

**HEPATOTOXICITY OF THIAZOLIDINEDIONE  
ANTIDIABETIC DRUGS: A STRUCTURAL TOXICITY  
RELATIONSHIP STUDY**

**SUDIPTA SAHA**

**NATIONAL UNIVERSITY OF  
SINGAPORE**

**2010**

**HEPATOTOXICITY OF THIAZOLIDINEDIONE  
ANTIDIABETIC DRUGS: A STRUCTURAL TOXICITY  
RELATIONSHIP STUDY**

**SUDIPTA SAHA**

**B. PHARM (JADAVPUR UNIVERSITY)**

**M. PHARM (JADAVPUR UNIVERSITY)**

**A THESIS SUBMITTED FOR THE DEGREE OF DOCTOR OF  
PHILOSOPHY**

**DEPARTMENT OF PHARMACY  
NATIONAL UNIVERSITY OF SINGAPORE**

**2010**

## ACKNOWLEDGEMENTS

I would like to give my sincere gratitude to my supervisors, Dr. Eric Chan Chun Yong and Dr. Chui Wai Keung, for their guidance on my PhD project. I am fortunate to be their student as they had granted me a great degree of freedom for creative research while carefully ensuring that my research did not lose its focus. As teachers, they also imparted to me the important values in research and importantly, the communication skills in scientific writing and presentation. The education I gained in my graduate study would serve as a strong foundation for me to continue to develop into an independent researcher.

I am also thankful to Dr Ho Han Kiat who guided me selflessly in numerous experiments pertaining to my research. While he is not my supervisor, I regarded him as an important mentor.

I am especially grateful to the laboratory supportive staff namely, Ms Ng Sek Eng and Ms Lye Pey Pey, for their constant technical support. In particular, I would like to show my deepest gratitude to Ms New Lee Sun who helped me significantly in the drug metabolism and LC/MS/MS experiments. I also wish to express my deep gratitude to the National University of Singapore for offering the research scholarship that supported my PhD candidature. In addition, I would like to acknowledge the academic research grants (R-148-050-088-101/133 and R-148-000-100-112) for providing financial resources for my research.

I would like to thank all my laboratory members namely Mainak Mal, Pasikanti Kishore Kumar, Phua Lee Cheng, Chng Hui Ting, Nikhil Sachdeva, Hriday Bera and Yang Hong for all their support and help during my candidature.

Last but not least, I am indebted to my dearest parents who are my first teachers in life and will remain my best companies forever. This thesis is dedicated to my parents and wife.

## Contents

	Page
Chapter 1 Introduction	
1.1 Hepatotoxicity and drug metabolism	1
1.2 Role of metabolism in hepatotoxicity	2
1.3 Symptoms and treatment of DM	3
1.4 Pharmacology and metabolism of TZD antidiabetic drugs	4
1.5 Potential mechanisms of TZD-induced hepatotoxicity	5
1.6 Mechanism of TGZ-induced hepatotoxicity	6
1.6.1 Formation of electrophilic reactive intermediates	6
1.6.2 Direct binding to PPAR <sub>γ</sub>	8
1.6.3 Mitochondrial dysfunction	9
1.6.4 Formation of TGZS	9
1.6.5 Apoptotic induction of hepatocytes and cancerous cells	11
1.6.6 Host Factors	11
1.7 Quantitative structure activity relationship (QSAR) of TZD antidiabetic drugs	12
1.8 Research questions	13
1.9 Hypothesis	14
1.10 Objectives	14
1.10.1 Chemical synthesis of analogues of TZD antidiabetic drug	15
1.10.2 Screening and identification of RMs using LC/MS/MS	15

	Page
1.10.3 Toxicity screening	17
1.10.4 Screening of PPAR <sub>γ</sub> binding affinities and aP2 gene expression	17
1.10.5 Synthesis and screening of TGZ and TGZS	19
1.10 Significance	19
1.11 Overview of proceeding chapters	20
Chapter 2 Synthesis of PRD analogues	
2.1 Introduction	21
2.2 Materials	22
2.3 Preparation of TSN	23
2.4 Preparation of PSN	20
2.5 Preparation of RSN	32
2.6 Preparation of CSN	37
2.7 Discussion	40
Chapter 3 RM profiling using HLM and THLE-2 cells	
3.1 Introduction	42
3.2 Materials	43
3.3 Methods	43
3.3.1 HLM incubation for RM profiling	43
3.3.2 THLE-2 cell culture	44
3.3.3 THLE-2 incubation for RM profiling	45
3.4 LC/MS/MS conditions	45

	Page
3.5 Results	46
3.5.1 RM profiling of TGZ and TSN	46
3.5.2 RM profiling of PGZ and PSN	50
3.5.3 RM profiling of RGZ and RSN	53
3.5.4 RM profiling of CGZ and CSN	55
3.6 Discussion	56
Chapter 4 Cytotoxicity assays	
4.1 Introduction	58
4.2 Materials	61
4.3 Methods	61
4.3.1 Stability studies of TZD and PRD analogues	61
4.3.1.1 BEGM incubation conditions	61
4.3.2.2 LC/MS/MS conditions	62
4.3.2 MTT viability assay	63
4.3.3 GSH depletion assay	64
4.3.3.1 Preparation of calibration curve	64
4.3.3.2 GSH depletion assay using THLE-2 cells	65
4.3.3.3 LC/MS/MS conditions	66
4.3.4 PC assay	67
4.4 Results	69
4.4.1 Stability studies	69
4.4.1.1 Stability studies of TGZ and TSN	69

	Page
4.4.1.2 Stability studies of PGZ and PSN	71
4.4.1.3 Stability studies of RGZ and RSN	73
4.4.1.4 Stability studies of CGZ and CSN	75
4.4.2 MTT viability assay	77
4.4.2.1 MTT viability assay of TGZ and TSN	77
4.4.2.2 MTT viability assay of PGZ and PSN	77
4.4.2.3 MTT viability assay of RGZ and RSN	80
4.4.2.4 MTT viability assay of CGZ and CSN	82
4.4.3 GSH consumption assay	83
4.4.3.1 GSH consumption assay of TGZ and TSN	83
4.4.3.2 GSH consumption assay of PGZ and PSN	85
4.4.3.3 GSH consumption assay of RGZ and RSN	86
4.4.3.4 GSH consumption assay of CGZ and CSN	87
4.4.4 PC assay	87
4.4.4.1 PC assay of TGZ and TSN	88
4.4.4.2 PC assay of PGZ and PSN	88
4.4.4.3 PC assay of RGZ and RSN	89
4.4.4.4 PC assay of CGZ and CSN	90
4.5 Discussion	91
Chapter 5 PPAR $\gamma$ binding and ap2 gene expression assays	
5.1 Introduction	95
5.2 Materials	95

	Page
5.3 Methods	96
5.3.1 PPAR $\gamma$ binding assay	96
5.3.1.1 PPAR $\gamma$ incubation conditions	96
5.3.1.2 LC/MS/MS conditions	97
5.3.2 aP2 gene expression assay	97
5.3.2.1 3T3-L1 cells	97
5.3.2.2 RNA isolation, PCR and qRT-PCR	98
5.4 Results	99
5.4.1 PPAR $\gamma$ binding assay	99
5.4.2 aP2 gene expression assay	102
5.2 Discussion	104
Chapter 6 Toxic effect of TGZS in THLE-2 cells	
6.1 Introduction	107
6.2 Preparation of TGZS	107
6.3 Methods	114
6.3.1 Sulfotransferase enzyme inhibition assay	114
6.3.1.1 THLE-2 cells incubation	114
6.3.1.2 LC/MS/MS conditions	114
6.3.2 Stability study of synthesized TGZS in BEGM	115
6.3.3 MTT viability assay	116
6.3.4 GSH depletion assay	16
6.3.5 PC assay	116



	Page
6.4 Results	116
6.4.1 Sulfotransferase enzyme inhibition assay	116
6.4.2 Stability profile of TGZS using BEGM	117
6.4.3 MTT viability assay	119
6.4.4 GSH depletion assay	121
6.4.5 PC assay	122
6.5 Discussion	123
Chapter 7 Conclusion, limitation and future direction	
7.1 Conclusion	127
7.1 Limitation and future direction	129
Bibliography	130
List of Publications	137

## Summary

Troglitazone (TGZ) was an orally active thiazolidinedione (TZD) hypoglycemic agent which was used for the treatment of non-insulin-dependent diabetes mellitus and withdrawn from the market in 2000 due to its hepatotoxicity. Pioglitazone (PGZ) and rosiglitazone (RGZ), the other two analogues of the TZD ring are non-toxic and still in the market. While the exact mechanism of TGZ toxicity remains unknown, it has been postulated that the formation of toxic reactive metabolites (RMs) may play an important role in the hepatotoxicity. On the other hand, the sulfation at 6-hydroxyl group of the chroman ring of TGZ may be partially responsible for hepatotoxicity. PGZ and RGZ also produce RMs but they are non-toxic in nature due to lower doses. Few cases of hepatotoxicity of RGZ and PGZ had also been published recently. The purpose of this study is to investigate the role of sulfur moiety of the TZD nucleus in inducing liver toxicity. To achieve this goal, the TZD analogues were synthesized chemically where the sulfur moiety of the TZD ring was replaced by the methylene group of the pyrrolidinedione (PRD) ring. Both these analogues were incubated independently with human liver microsomes and glutathione (GSH). In a separate experiment, the TZD and PRD analogues were incubated with normal human hepatocytes (THLE-2 cells). Reactive metabolite glutathione (RM-GSH) adducts were formed during incubation which were separated by ultra performance liquid chromatography (UPLC) and identified using mass spectrometry (MS). 3-(4,5-Dimethylthiazol-2-yl)-2,5-diphenyltetrazolium (MTT), glutathione (GSH) and protein carbonyl (PC) assays were performed to check the mechanism of toxicity of both these analogues using THLE-2 cells. Finally, peroxisome proliferator activated receptor gamma (PPAR<sub>γ</sub>) binding activity and  $\alpha$ P2 gene expression assays were performed to check the binding affinities of both these analogues. Our results indicated collectively that the TZD analogues were more toxic than the

PRD analogues in THLE-2 cells. As both analogues were shown to bind to PPAR $\gamma$ , the substitution of the TZD ring by the PRD ring may be beneficial from a drug design perspective.

Furthermore, we synthesized sulfo-conjugated troglitazone (TGZS) and toxicity studies were performed using THLE-2 cells. Our MTT, GSH and PC results suggested that TGZS was more toxic than its parent TGZ and may be partially responsible for TGZ-induced hepatotoxicity via the oxidative stress mechanism.

In conclusion, our study suggested that the TZD antidiabetic drugs may be partially responsible for its liver toxicity in humans via oxidative stress mechanism through the RMs formation.

## ABBREVIATIONS

ACN	Acetonitrile
aP2	adipocyte fatty acid
BEBM	bronchial epithelial basal media
BEGM	bronchial epithelial growth media
BSEP	bile salt export pump
CDCl <sub>3</sub>	deuterated chloroform
CGZ	Ciglitazone
<sup>13</sup> CNMR	carbon nuclear magnetic resonance
CSN	Cisuccinimide
CYP450	cytochrome P450
DMEM	dullbecco's modified eagle's media
DMF	Dimethylformamide
DMSO-d <sub>6</sub>	deuterated dimethyl sulfoxide
EDTA	ethylenediamine tetraacetic acid
ESI	electrospray ionization
EtOAc	ethyl acetate
GSH	Glutathione
GSSG	glutathione disulfide
h	Hour
HLM	human liver microsomes
<sup>1</sup> HNMR	proton nuclear magnetic resonance
HPLC	high performance liquid chromatography

LBD	ligand-binding domain
LC/MS/MS	liquid chromatography tandem mass spectrometry
LLE	liquid-liquid extraction
Min	Minute
MRM	multiple reaction monitoring
mRNA	messenger ribonucleic acid
MS	mass spectrometry
MTBE	methyl tert-butyl ether
MTT	3-(4,5-Dimethylthiazol-2-yl)-2,5-diphenyltetrazolium
NADPH	nicotinamide adenine-di-nucleotide phosphate hydrogen
Na <sub>2</sub> EDTA•2H <sub>2</sub> O	ethylenediaminetetraacetic acid disodium salt dehydrate
NEM	N-ethylmaleimide
NL	neutral loss
PC	protein carbonyl
PCR	polymerase chain reaction
PGZ	Pioglitazone
PIS	product ion scan
PPAR <sub>γ</sub>	peroxisome proliferator activated receptor gamma
PRD	2,5-pyrrolidinedione
PSN	Piosuccinimide
QC	quality control
QR	Quercetin
QRS	quercetin sulphate
qRT-PCR	quantitative real time polymerase chain reaction

QSAR	quantitative structure activity relationship
QTRAP MS	quadrupole linear ion trap mass spectrometer
RGZ	Rosiglitazone
RM-GSH	reactive metabolite glutathione adduct
RMs	reactive metabolites
RNA	ribonucleic acid
RSN	Rosisuccinimide
S	Second
SAR	structure activity relationship
STR	structural toxicity relationship
TA	tocopherol acetate
TCA	trichloroacetic acid
TGZ	Troglitazone
TGZS	troglitazone sulphate
THF	Tetrahydrofuran
THLE-2 cells	normal human hepatocytes
TSN	Trosuccinimide
TZD	2,4-thiazolidinedione
UPLC/MS/MS	ultra performance liquid chromatography tandem mass spectrometry
3T3-L1 cells	human adipocytes

## LIST OF FIGURES

FIGURE		PAGE
1	Relationship between drug metabolism and toxicity. Toxicity may be acquired through either accumulation of parent drug or via metabolic activation, through formation of toxic RMs. If RMs are not detoxified, they can bind covalently with biological macromolecules which may lead to drug toxicity (Park et al., 2005).	2
2	Structures of TZD antidiabetic drugs (A) TGZ (* 6-hydroxyl group of the chroman ring of TGZ), (B) RGZ, (C) PGZ and (D) CGZ.	7
3	RM-GSH conjugates of TGZ (M1-M5 and ML3) (Kassahun et al., 2001; Prabhu et al., 2002).	10
4	Pharmacophoric elements of TZD antidiabetic drugs.	13
5	Summary of the proposed research work.	17
6	General procedure for the synthesis of TZD antidiabetic drugs. (A) sodium hydride, anhydrous DMF, 4-fluorobenzaldehyde, RT, 12 h; (B) TZD, piperidine, ethanol, reflux, 24 h; (C) 10% Pd/C, hydrogen gas, ethanol, 12 h.	22
7	Synthesis of TSN. (A) Triphenylphosphine, methanol, reflux, 1.5 h; (B) dibutylamine, acetic acid, 24 h, reflux; (C) lithium aluminium hydride, anhydrous THF, 0°C, 4-5 h; (D) allyl bromide, acetone AR, potassium carbonate, reflux, 48 h; (E) sodium hydride, anhydrous DMF, 4-fluorobenzaldehyde, RT, 12h; (F) 3-(triphenylphosphoranylidene)pyrrolidine-2,5-dione, methanol, reflux, 3 h; (G) lithium chloride (anhydrous), sodium borohydride, anhydrous THF, RT and 10% Pd/C, hydrogen gas, ethanol, 12 h.	24
8	<sup>13</sup> C NMR interpretation of (A) methyl-6-hydroxy-2,5,7,8-tetramethylchroman-2-carboxylate, (B) 4-((6-(allyloxy)-2,5,7,8-tetramethylchroman-2-yl)methoxy)benzaldehyde and (C) TSN.	25
9	Synthesis of PSN. (A) 4-Fluorobenzaldehyde, sodium hydride, DMF, RT, 12 h; (B) 3-(triphenylphosphoranylidene)pyrrolidine-2,5-dione,	31

	methanol, reflux, 2 h; (C) 10% Pd/C, hydrogen gas, ethanol, 12 h.	
10	<sup>13</sup> C NMR interpretation of (A) (3E)-3-{4-[2-(5-ethylpyridin-2-yl)ethoxy]benzylidene}pyrrolidine-2,5-dione and (B) PSN	31
11	Synthesis of RSN. (A) Di- <i>tert</i> -butyl dicarbonate, chloroform, RT, 24 h; (B) 4-hydroxybenzaldehyde, triphenylphosphine, DIAD, dry THF, 0°C, RT, 18 h; (C) 3-(triphenylphosphoranylidene)pyrrolidine-2,5-dione, methanol, reflux, 2 h; (D) 10% Pd/C, hydrogen gas, ethanol, 12 h; (E) 0.5N HCl in dioxane, chloroform, RT, 2 h; (F) 2-chloropyridine, absolute ethanol, reflux, 24 h.	34
12	<sup>13</sup> C NMR interpretation RSN.	34
13	Synthesis of CSN. (A) Iodine, sodium borohydride, anhydrous THF, 0°C, RT; (B) 4-hydroxybenzaldehyde, triphenylphosphine, DIAD, dry THF, 0°C, RT, 18 h; (C) methanol, reflux, 2 h, 3-(triphenylphosphoranylidene)pyrrolidine-2,5-dione; (D) 10% Pd/C, hydrogen gas, ethanol, 12 h.	38
14	<sup>13</sup> C NMR interpretation of (A) (3Z)-3-{4-[(1-methylcyclohexyl)methoxy]benzylidene}pyrrolidine-2,5-dione and (B) CSN.	38
15	NL scan at <i>m/z</i> 129 amu of (A) 24 h TGZ-THLE-2 sample and (B) 60 min TGZ-HLM-GSH sample. PIS of (C) RM1, <i>m/z</i> 722 (D) RM2, <i>m/z</i> 747, (E) RM3, <i>m/z</i> 737 and (F) RM4, <i>m/z</i> 781.	48, 49
16	NL scan of at <i>m/z</i> 129 amu of (A) 60 min PGZ-HLM-GSH sample and (B) 24 h PGZ-THLE-2 sample. PIS of (C) RM5, <i>m/z</i> 636 (D) RM6, <i>m/z</i> 637.	52, 53
17	NL scan of at <i>m/z</i> 129 amu of (A) 60 min RGZ-HLM-GSH and (B) 24 h RGZ-THLE-2 sample. PIS of (C) RM7, <i>m/z</i> 637 and (D) RM8, <i>m/z</i> 638.	54, 55
18	Representative LC/MS/MS chromatograms of (A) TGZ (6.44 min), (B) TSN (8.11 min) in BEGM.	69
19	Stability profiles of TSN at (A) 1 and (B) 50 μM, TGZ at (C) 1 and (D) 50 μM in BEGM at 37°C up to 72 h (average±SD, n=3).	70
20	Representative LC/MS/MS chromatograms of (A) PGZ (3.13 min), (B) PSN (2.66 min) in BEGM.	71



21	Stability studies of PSN at (A) 1 and (B) 50 $\mu$ M, PGZ at (C) 1 and (D) 50 $\mu$ M in BEGM at 37°C up to 72 h (average $\pm$ SD, n=3).	72
22	Representative LC/MS/MS chromatograms of (A) RGZ (2.59 min), (B) RSN (5.39 min) in BEGM.	73
23	Stability studies of RSN at (A) 1 and (B) 50 $\mu$ M, RGZ at (C) 1 and (D) 50 $\mu$ M in BEGM at 37°C up to 72 h (average $\pm$ SD, n=3).	74
24	Representative LC/MS/MS chromatograms of (A) CGZ (7.65 min) and (D) CSN (7.31 min) in BEGM.	75
25	Stability studies of CSN at (A) 1 and (B) 50 $\mu$ M, CGZ at (C) 1 and (D) 50 $\mu$ M in BEGM at 37°C up to 72 h (average $\pm$ SD, n=3).	76
26	(A) Percentage MTT cell viabilities of THLE-2 cells at varying concentrations of TGZ and TSN. Statistical differences were demonstrated between control and test compounds (one-way ANOVA, P<0.05) and between TGZ and TSN (paired T-test, P<0.05) at and above 25 and 50 $\mu$ M concentration, respectively. (B) Percentage MTT cell viabilities of THLE-2 cells at varying concentrations of TGZ and TSN co-incubated with 20 $\mu$ M TA. Statistical differences were observed between TGZ and TSN in terms of percentage cell viability at and above 100 $\mu$ M (paired T-test, P<0.05).	78
27	(A) Percentage MTT cell viabilities of THLE-2 cells at varying concentrations of PGZ and PSN. Statistical differences were demonstrated between control and test compounds (one-way ANOVA, P<0.05) at and above 50 $\mu$ M concentration. Statistical differences were also observed between PGZ and PSN (paired T-test, P<0.05) at 50, 75 and 100 $\mu$ M. (B) Percentage MTT cell viabilities of THLE-2 cells at varying concentrations of PGZ and PSN co-incubated with 20 $\mu$ M TA. Statistical differences were observed between PGZ and PSN in terms of percentage cell viability at 75, 100 and 125 $\mu$ M (paired T-test, P<0.05).	79
28	(A) Percentage MTT cell viabilities of THLE-2 cells at varying concentrations of RGZ and RSN. Statistical differences were demonstrated between control and test compounds (one-way ANOVA, P<0.05) at and above 25 $\mu$ M concentration. (B) Percentage MTT cell viabilities of THLE-2 cells at varying concentrations of RGZ and RSN	81

co-incubated with 20  $\mu$ M TA.

- 29 (A) Percentage MTT cell viabilities of THLE-2 cells at varying concentrations of CGZ and CSN. Statistical differences were demonstrated between control and test compounds (one-way ANOVA,  $P < 0.05$ ) at and above 25  $\mu$ M concentration. (B) Percentage MTT cell viabilities of THLE-2 cells at varying concentrations of CGZ and CSN co-incubated with 20  $\mu$ M TA. 82
- 30 Representative LC/MS/MS chromatogram of GSH-NEM complex (3.13 min). 84
- 31 GSH depletion in THLE-2 cells at varying concentrations of TGZ and TSN. Statistical differences were demonstrated between control and test compounds (one-way ANOVA,  $P < 0.05$ ) and between TGZ and TSN (paired T-test,  $P < 0.05$ ) at and above 25 and 75  $\mu$ M, respectively. 84
- 32 GSH depletion in THLE-2 cells at varying concentrations of PGZ and PSN. Statistical differences were demonstrated between control and test compounds (one-way ANOVA,  $P < 0.05$ ) at and above 25  $\mu$ M. Statistical differences were also observed between TGZ and TSN (paired T-test,  $P < 0.05$ ) from 25 to 100  $\mu$ M. 85
- 33 GSH depletion in THLE-2 cells at varying concentrations of RGZ and RSN. Statistical differences were demonstrated between control and test compounds (one-way ANOVA,  $P < 0.05$ ) and between RGZ and RSN (paired T-test,  $P < 0.05$ ) at and above 100 and 25  $\mu$ M, respectively. 86
- 34 GSH depletion in THLE-2 cells at varying concentrations of CGZ and CSN. Statistical differences were demonstrated between control and test compounds (one-way ANOVA,  $P < 0.05$ ) at and above 25  $\mu$ M. Statistical differences were observed between CGZ and CSN at 10, 25 and 50  $\mu$ M (paired T-test,  $P < 0.05$ ). 87
- 35 PC assay of THLE-2 cells at varying concentrations of TGZ and TSN. Statistical differences were demonstrated between control and test compounds (one-way ANOVA,  $P < 0.05$ ) and between TGZ and TSN (paired T-test,  $P < 0.05$ ) at 50  $\mu$ M. 88

36	PC assay of THLE-2 cells at varying concentrations of PGZ and PSN. Statistical differences were demonstrated between control and test compounds (one-way ANOVA, $P < 0.05$ ) at 50 $\mu\text{M}$ . Statistical differences were observed between PGZ and PSN at 1 and 50 $\mu\text{M}$ (paired T-test, $P < 0.05$ ).	89
37	PC assay of THLE-2 cells at varying concentrations of RGZ and RSN. Statistical difference was demonstrated between RGZ and RSN (paired T-test, $P < 0.05$ ) at 50 $\mu\text{M}$ .	90
38	PC assay of THLE-2 cells at varying concentrations of CGZ and CSN. Statistical differences were demonstrated between control and test compounds (one-way ANOVA, $P < 0.05$ ) at 50 $\mu\text{M}$ . Statistical differences were observed between CGZ and CSN at 10 $\mu\text{M}$ (paired T-test, $P < 0.05$ ).	91
39	(A) Percentage binding to PPAR $_{\gamma}$ -LBD at varying concentrations of TGZ and TSN. Statistical differences were observed between TGZ and TSN in terms of percentage binding to PPAR $_{\gamma}$ -LBD at and above 50 nM (paired T-test, $P < 0.05$ ). (B) Percentage binding to PPAR $_{\gamma}$ -LBD at varying concentrations of PGZ and PSN. Statistical differences were observed between PGZ and PSN in terms of percentage binding to PPAR $_{\gamma}$ -LBD at 100 nM (paired T-test, $P < 0.05$ ).	100
40	(A) Percentage binding to PPAR $_{\gamma}$ -LBD at varying concentrations of RGZ and RSN. Statistical differences were observed between RGZ and RSN in terms of percentage binding to PPAR $_{\gamma}$ -LBD at 50 and 100 nM (paired T-test, $P < 0.05$ ). (B) Percentage binding to PPAR $_{\gamma}$ -LBD at varying concentrations of CGZ and CSN. Statistical differences were observed between CGZ and CSN in terms of percentage binding to PPAR $_{\gamma}$ -LBD at 500.0 nM (paired T-test, $P < 0.05$ ).	101
41	(A) Relative amount of mRNA expression of aP2 gene at 50 $\mu\text{M}$ concentration of TGZ and TSN. Statistical differences were observed between TGZ and TSN at 50 $\mu\text{M}$ (paired T-test, $P < 0.05$ ). (B) Relative amount of aP2 gene expression at 50 $\mu\text{M}$ concentration of PGZ and PSN.	103
42	Relative amount of aP2 gene expression at 50 $\mu\text{M}$ concentration of RGZ and RSN. (B) Relative amount of aP2 gene expression at 50 $\mu\text{M}$ concentration of CGZ and CSN.	104

43	Synthesis of TGZS. (A) Tert-butyldimethylsilyl chloride, imidazole, anhydrous DMF, RT, 36 h; (B) sodium hydride, anhydrous DMF, 4-fluorobenzaldehyde, RT, 12 h; (C) TZD, 2-aminoethanol, reflux, 24 h and then 10% Pd/C, H <sub>2</sub> gas, EtOH, 12 h; (D) sulphur trioxide-N-triethylamine complex, potassium carbonate, anhydrous DMF, RT for 1h then 40°C for 2 h.	112
44	<sup>13</sup> C NMR interpretation (A) 6-(tert-butyl-dimethyl-silanyloxy)-2,5,7,8-tetramethyl-chroman-2-yl]-methanol; (B) TGZ and (C) TGZS.	113
45	(A) Representative LC/MS/MS chromatogram of TGZS in “24 h TGZ–THLE–2” sample (retention time 4.92 min). (B) Representative LC/MS/MS chromatogram of “24 h TGZ–QR–THLE–2” sample (QRS1, retention time 3.09 min; QRS2, retention time 6.68 min).	117
46	Stability profile of TGZS at (A) 1.0 and (B) 50.0 μM in BEGM at 37°C up to 72 h.	118
47	(A) Percentage MTT cell viabilities of THLE–2 cells at varying concentrations of TGZ and TGZS. Statistical differences were demonstrated between control and test compounds (one–way ANOVA, P<0.05) and between TGZ and TGZS (paired T–test, P<0.05) at and above 10 μM concentration, respectively. (B) Percentage MTT cell viabilities of THLE–2 cells at varying concentrations of TGZ and TGZS co–incubated with 50 μM of QR. Statistical differences were observed between TGZ and TGZS in terms of percentage cell viability at and above 50 μM (paired T–test, P<0.05). (C) Percentage MTT cell viabilities of THLE–2 cells at varying concentrations of TGZ and TGZS co–incubated with 20 μM of TA. Statistical differences were observed between TGZ and TGZS in terms of percentage cell viability at and above 25 μM (paired T–test, P<0.05).	120
48	Percentage MTT cell viabilities of THLE–2 cells at varying concentrations of QR	121
49	<b>G</b> SH depletion in THLE–2 cells at varying concentrations of TGZ and TGZS. Statistical differences were demonstrated between control and test compounds (one–way ANOVA, P<0.05) and between TGZ and TGZS	122

(paired T-test,  $P < 0.05$ ) at and above 50  $\mu\text{M}$ , respectively.

- 50 PC assay of THLE-2 cells at varying concentrations of TGZ and TGZS. 123  
Statistical differences were demonstrated between control and test  
compounds (one-way ANOVA,  $P < 0.05$ ) and between TGZ and TGZS  
(paired T-test,  $P < 0.05$ ) at 50  $\mu\text{M}$ .

## LIST OF TABLES

TABLE		PAGE
1	TZD antidiabetic drugs (TGZ, RGZ, PGZ and CGZ) and the respective proposed PRD analogues (TSN, RSN, PSN and CSN) (* Positions where TZD and PRD rings are covalently bonded to the structural back bones). Values in parenthesis refer to the cLogP values calculated using ChemDraw Ultra version 6.0.	16
2	Optimized MS parameters for the detection of RM-GSH adducts.	46
3	Optimized MS parameters for stability studies of the TZD analogues.	63
4	Optimized MS parameters for stability studies of the PRD analogues.	63
5	Optimized LC conditions for GSH depletion assay (New and Chan, 2008)	67
6	Optimized MS parameters for GSH depletion assay.	67
7	Expression level of mRNA in 3T3-L1 cells (aP2/ $\beta$ -actin)	105
8	Optimized MS parameters for identification and stability profiling of TGZS and QRS.	115

# Chapter 1

## Introduction

### *1.1 Hepatotoxicity and drug metabolism*

Drug-induced liver failure is a significant health problem throughout the world in the twenty-first century. At the same time, drug-induced liver injury is one of the most common reasons for the withdrawal of approved drugs from the market and accounts for approximately 50% of the total cases of acute liver failure in the United States (Lee, 2003). Recent evidence suggested that more than 600 drugs are associated with hepatotoxicity in the United States (Lee, 2003).

The biotransformation of drugs takes place in the liver (both phase I and II). Cytochrome P450 enzymes (CYP450) are mainly responsible for the metabolism of most drugs and other xenobiotics. Different types of metabolites are generated from the biotransformation of drugs. One is the inactive metabolite which is relatively more polar in nature than the parent drug and easily eliminated via the renal system. Another is the highly electrophilic reactive metabolite (RM) which can interact with vital intracellular macromolecules resulting in toxicity. RMs are detoxified naturally through the binding with endogenous nucleophiles such as glutathione (GSH) and proteins. GSH can bind with RMs nonenzymatically or enzymatically by the action of glutathione S-transferases. When excess RMs bind covalently with cellular macromolecules (e.g. proteins and/or nucleic acids), serious toxicity may result (Fig. 1). Currently, the pharmaceutical industry has adopted the screening of RMs during early candidate profiling in drug discovery and development.

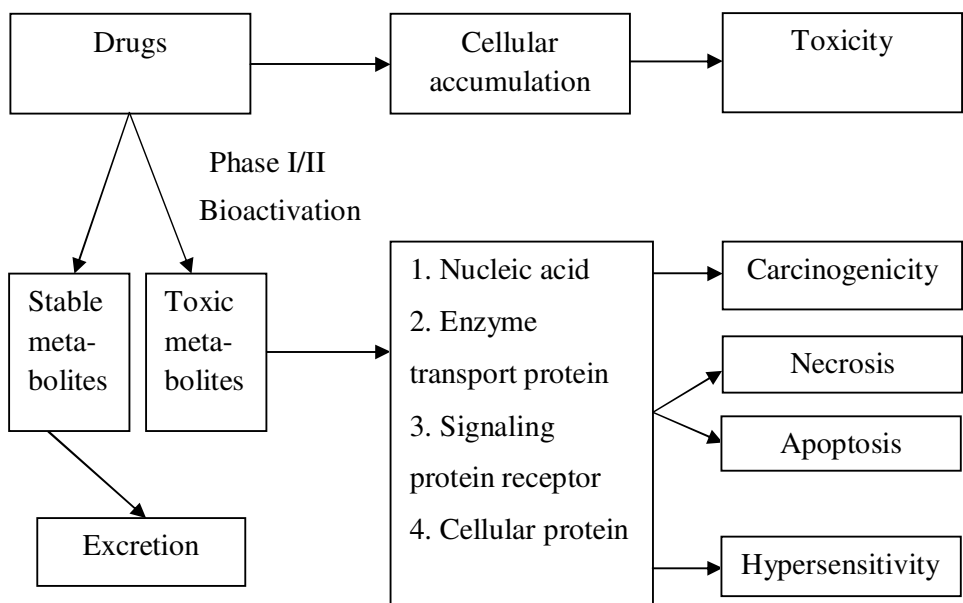


**Fig. 1** Relationship between drug metabolism and toxicity. Toxicity may be acquired through either accumulation of parent drug or via metabolic activation, through formation of toxic RMs. If RMs are not detoxified, they can bind covalently with biological macromolecules which may lead to drug toxicity (Park et al., 2005).

### 1.2 Role of metabolism in hepatotoxicity

The most prevalent hypothesis for metabolism related hepatotoxicity is the hapten carrier hypothesis (Park et al., 1998; Utrecht., 1999). The hypothesis suggested that all small molecules are not immunogenic in nature. They produce immune response during binding to larger molecule like proteins. Drugs and their RMs act as hapten and bind with proteins and cellular molecules irreversibly to perform cellular toxicity.

Drug molecules were either withdrawn from market or given black box warning due to their potential cause of hepatotoxicity. Bromfenac, the second generation non-steroidal anti-inflammatory drug was withdrawn from market in 1998 due to the formation of acyl glucuronide conjugate during metabolism which might be reacted with hepatic proteins



(Rabkin et al., 1999). The antidepressant drug, nefazodone was withdrawn from market in 2003 due to its hepatotoxicity nature. It produced hydroxyl and quinonimine intermediates after metabolic activation which was trapped by GSH (Kalgutkar et al., 2005).

The anti-tubercular drug, isoniazid received black box warning in 1969 which generated acetylhydrazine after metabolic activation and might be reacted with cellular macromolecules (Nelson et al., 1976). The anti-fungal drug, ketoconazole was given black box warning in 1980 which produced N-desmethyl ketoconazole during metabolism and might be reacted with hepatic cells (Heel et al., 1982).

Another classical example of drug induced hepatotoxicity is troglitazone which was used as antidiabetic drugs and withdrawn from market in 2000 (Chojkier, 2005). It produced sulfoxide and  $\alpha$ -ketoisocyanate intermediates after metabolic activation which might have tendency to bind with GSH.

### *1.3 Symptoms and treatment of diabetes mellitus*

Diabetes mellitus affected an estimated 16 million people in the United States in 1998 (Harris et al., 1998). At present, one out of eleven people (~ 10% of population) is affected by diabetes in Singapore ([www.diabetes.org.sg](http://www.diabetes.org.sg)). Type II diabetes mellitus (also known as non-insulin-dependent diabetes mellitus) is the fourth leading cause of death in the United States which is also a major contributor to blindness and chronic renal failure. The disease is linked to several long-term complications like retinopathy, nephropathy, neuropathy, hypertension, atherosclerosis, and hyperlipidemia (Bethesda, 1995; Harris et al., 1998).

Diagnosis and complications of diabetes mellitus have been described as a mixture of metabolic disorders which are characterized by hyperglycemia. There are several treatments

of diabetes mellitus comprising non-pharmacologic interventions such as diet modification and exercise and pharmacological interventions such as sulfonylureas, metformin, acarbose, 2,4-thiazolidinediones (TZDs) and insulin administered either alone or in combination for the treatment of type II diabetes mellitus (UK Prospective Diabetes Study Group, 1998; American Diabetes Association, 2000).

In the introduction, we focus our discussion on the TZD antidiabetic drugs as this group of drugs is implicated in hepatotoxicity via possible metabolic activation.

#### *1.4 Pharmacology and metabolism of TZD antidiabetic drugs*

Troglitazone (TGZ, Fig. 2) and the other TZD antidiabetic drugs such as rosiglitazone (RGZ, Fig. 2) and pioglitazone (PGZ, Fig. 2) lower the blood glucose concentration by partial agonism to peroxisome proliferator activated receptor gamma (PPAR<sub>γ</sub>) (Henry, 1997). PPAR<sub>γ</sub> is a ligand activated transcription factor which is similar to the retinoid X receptor (Zhang et al., 1992; Kliewer et al., 1992) and interacts with genes during glucose and lipid metabolism. Among the effects, researchers proposed that TGZ and RGZ induce human adipocyte fatty acid (aP2) binding protein gene expression in adipocytes (Kletzien et al., 1992; Ibrahimi et al., 1994). Once PPAR<sub>γ</sub> is stimulated, glucose transporter-4 production and translocation occur inside the cell system. As a result, TGZ and other glitazones may raise serum triglycerides level or alter thyroid metabolism (Miller et al., 1997; Sherman et al., 1999; Rizvi et al., 1999) and inhibit phosphoenolpyruvate carboxylase enzyme, which is mainly responsible for hepatic gluconeogenesis (Camp et al., 2000). TGZ has no direct action on insulin formation and secretion, but increases the insulin sensitivity of adipose tissue and skeletal muscle during hyperglycemia and decreases hepatic glucose production (Wagstaff et al., 2002).

*In vitro* and *in vivo* experiments suggested that TGZ is mainly metabolized by cytochrome 3A4 (CYP3A4) and 2C8 (CYP2C8) enzymes (Sahi et al., 2000; Ramachandran et al., 1999; He et al., 2001). The metabolism of TGZ in liver includes oxidation (phase I metabolism), sulfation and glucuronidation (phase II metabolism). The glucuronide metabolite of TGZ is found in human plasma at very low concentration while the major metabolites of TGZ in humans are the sulfate (TGZS, 70%, Fig. 2) and quinone (10%) conjugates, respectively (Loi et al., 1997; Loi et al., 1999).

RGZ is mainly metabolized by CYP2C8 and to a lesser extent by cytochrome 2C9 enzyme (CYP2C9) in liver to the corresponding ortho- or para-hydroxyl and N-desmethyl RGZ (phase I metabolism). These metabolites are conjugated subsequently with sulfate and glucuronic acid (phase II metabolism) (Malinowski and Bolesta, 2000).

PGZ is also oxidized by CYP2C8 and CYP3A4 to the corresponding hydroxyl and carboxyl metabolite of PGZ (phase I metabolism) (Jaakkola et al., 2005). These metabolites are excreted after sulfate and glucuronide conjugation (phase II metabolism).

### *1.5 Potential mechanisms of TZD-induced hepatotoxicity*

TGZ was withdrawn from the market in 2000 due to fatalities caused by liver toxicity (Chojkier, 2005). While H<sub>2</sub>-receptor antagonists having thiazolidine ring (ebrotidine, famotidine) were also withdrawn from market due to similar toxic liabilities (Andrade et al., 1999; Castillo et al., 2000), the other PPAR<sub>γ</sub> agonists such as RGZ and PGZ which contain the TZD ring are still used clinically for the treatment of diabetes. However, RGZ was recently found to be associated with cardiotoxicity (Burce et al., 2007) and hepatic injury (four reports) (Park et al., 2005). On the other hand, there were also six reports of hepatic injury in the case of PGZ (Park et al., 2005; Baughmam et al., 2005). Nonetheless, there were

no severe case reports regarding the hepatotoxicity of PGZ and RGZ till date. Ciglitazone (CGZ, Fig. 2), another TZD antidiabetic drug candidate, was also withdrawn from phase-II clinical trial due to its poor efficacy (Day, 1999). The exact nature of TGZ inducing hepatotoxicity has not been established but many mechanisms had been proposed (Smith, 2003). As TZD drugs are still used clinically, it becomes necessary to investigate the mechanism of toxicity of TGZ.

### *1.6 Mechanism of TGZ-induced hepatotoxicity*

The exact nature of TGZ-induced hepatotoxicity has not been established, but many mechanisms had been proposed (Smith, 2003; Masubichi, 2006). These potential mechanisms include the formation of electrophilic reactive intermediates (section 1.6.1), direct binding to PPAR $\gamma$  (section 1.6.2), mitochondrial dysfunction (section 1.6.3), formation of TGZS (section 1.6.4), apoptotic induction of hepatocytes and cancer cells (section 1.6.5) and a combination of host factors (section 1.6.6). All these proposed mechanisms are briefly discussed below. Sections 1.6.2, 1.6.3 and 1.6.5 are related to the direct toxicity of TGZ to liver cell, while sections 1.6.1 and 1.6.4 are related to the metabolism-based toxicity of TGZ.

#### *1.6.1 Formation of electrophilic reactive intermediates*

Recently available data proposed that TGZ produces hepatotoxicity via the formation of RMs (Kassahun et al., 2001). One postulation was that the sulfur moiety of the TZD ring might be oxidized by CYP3A4 enzyme to the corresponding electrophilic sulfoxide and  $\alpha$ -ketoisocyanate intermediates that might react with GSH. Six reactive metabolite glutathione adducts (RM-GSH, Fig. 3) (M1 to M5 and ML3) of TGZ had already been identified

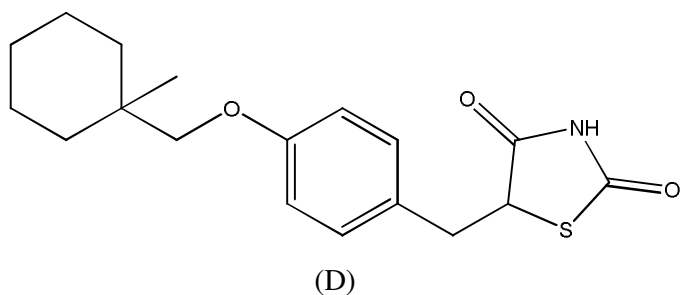
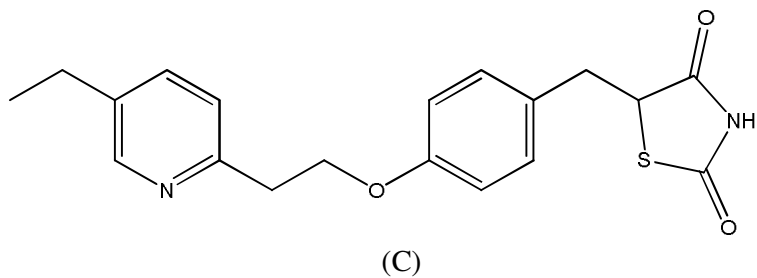
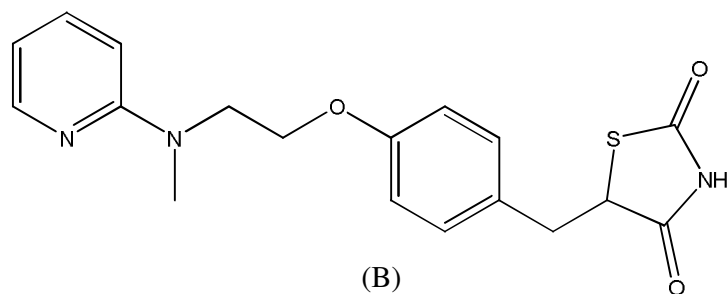
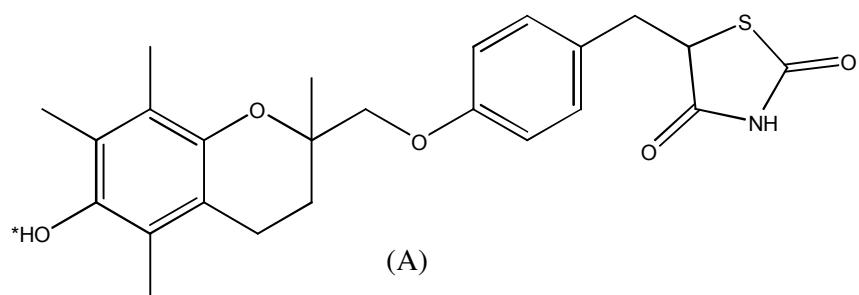


**Fig. 2** Structures of TZD antidiabetic drugs (A) TGZ (\* 6-hydroxyl group of the chroman ring of TGZ), (B) RGZ, (C) PGZ and (D) CGZ.

*in vitro* using human liver microsomes (HLM) and *in vivo* using Sprague-dawley rats ((Kassahun et (Kassahun et al., 2001; Prabhu et al., 2002)). Among these six RMs of TGZ, one was related to a quinone metabolite, while the other five RMs arose from the TZD moiety. The presence of a quinone metabolite appeared to be the potential cause of TGZ toxicity as the safer analogues such as RGZ and PGZ do not contain a chroman ring nor generate the quinone metabolite (Fig. 2). However, it had been shown that the quinone metabolite of TGZ was not as cytotoxic as compared to the parent drug in human and porcine hepatocytes (Tetty et al., 2001; Kostrubsky et al., 2000). On the other hand, all TZD drugs, including RGZ and PGZ, are capable of TZD-ring opening to generate reactive intermediates. Therefore, it becomes difficult to account for the higher level of toxicity of TGZ as compared to RGZ and PGZ. For example, RMs of RGZ and PGZ that are related to the TZD ring had been identified (Alvarez-Sánchez et al., 2006). Nonetheless, one must be mindful that RGZ and PGZ are prescribed at much lower doses clinically than TGZ (Malinowski and Bolesta, 2000), and thus present a reduced risk for toxicity given a similar adduction potential. As the TZD ring may be implicated in toxicity due to the formation of reactive intermediates, it is important to question, investigate and understand the role of the TZD ring in toxicities related to this class of drugs.

### *1.6.2 Direct binding to PPAR<sub>γ</sub>*

All the TZD antidiabetic drugs are specific ligands for PPAR<sub>γ</sub> (Berger and Moller, 2002; Hihi et al., 2002). PPAR<sub>γ</sub> belongs to the nuclear receptor family that regulates the gene expressions during glucose and lipid metabolism. There are several postulations regarding the binding of TZD drugs to PPAR<sub>γ</sub> which include alteration of glucose and lipid metabolism and changes in the expressed genes that control apoptosis, a form of cell suicide or cell death.

Apoptosis is manifested by cell shrinkage, nuclear and DNA fragmentation and removal of cells by phagocytosis. Apoptotic induction by TGZ in hepatocytes depends on its binding to PPAR $\gamma$ . While other TZD drugs (RGZ and PGZ) were shown to bind to PPAR $\gamma$ , they were found to be less toxic in inducing apoptosis in cultured liver cells *in vitro* (Lloyd et al., 2002). Therefore, direct binding to PPAR $\gamma$  may be another cause of TGZ-induced hepatotoxicity.

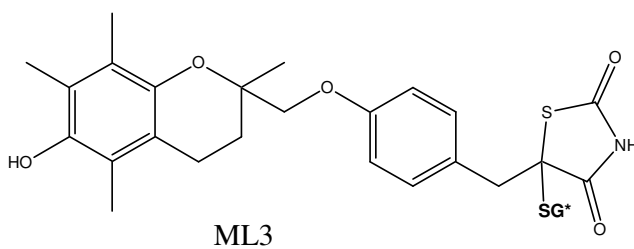
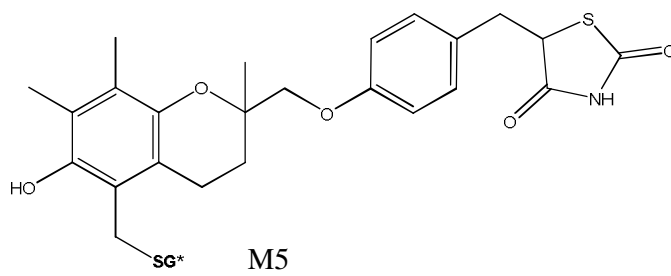
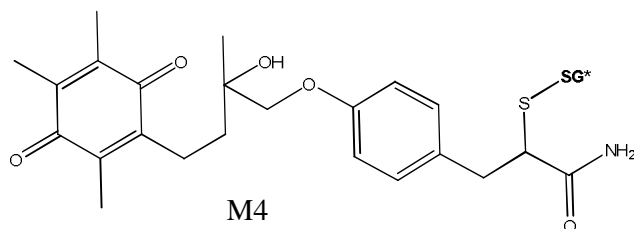
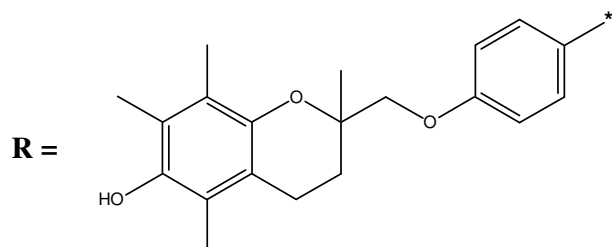
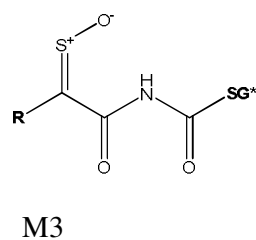
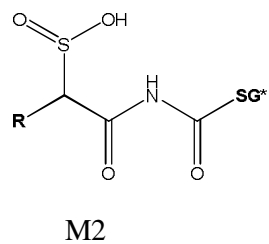
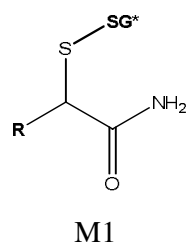
### *1.6.3 Mitochondrial dysfunction*

It had been shown that TGZ has direct effect on mitochondria producing depletion of adenosine-tri-phosphate and release of cytochrome c, which in turn induces cell death via apoptosis. TGZ had been shown to produce a rapid decline in mitochondrial membrane potential and adenosine-tri-phosphate depletion during its incubation with hepatocytes (Haskins et al., 2001). Therefore, mitochondrial dysfunction may be another possible outcome of TGZ-inducing hepatotoxicity.

### *1.6.4 Formation of TGZS*

The major metabolite of TGZ is TGZS (Loi et al., 1997; Loi et al., 1999). The phase II sulfation of TGZ occurs at the 6-hydroxyl group of its chroman ring (Fig. 2). While the formation of sulfate metabolites of TGZ and its biliary excretion form part of the drug elimination process, Kostrubsky et al. (2000) proposed that diabetic patients with cholestasis may have less capacity to excrete TGZS through the bile and the risk of hepatotoxicity may be increased.

Another probable mechanism of hepatotoxicity is the inhibition of bile salt export pump (BSEP) by TGZS causing accumulation of bile salts in the liver. As BSEP plays an



**SG\*** = deprotonated GSH

**Fig. 3** RM-GSH conjugates of TGZ (M1-M5 and ML3) (Kassahun et al., 2001; Prabhu et al., 2002).



important role in removing bile salts from liver cells using energy in the form of adenosine-tri-phosphate (Kullak et al., 2000), the accelerated accumulation of bile salts may lead to cholestasis and subsequent hepatocyte apoptosis. High concentration of bile salt levels have been shown to induce liver cell death and mitochondrial dysfunction due to their detergent properties (Delzenne et al., 1992; Gores et al., 1998). The cholestatic potential of TGZ and TGZS had been studied previously *in vitro* and *in vivo* in rats (Funk et al., 2001). With the increasing findings of toxic phase II metabolites, it is also important to investigate and elucidate whether TGZS has any direct toxic effect on normal human hepatocytes besides BSEP inhibition.

#### *1.6.5 Apoptotic induction of hepatocytes and cancer cells*

It has been shown that TGZ produces apoptotic induction of normal hepatocytes by activation of c-Jun N-terminal protein kinase and p53 mitogen protein kinase (Masubichi, 2006). It releases cytochrome-c and declines mitochondrial membrane potential during incubation with normal human hepatocytes. It causes death of cancerous cells via either PPAR<sub>γ</sub> activation or by changing the mitochondrial morphology (Masubichi, 2006).

#### *1.6.6 Host factors*

Multiple host factors might have predisposed the patients to hepatotoxicity induced by TGZ. These factors include the presence of diabetes with ongoing cholestasis, the concomitant use of other cholestatic drugs, impaired liver function leading to low rates of drug metabolism and clearance, low CYP3A4 activity or inhibition of CYP3A4 activity by

other drugs, dietary factors and obesity/ hypertriglyceridemia/ insulin resistance syndrome leading to non-alcoholic steatohepatitis (Kawai et al., 1997; Kostrubsky et al., 2000).

### *1.7 Quantitative structure activity relationship (QSAR) of TZD antidiabetic drugs*

TZD antidiabetic drugs have a few pharmacophoric elements which are essential for binding to PPAR $\gamma$ . Based on X-ray crystallographic study and molecular modeling, a U shaped pharmacophore had been identified for PPAR $\gamma$  agonists. The four heads of the TZD ring (S, NH and two C=O) are bound with PPAR $\gamma$  by hydrogen bonds (Khanna et al., 2005; Ramachandran et al., 2004).

QSAR study of TZD antidiabetic drugs exerted that both parts B and C are most essential for binding to the receptor (Fig. 4). On one hand, part A has various substitutions (TGZ – chroman, RGZ and PGZ – pyridine, and CGZ – cyclohexane ring) which appear to be not essential for binding to the receptor. On the other hand, the pyridine moiety of RGZ and PGZ enhance the binding affinity of these drugs to the receptor as compared to the chroman moiety of TGZ (Ramachandran et al., 2004). Comparative Molecular Field Analysis (CoMFA) data showed that when the sulfur moiety of TZD ring (part C) was substituted by oxygen moiety, there was no change in the IC<sub>50</sub> of the substituted compounds (Momose et al., 2002). Robert et al. (1991) had prepared some 2,4-oxazolidinedione derivatives as potent hypoglycemic agents with similar IC<sub>50</sub> values like TZD antidiabetic drugs.

This substitution established an important finding that there was no significant change in the biological activity when the sulfur moiety of the TZD ring was replaced by the bioisosteric oxygen moiety. In view with the above findings, we replaced the sulfur moiety with the bioisosteric methylene moiety to perform pharmacological activity and toxicity.

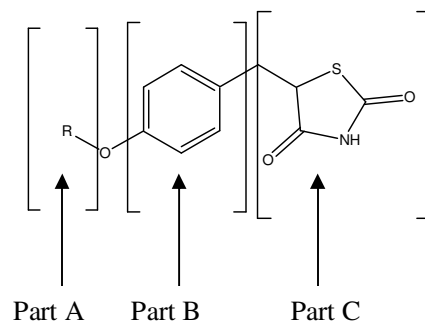


**Fig. 4** Pharmacophoric elements of TZD antidiabetic drugs

### *1.8 Research questions*

The above review raised two important research questions.

- While all the TZD antidiabetic drugs possess the common TZD ring, TGZ is hepatotoxic and yet RGZ and PGZ demonstrate better safety profiles. The TZD ring is an important pharmacophoric element but implicated in the formation of RMs (Fig 5). This raised the question of what is the role of the TZD ring in inducing hepatotoxicity.
- TGZS is the major metabolite of TGZ in human plasma after the intravenous administration of parent TGZ. While the majority phase II metabolites are non-toxic, TGZS was found to inhibit BSEP and might be implicated in cholestasis (Fig 5). This raised an important question of whether TGZS exerts any direct toxic effect on human liver cells.

### *1.9 Hypothesis*

We hypothesize that the sulfur moiety of the TZD ring of glitazones and the phase II metabolite of TGZ, TGZS, are the toxicophores that may account for drug-induced toxicity in human.

### *1.10 Objectives*

The overarching aim of my thesis is to investigate and elucidate the structural toxicity relationship (STR) of the TZD antidiabetic drugs with respect to human liver toxicity. The five key objectives of this project are summarized below.

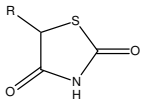
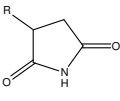
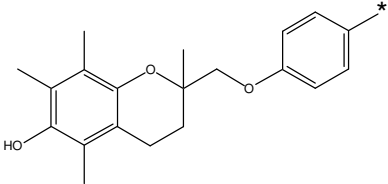
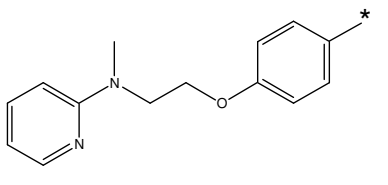
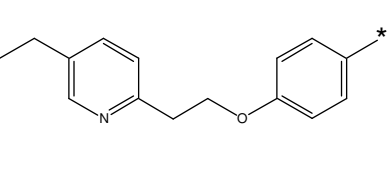
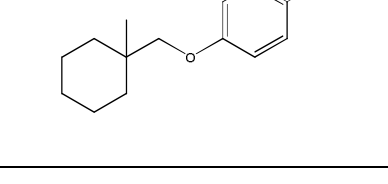
1. To synthesize and characterize the chemical analogues of the TZD antidiabetic drugs. These compounds were used for the STR study of TZD antidiabetic drugs.
2. To screen and identify the RMs of the TZD drugs and their chemical analogues using liquid chromatography tandem mass spectrometry (LC/MS/MS). These experiments were performed to explore and ascertain the metabolic potential of these compounds in generating electrophilic intermediates.
3. To characterize the cytotoxicities of the TZD drugs, their analogues using metabolically-active normal human hepatocytes (THLE-2 cells) (Andrea et al., 1993). Various cytotoxic assays were performed to elucidate the STR of the TZD drugs.
4. To characterize the PPAR<sub>γ</sub> binding affinities using the PPAR<sub>γ</sub> ligand-binding domain (LBD) and measure aP2 gene expression using human adipose cells (3T3-L1) of the TZD drugs and their analogues.
5. To synthesize and characterize TGZS and screen the cytotoxicities of TGZ and TGZS using THLE-2 cells.

### *1.10.1 Chemical synthesis of analogues of TZD antidiabetic drug*

The thia (-S-) group of TZD is implicated in the formation of RMs. In order to investigate the role of the TZD ring in inducing liver toxicity via the formation of RMs, chemical analogues of TGZ, RGZ, PGZ and CGZ where the TZD ring was replaced by the pyrrolidine-2,5-dione (PRD) ring, were synthesized and investigated (Fig. 5). In terms of physicochemical properties, the PRD (succinimide) ring shares similar five-membered ring structure, molecular size and lipophilicity (Table 1) with the TZD ring. On the other hand, the PRD ring lacks the -S- group and possesses the -CH<sub>2</sub>- group. The generated analogues namely, TSN, RSN, PSN and CSN (Table 1) were used subsequently for the STR studies and to ascertain if the isosteric replacement of the TZD with PRD ring affected the PPAR<sub>γ</sub>-related biological effects.

### *1.10.2 Screening and identification of RMs using LC/MS/MS*

Some xenobiotics can be metabolized by CYP450 enzymes to form RMs which bind covalently with GSH. In order to profile and identify RMs of the TZD antidiabetic drugs and the proposed synthetic PRD analogues, these compounds were incubated with HLM and GSH. In a separate experiment, the TZD and PRD analogues were incubated with THLE-2 cells. Any RM-GSH adducts formed during incubation that were separated by ultra performance liquid chromatography (UPLC) and identified using mass spectrometry (MS).

Structural Backbone (R)	 <b>TZD</b>	 <b>PRD</b>
	<b>Troglitazone (TGZ)</b>  <b>(5.08)</b>	<b>Trosuccinimide (TSN)</b>  <b>(4.34)</b>
	<b>Rosiglitazone (RGZ)</b>  <b>(3.21)</b>	<b>Rosisuccinimide (RSN)</b>  <b>(2.46)</b>
	<b>Pioglitazone (PGZ)</b>  <b>(3.58)</b>	<b>Piosuccinimide (PSN)</b>  <b>(2.84)</b>
	<b>Ciglitazone (CGZ)</b>  <b>(4.27)</b>	<b>Cisuccinimide (CSN)</b>  <b>(3.53)</b>

**Table 1** TZD antidiabetic drugs (TGZ, RGZ, PGZ and CGZ) and the respective proposed PRD analogues (TSN, RSN, PSN and CSN). \* Positions where TZD and PRD rings are covalently bonded to the structural back bones. Values in parentheses refer to the cLogP values calculated using ChemDraw Ultra version 6.0.

### 1.10.3 Toxicity screening

RMs can produce toxicity by redox cycling with molecular oxygen to produce superoxide anion radical and subsequent oxidative stress (Bolton et al., 2000; Thor et al., 1982; Schulz et al., 1996). The formation of oxygen radicals may lead to GSH and protein oxidation and the peroxidation of membrane lipids. In addition to the profiling of RMs using LC/MS/MS, the TZD antidiabetic drugs and the PRD analogues were screened for toxicity *in vitro* using THLE-2 cells. MTT [3-(4,5-Dimethylthiazol-2-yl)-2,5-diphenyltetrazolium], GSH and protein carbonyl (PC) assays were performed as part of toxicity screening (Fig. 5).

### 1.10.4 Screening of PPAR<sub>γ</sub> binding affinities and aP2 gene expression

All TZD antidiabetic drugs are specific ligands for PPAR<sub>γ</sub>. Determination of PPAR<sub>γ</sub> binding activity of the TZD drugs and the PRD analogues were performed using PPAR<sub>γ</sub>-LBD at 0 and 24 h. Various concentrations of the test compounds were incubated with PPAR<sub>γ</sub>-LBD for 24 h. Percentage of drug binding was measured using LC/MS/MS.

It was postulated that all the TZD antidiabetic drugs exhibited their activity by activating PPAR<sub>γ</sub> target genes, among which aP2 gene is a robust indicator (Kletzien et al., 1992; Ibrahimi et al., 1994). It was also demonstrated that aP2 genes were expressed in 3T3-L1 cells, a cell line that had similar morphological and biochemical pattern like human adipocytes (Kletzien et al., 1992). In my project, aP2 gene expression assays were performed of all the test compounds via polymerase chain reaction (PCR) and quantitative real-time polymerase chain reaction (qRT-PCR) using 3T3-L1 cells.

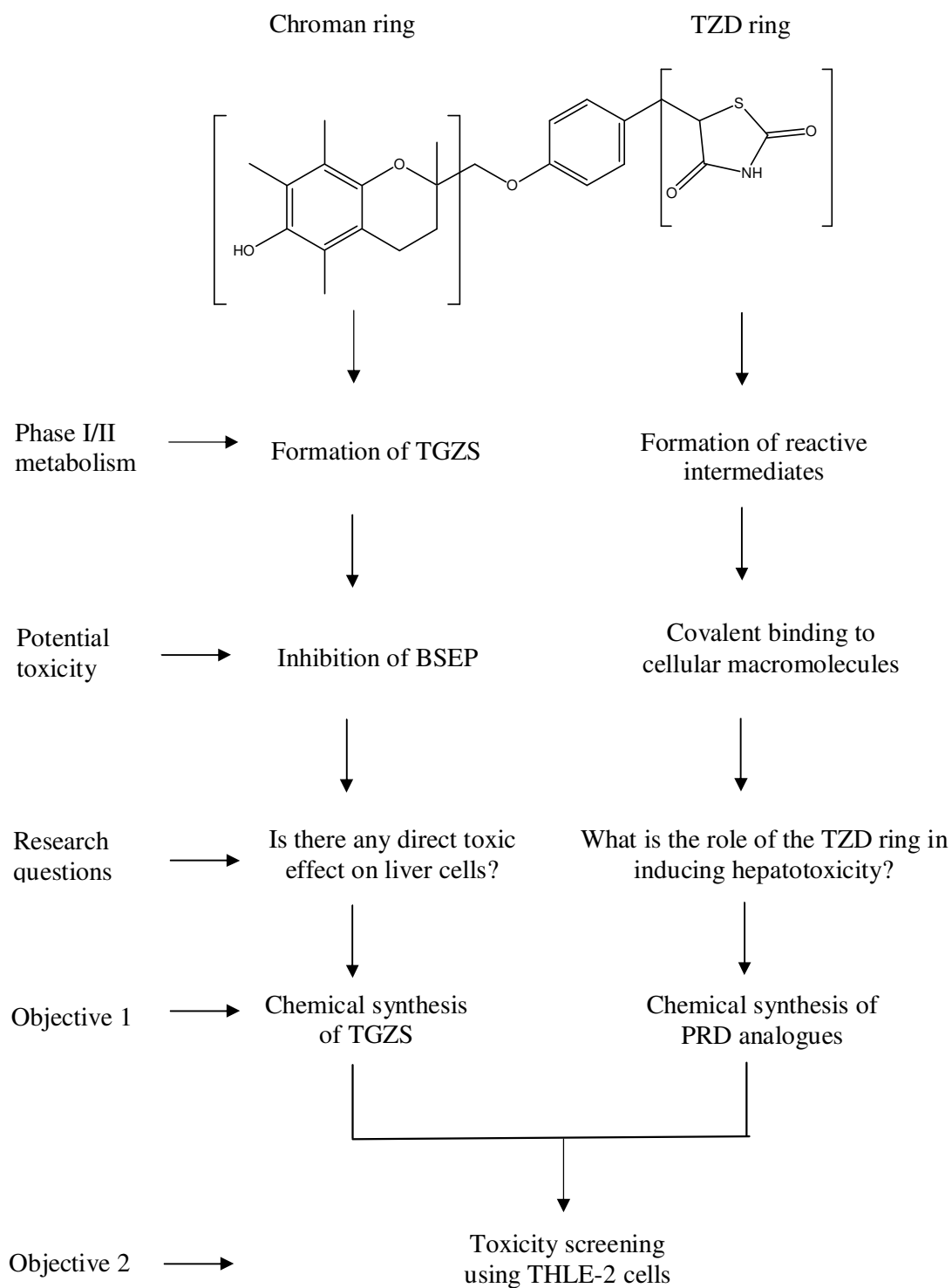


**Fig. 5** Summary of the proposed research work



### *1.10.5 Synthesis and cytotoxicity screening of TGZ and TGZS*

The 6-hydroxy group of TGZ is responsible for the formation of TGZS. TGZS inhibits BSEP that might lead to subsequent cholestasis and hepatocyte injury. In order to investigate the involvement of the chroman ring of TGZ in inducing direct hepatotoxicity, TGZS was further synthesized to complement the STR study.

Similar cytotoxicity experiments (MTT, GSH and PC assays) were separately performed using TGZ and TGZS (Fig. 5)

### *1.11 Significance*

The finding of this project establishes a correlation between toxicity effect and pharmacological response related to the TZD drugs. While structural changes leading to different pharmacological effect have been well studied in the context of antidiabetic drugs, much less is known about their impact on their toxicity. This study considers how chemical modification may contribute to both toxicological and pharmacological effects simultaneously. The knowledge generated can help support the future design of efficacious but less toxic antidiabetic agents. In our project, the structural modification involves changing the sulfur moiety with the bioisosteric methylene moiety. We believe that our data will provide useful information for the wider scientific community as they consider the use of such functional groups for other drug design.

On a broader perspective, this study underscores the value of incorporating both structure activity relationship (SAR) and STR studies in the early stage of drug discovery, so as to elucidate the key chemical features that correlate with maximal therapeutic benefit.

### *1.12 Overview of proceeding chapters*

Chapter two will be focussed on the synthesis of the PRD analogues. Chapters three and four will investigate and discuss the potential mechanism of toxicity related to the TZD and PRD analogues. PPAR $\gamma$  binding activity and aP2 gene expression study will be discussed in chapter five while the comparison of hepatotoxicity between TGZS and TGZ will be discussed in chapter six. The conclusion related to my project will be featured in the final chapter (seven).

## Chapter 2

### Synthesis of PRD analogues

#### 2.1 Introduction

Chapter two focuses mainly on the synthesis of the PRD analogues where the sulfur moiety of the TZD ring was replaced by the methylene moiety of the PRD ring. These two nuclei share similar five-member ring structure, molecular size and lipophilicity (discussed in chapter one).

The TZD antidiabetic drugs are generally prepared by the following procedures as described below. Etherification was performed using Williamson ether synthesis where ether linkages were formed between alcohol and p-fluorobenzaldehyde in presence of strong base. Later, TZD ring was reacted with corresponding aldehyde in presence of basic amines to form -ene- compounds (Knoevenagel synthesis). Finally, reduction step was conducted in presence of 10% palladium–charcoal (Pd/C) and hydrogen atmosphere to get desired TZD compounds (Lee et al., 2005; Fan et al., 2004; Huang et al., 2006).

The PRD analogues were prepared as outlined in Fig. 7 to 14 using the procedures described below. For all the chemical analyses of synthesized intermediates and final products, proton nuclear magnetic resonance ( $^1\text{H}$  NMR) and carbon nuclear magnetic resonance ( $^{13}\text{C}$  NMR) spectra were recorded on a Bruker 300 MHz NMR spectrometer (Rheinstetten, Germany) using deuterated dimethyl sulfoxide (DMSO- $d_6$ ) (2.5 and 40.0-41.1 ppm for  $^1\text{H}$  and  $^{13}\text{C}$ , respectively) and deuterated chloroform ( $\text{CDCl}_3$ ) (7.26 and 76.6-77.4 ppm for  $^1\text{H}$  and  $^{13}\text{C}$ , respectively) as solvent peaks. Direct-infusion mass spectroscopy (MS) data were acquired using a hybrid triple quadrupole linear ion trap MS (QTRAP MS)

equipped with an electrospray ionization (ESI) source (2000 QTRAP, Applied Biosystems, Foster City, CA, USA).

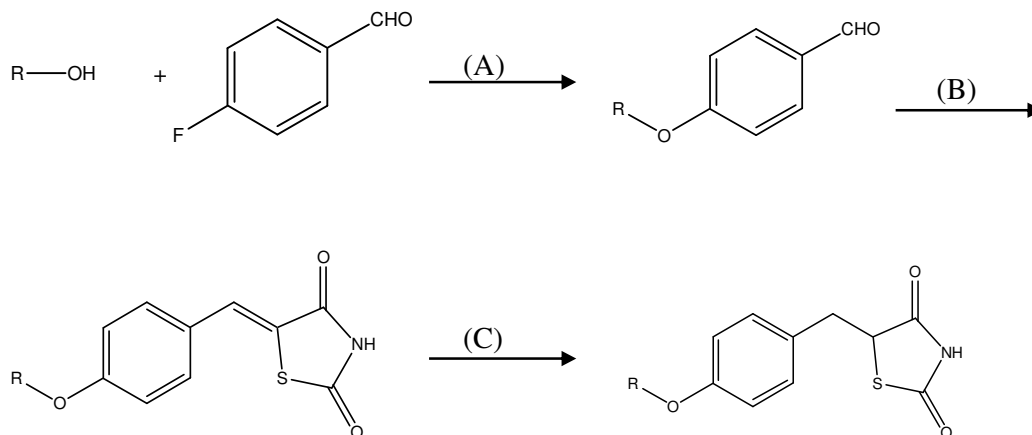


**Fig. 6** General procedure for the synthesis of TZD antidiabetic drugs. (A) sodium hydride, anhydrous DMF, 4-fluorobenzaldehyde, RT, 12 h; (B) TZD, piperidine, ethanol, reflux, 24 h; (C) 10% Pd/C, hydrogen gas, ethanol, 12 h.

## 2.2 Materials

HPLC-grade acetonitrile (ACN) was purchased from Tedia Company Inc. (Fairfield, OH, USA). Formic acid (99% purity) and glacial acetic acid were purchased from VWR International Ltd. (Leicestershire, UK). DMSO (ACS grade) was obtained from Panreac Quimica SA (Barcelona, Spain). Dichloromethane was purchased from Merck (Merck Pte. Ltd., Singapore). Water was purified using a Milli-Q water purification system (Millipore, Bedford, MA, USA). All the other chemicals related to the synthesis of the PRD analogues were purchased from Sigma-Aldrich (Saint Louis, MO, USA). All other reagents and chemicals used for the experiments were of analytical grades.

### 2.3 Preparation of TSN ( $C_{25}H_{29}NO_5$ )

The synthetic routes of TSN are illustrated in Fig. 7.

#### 2.3.1 Synthesis of 3-(triphenylphosphoranylidene)pyrrolidine-2,5-dione [I (A)]

A mixture of maleimide (1 g, 10.30 mmol), triphenylphosphine (2.70 g, 10.30 mmol) and acetone (30 mL) was heated under reflux for 1 h. After cooling, the resulting precipitate was filtered, washed with acetone (100 mL) and recrystallized using acetone. The crystal was filtered and dried under vacuum at 40°C overnight to give a white solid [I (A)] (Fig. 7) (2.8 g, yield 75%). Melting point 227°C.  $^1\text{H}$  NMR (DMSO- $d_6$ )  $\delta$ : 4.76 (s, 2H,  $-\text{CH}_2-$ ), 7.58-7.64 (m, 15H,  $-\text{C}_6\text{H}_5$ ), 8.67 (s, 1H,  $>\text{NH}$ ). MS (ESI+)  $m/z$  ( $\text{M}+\text{H}$ ) $^+$  360.3.

#### 2.3.2 Synthesis of methyl-6-hydroxy-2,5,7,8-tetramethylchroman-2-carboxylate [II (A)]

A mixture of paraformaldehyde (0.99 g, 32.8 mmol), methyl methacrylate (17.44 mL, 164 mmol), dibutylamine (0.7 mL, 3.92 mmol) and 25 mL acetic acid were stirred at room temperature ( $28 \pm 4^\circ\text{C}$ ) for 30 min and 2,3,5-trimethylbenzene-1,4-diol (5 g, 32.8 mmol) was added to it. Then the mixture was heated under reflux for another 24 h and cooled to RT. The reaction mixture was kept at 4°C overnight to promote crystal formation. The resulting crystal was filtered, recrystallized with methanol (20 mL) and dried under vacuum at 40°C to give a white solid [II (A)] (Fig. 7) (4.2 g, 48% yield). Melting point 160-162°C.  $^1\text{H}$  NMR: (DMSO- $d_6$ )  $\delta$ : 1.50 (s, 3H,  $-\text{CH}_3$ ), 1.73-1.80 (m, 1H,  $-\text{CH}_2-$ ), 1.97 (s, 3H,  $-\text{CH}_3$ ), 2.03 (s, 3H,  $-\text{CH}_3$ ), 2.05 (s, 3H,  $-\text{CH}_3$ ), 2.27-2.38 (m, 2H,  $-\text{CH}_2-$ ), 2.55-2.58 (m, 1H,  $-\text{CH}_2-$ ), 3.20 (s, 3H,  $-\text{OCH}_3$ ), 7.48 (s, 1H,  $-\text{OH}$ ).  $^{13}\text{C}$  NMR: (DMSO- $d_6$ )  $\delta$ : 11.65, 11.70, 12.62, 20.32,

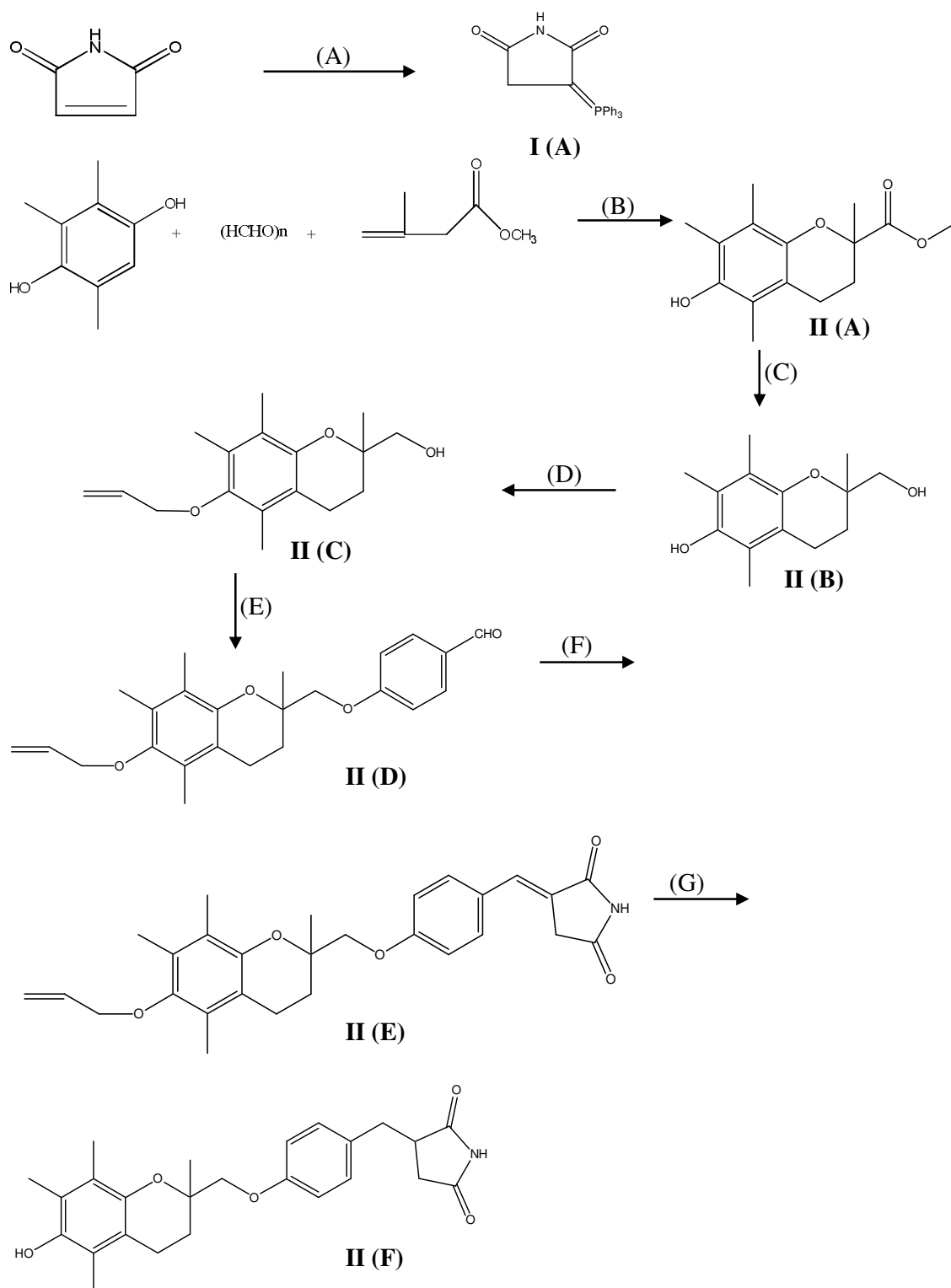


**Fig. 7** Synthesis of TSN. (A) Triphenylphosphine, methanol, reflux, 1.5 h; (B) dibutylamine, acetic acid, 24 h, reflux; (C) lithium aluminium hydride, anhydrous THF, 0°C, 4-5 h; (D)

allyl bromide, acetone AR, potassium carbonate, reflux, 48 h; (E) sodium hydride, anhydrous DMF, 4-fluorobenzaldehyde, RT, 12 h; (F) 3-(triphenylphosphoranylidene)pyrrolidine-2,5-dione, methanol, reflux, 3 h; (G) lithium chloride (anhydrous), sodium borohydride, anhydrous THF, RT and 10% Pd/C, hydrogen gas, ethanol, 12 h.

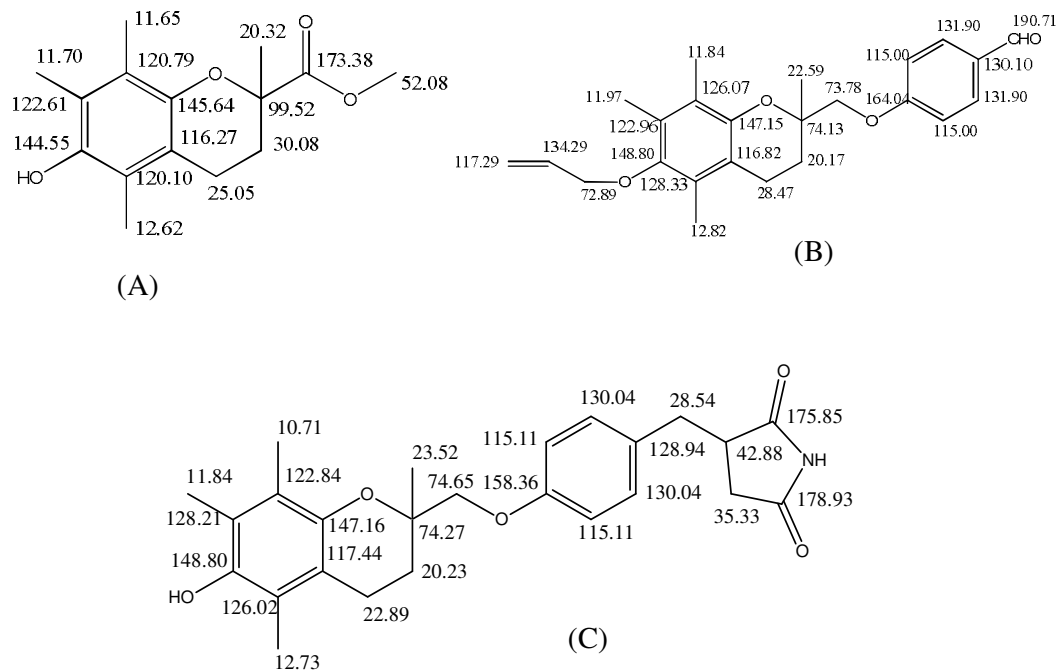


**Fig. 8**  $^{13}\text{C}$  NMR interpretation of (A) methyl-6-hydroxy-2,5,7,8-tetramethylchroman-2-carboxylate, (B) 4-(((6-(allyloxy)-2,5,7,8-tetramethylchroman-2-yl)methoxy)benzaldehyde and (C) TSN.

25.05, 30.08, 52.08, 99.52, 116.27, 120.10, 120.79, 122.61, 144.55, 145.55 and 173.38 (Fig. 8A). MS (ESI+)  $m/z$  (M+H) $^+$  265.3.

### 2.3.3 Synthesis of 2-(hydroxymethyl)-2,5,7,8-tetramethylchroman-6-ol [II (B)]

A solution of methyl-6-hydroxy-2,5,7,8-tetramethylchroman-2-carboxylate (4 g, 16.9 mmol) in anhydrous tetrahydrofuran (THF, 20 mL) was added dropwise to a stirred solution

of lithium aluminium hydride (0.644 g, 16.9 mmol) in anhydrous THF (10 mL) under nitrogen atmosphere at 0°C over 30 min. It was stirred for another 6 h under nitrogen atmosphere at RT. The reaction mixture was quenched using 0.25 N sodium hydroxide (5 mL). Subsequently, the mixture was stirred for 1 h at RT, filtered and concentrated by evaporation under reduced pressure. The concentrate thus obtained was purified by column chromatography on silica gel (60–120 mesh) using a mixture of n-hexane/ethyl acetate (EtOAc) (2:1 v/v) as eluent to give a white solid [II (B)] (Fig. 7) (2.4 g, 67% yield). Melting point 183°C. <sup>1</sup>H NMR: (DMSO-d<sub>6</sub>) δ: 1.12 (s, 3H, -CH<sub>3</sub>), 1.59-1.68 (m, 1H, -CH<sub>2</sub>-), 1.76-1.85 (m, 1H, -CH<sub>2</sub>-), 1.96 (s, 3H, -CH<sub>3</sub>), 2.00 (s, 3H, -CH<sub>3</sub>), 2.03 (s, 3H, -CH<sub>3</sub>), 3.27-3.29 (m, 2H, -CH<sub>2</sub>-), 3.9-4.3 (m, 1H, -CH<sub>2</sub>-), 4.82 (t, 1H, J=6 Hz, -CH<sub>2</sub>-), 7.41 (s, 1H, -OH). MS (ESI+) *m/z* (M+H)<sup>+</sup> 237.1.

#### 2.3.4 Synthesis of (6-(allyloxy)-2,5,7,8-tetramethylchroman-2-yl)methanol [II (C)]

A mixture of 2-(hydroxymethyl)-2,5,7,8-tetramethylchroman-6-ol (2.3 g, 9.74 mmol), allyl bromide (1.8 mL, 19.4 mmol) and anhydrous potassium carbonate (2.68 g, 19.4 mmol) in 20 mL acetone was refluxed for 48 h. The reaction mixture was cooled to RT, filtered and concentrated by evaporation under reduced pressure. The resulting concentrate was further purified by column chromatography on silica gel (60–120 mesh) using a mixture of n-hexane/EtOAc (5:1 v/v) as eluent to give a white solid [II (C)] (Fig. 7) (1.9 g, 70% yield). Melting point 78–79°C. <sup>1</sup>H NMR: (CDCl<sub>3</sub>) δ: 1.23 (s, 3H, -CH<sub>3</sub>), 1.68-1.74 (m, 1H, -CH<sub>2</sub>-), 1.98-2.04 (m, 1H, -CH<sub>2</sub>-), 2.09 (s, 3H, -CH<sub>3</sub>), 2.14 (s, 3H, -CH<sub>3</sub>), 2.18 (s, 3H, -CH<sub>3</sub>), 2.64 (t, 2H, J=9 Hz, -CH<sub>2</sub>-), 3.61 (d, 2H, J=6 Hz, -CH<sub>2</sub>-), 4.18 (d, 2H, J=6 Hz, -OCH<sub>2</sub>-), 5.24 (d, 1H, J=9 Hz, =CH<sub>2</sub>), 5.46 (d, 1H, J=9 Hz, =CH<sub>2</sub>), 6.06-6.10 (m 1H, =CH-). MS (ESI+) *m/z* (M+H)<sup>+</sup> 277.2.



### 2.3.5 Synthesis of 4-((6-(allyloxy)-2,5,7,8-tetramethylchroman-2-yl)methoxy)benzaldehyde [II (D)]

Sodium hydride (60% in mineral oil, 0.315 g, 13.04 mmol) and 6-(allyloxy)-2,5,7,8-tetramethylchroman-2-yl)methanol (1.8 g, 6.52 mmol) in anhydrous dimethylformamide (DMF) (20 mL) was stirred for 30 min under nitrogen atmosphere at RT. Subsequently, 4-fluorobenzaldehyde (1.4 mL, 13.04 mmol) was added slowly dropwise to the reaction mixture under nitrogen atmosphere at RT. After stirring at the same temperature for overnight, the reaction mixture was quenched with aqueous ammonium chloride (20 mL). 30 mL of ice-water (30 mL) was added and the resultant mixture was extracted with EtOAc (50 mL, two times). The organic layer was washed with water and brine, dried over anhydrous sodium sulfate and concentrated by evaporation under reduced pressure. The concentrate thus obtained was purified by column chromatography on silica gel (60–120 mesh) using a mixture of n-hexane/EtOAc (4:1 v/v) as eluent to give a yellow liquid [II (D)] (Fig. 7) (0.41 g, 16.1% yield). <sup>1</sup>H NMR: (CDCl<sub>3</sub>) δ: 1.24-1.29 (m, 1H, -CH<sub>2</sub>-), 1.44 (s, 3H, -CH<sub>3</sub>), 1.94-2.01 (m, 1H, -CH<sub>2</sub>-), 2.08 (s, 3H, -CH<sub>3</sub>), 2.15 (s, 3H, -CH<sub>3</sub>), 2.19 (s, 3H, -CH<sub>3</sub>), 2.62 (t, 2H, J=6 Hz, -CH<sub>2</sub>-), 3.99-4.12 (m, 2H, -CH<sub>2</sub>-), 4.19 (d, 2H, J=6 Hz, -OCH<sub>2</sub>-), 5.24 (d, 1H, J=12 Hz, =CH<sub>2</sub>), 5.46 (d, 1H, J=18 Hz, =CH<sub>2</sub>), 6.06-6.11 (m, 1H, =CH-), 7.03 (d, 2H, J=6 Hz, -C<sub>6</sub>H<sub>4</sub>-), 7.81 (d, 2H, J=6 Hz, -C<sub>6</sub>H<sub>4</sub>-), 9.88 (s, 1H, -CHO). <sup>13</sup>C NMR: (DMSO-d<sub>6</sub>) δ: 11.84, 11.97, 12.82, 14.19, 20.17, 22.59, 28.47, 72.89, 73.78, 74.13, 115.00, 116.82, 117.29, 122.96, 126.07, 128.33, 130.10, 131.90, 134.29, 147.14, 148.80, 164.04 and 190.71 (Fig. 8B). MS (ESI+) *m/z* (M+H)<sup>+</sup> 381.4.

### 2.3.6 Synthesis of (E)-3-(4-((6-(allyloxy)-2,5,7,8-tetramethylchroman-2-yl)methoxy)benzylidene)pyrrolidine-2,5-dione [II (E)]

A mixture of 3-(triphenylphosphoranylidene)pyrrolidine-2,5-dione (370 mg, 1.04 mmol), 4-(((6-(allyloxy)-2,5,7,8-tetramethylchroman-2-yl)methoxy)benzaldehyde (400 mg, 1.04 mmol) in methanol (20 mL) was heated under reflux for 1.5 h and then cooled at RT. The reaction mixture was concentrated by evaporation under reduced pressure. The concentrate thus obtained was further purified by column chromatography on silica gel (60–120 mesh) using a mixture of n-hexane/EtOAc (3:1 v/v) as eluent to give a white solid [II (E)] (Fig. 7) (0.21 g, 41.4% yield). Melting point 122–123°C. <sup>1</sup>H NMR: (CDCl<sub>3</sub>) δ: 1.43 (s, 3H, -CH<sub>3</sub>), 1.94-2.01 (m, 1H, -CH<sub>2</sub>-), 2.07 (s, 3H, -CH<sub>3</sub>), 2.14 (s, 3H, -CH<sub>3</sub>), 2.18 (s, 3H, -CH<sub>3</sub>), 2.61 (t, 2H, J=6 Hz, -CH<sub>2</sub>-), 3.56 (s, 2H, -CH<sub>2</sub>-), 3.94-4.06 (m, 2H, -CH<sub>2</sub>-), 4.18 (d, 2H, J=6 Hz, -OCH<sub>2</sub>-), 5.24 (d, 1H, J=9 Hz, =CH<sub>2</sub>), 5.46 (d, 1H, J=18 Hz, =CH<sub>2</sub>), 6.05-6.11 (m, 1H, -CH=), 6.98 (d, 2H, J=9 Hz, -C<sub>6</sub>H<sub>4</sub>-), 7.43 (d, 2H, J=6 Hz, -C<sub>6</sub>H<sub>4</sub>-), 7.55 (s, 1H, -CH=), 9.04-9.13 (br s, 1H, >NH). MS (ESI+) *m/z* (M+H)<sup>+</sup> 462.3.

### 2.3.7 Synthesis of (R,S)-3-(4-(((6-(allyloxy)-2,5,7,8-tetramethylchroman-2-yl)methoxy)benzyl)pyrrolidine-2,5-dione (TSN) [II (F)]

Lithium chloride (20 mg, 0.433 mmol) in anhydrous THF (10 mL) was taken into a two-necked round bottom flask at 0°C under nitrogen atmosphere. Sodium borohydride (25 mg, 0.433 mmol) was added to the mixture very quickly. The reaction mixture was stirred for 5 min and (E)-3-(4-(((6-(allyloxy)-2,5,7,8-tetramethylchroman-2-yl)methoxy)benzylidene)pyrrolidine-2,5-dione (150 mg, 0.433 mmol) in anhydrous THF (5 mL) was added to it dropwise with constant stirring. After complete addition, the reaction mixture was brought to RT and stirred for another 30 min. The reaction mixture was quenched with 2 mL water and evaporated to dryness under reduced pressure. 5 mL of water was added to reaction mixture and liquid-liquid extraction (LLE) was performed with ether (20 mL, 2 times). The ether

layer was dried over anhydrous sodium sulfate and concentrated under reduced pressure to form a yellow liquid. Next, the reduction step was performed without further purification. The above-mentioned liquid was dissolved in 20 mL ethanol taken in a parr bottle and 50 mg of (Pd/C) (10%) was added to it. The compound was hydrogenated under hydrogen atmosphere (pressure 40 psi) at RT for 8 h. The mixture was filtered using celite and concentrated by evaporation under reduced pressure to give a white solid. The compound was further purified by column chromatography on silica gel (60–120 mesh) using a mixture of n-hexane/EtOAc (10:1 v/v) as eluent to give a white solid [II (F)] (Fig. 7) (0.5 g, 10.2% yield, 98.7% purity). Melting point 205–207°C. <sup>1</sup>H NMR: (CDCl<sub>3</sub>) δ: 1.42 (s, 3H, -CH<sub>3</sub>), 2.08 (s, 3H, -CH<sub>3</sub>), 2.13 (s, 3H, -CH<sub>3</sub>), 2.18 (s, 3H, -CH<sub>3</sub>), 2.43-2.51 (m, 1H, -CH<sub>2</sub>-), 2.60-2.64 (m, 2H, -CH<sub>2</sub>-), 2.68-2.74 (m, 1H, -CH<sub>2</sub>-), 2.84-2.89 (m, 1H, -CH<), 3.14 (d, 2H, J=12 Hz, -CH<sub>2</sub>-), 3.61 (t, 2H, J=6 Hz, -CH<sub>2</sub>-), 3.85 (d, 1H, J=9 Hz, -CH<sub>2</sub>-), 3.95 (d, 1H, J=9 Hz, -CH<sub>2</sub>-), 6.85 (d, 2H, J=9 Hz, -C<sub>6</sub>H<sub>4</sub>-), 7.07 (d, 2H, J=6 Hz, -C<sub>6</sub>H<sub>4</sub>-), 8.80 (s, 1H, >NH), <sup>13</sup>C NMR: (DMSO-d<sub>6</sub>) δ: 10.71, 11.84, 12.73, 20.23, 22.89, 23.52, 28.54, 35.33, 42.88, 74.27, 74.65, 115.11, 117.44, 122.84, 126.02, 128.27, 128.94, 130.04, 147.16, 148.80, 158.36, 175.85 and 178.93 (Fig. 8C). MS (ESI-) *m/z* (M-H)<sup>-</sup> 422.0.

#### 2.4 Preparation of PSN (C<sub>20</sub>H<sub>22</sub>N<sub>2</sub>O<sub>3</sub>)

The synthetic routes of PSN are illustrated in Fig.9.

##### 2.4.1 Synthesis of 4-[2-(5-ethylpyridine-2-yl)ethoxy]benzaldehyde [III (A)]

To a suspension of sodium hydride (60% mineral oil, 222 mg, 9.26 mmol) in anhydrous DMF (20 mL), 2-(5-ethylpyridine-2-yl)ethanol (700 mg, 4.63 mmol) was added and the

mixture was stirred for 30 min. Subsequently, 4-fluorobenzaldehyde (1 mL, 9.26 mmol) was added slowly to the reaction mixture under nitrogen atmosphere at RT. After stirring at the same temperature for 3 h, the reaction mixture was quenched with aqueous ammonium chloride (20 mL), poured into ice-water (30 mL), and extracted with EtOAc (80 mL). The extract was washed with water and brine (50 mL, 2 times), dried over anhydrous sodium sulfate and concentrated by evaporation under reduced pressure. The concentrate thus obtained was purified by column chromatography on silica gel (60–120 mesh) using a mixture of n-hexane/EtOAc (4:1 v/v) as eluent to give a yellow liquid [III (A)] (Fig. 9) (0.398 g, 57% yield). <sup>1</sup>H NMR (DMSO-d<sub>6</sub>) δ: 1.17 (t, 3H, J=9, 15 Hz, -CH<sub>3</sub>), 2.57 (q, 2H, J=9 Hz, -CH<sub>2</sub>-), 3.18 (t, 2H, J= 6 Hz, -CH<sub>2</sub>-), 4.46 (t, 2H, J =6 Hz, -OCH<sub>2</sub>-), 7.10 (d, 2H, J=9 Hz, -C<sub>6</sub>H<sub>4</sub>-), 7.30 (d, 1H, J=9 Hz, -C<sub>5</sub>H<sub>3</sub>N-), 7.57 (d, 1H, J=9 Hz, -C<sub>5</sub>H<sub>3</sub>N-), 7.83 (d, 2H, J=6 Hz, -C<sub>6</sub>H<sub>4</sub>-), 8.37 (s, 1H, -C<sub>5</sub>H<sub>3</sub>N-), 9.85 (s, 1H, -CHO). MS (ESI) *m/z* (M+H)<sup>+</sup> 256.3.

#### 2.4.2 Synthesis of (3E)-3-{4-[2-(5-ethylpyridin-2-yl)ethoxy]benzylidene}pyrrolidine-2,5-dione [III (B)]

A mixture of 3-(triphenylphosphoranylidene)pyrrolidine-2,5-dione (250 mg, 0.69 mmol), 4-[2-(5-ethylpyridin-2-yl)ethoxy]benzaldehyde (175 mg, 0.69 mmol) and methanol (20 mL) was heated under reflux for 1.5 h and then cooled at RT. The resulting crystal was filtered, washed with methanol (20 mL) and dried under vacuum at 40°C to give a white solid [III (B)] (Fig. 9) (0.33g, 98% yield). Melting point 224°C. <sup>1</sup>H NMR (DMSO-d<sub>6</sub>) δ: 1.23 (t, 3H, J=9, 15 Hz, -CH<sub>3</sub>), 2.76 (q, 2H, J=9 Hz, -CH<sub>2</sub>-), 3.48 (t, 2H, J=9 Hz, -CH<sub>2</sub>-), 3.59 (s, 2H, -CH<sub>2</sub>-), 4.48 (t, 2H, J=9 Hz, -OCH<sub>2</sub>-), 7.01 (d, 2H, J=6 Hz, -C<sub>6</sub>H<sub>4</sub>-), 7.32 (s, 1H, -CH=), 7.55 (d, 2H, J=6 Hz, -C<sub>6</sub>H<sub>4</sub>-), 7.95 (d, 1H, J=9 Hz, -C<sub>5</sub>H<sub>3</sub>N-), δ: 8.37 (d, 1H, J=6 Hz, -C<sub>5</sub>H<sub>3</sub>N-), δ: 8.71 (s, 1H, -C<sub>5</sub>H<sub>3</sub>N-), δ: 11.36 (s, 1H, >NH). <sup>13</sup>C NMR (DMSO-d<sub>6</sub>) δ: 14.56, 24.53, 32.52,

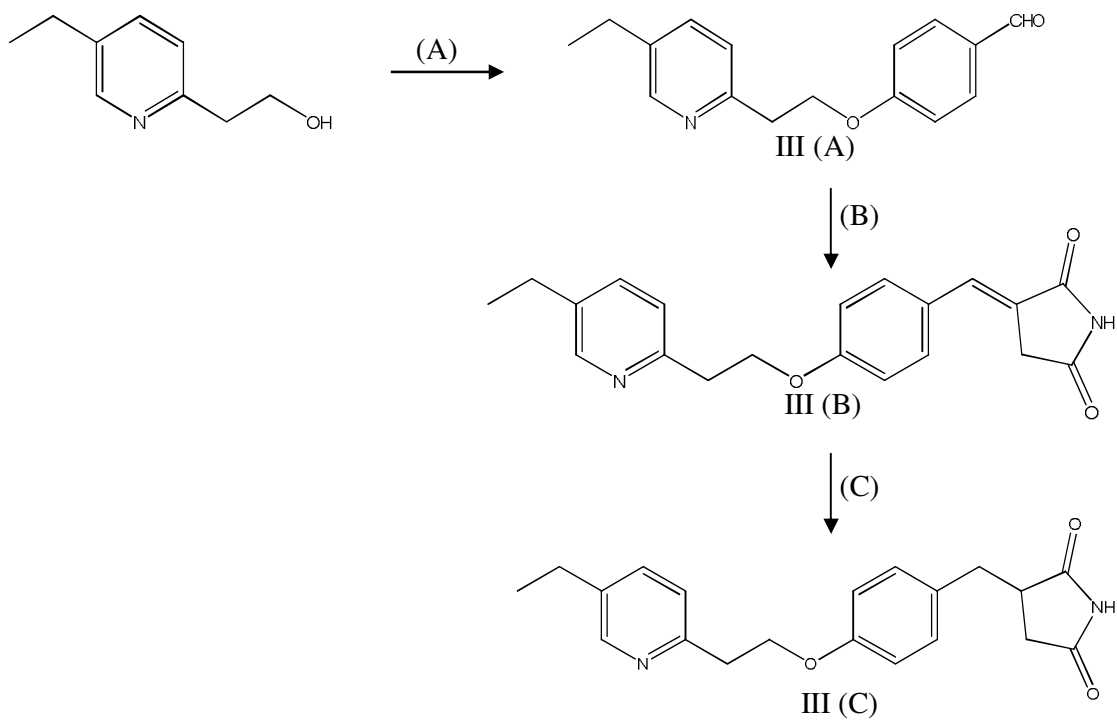


**Fig. 9** Synthesis of PSN. (A) 4-Fluorobenzaldehyde, sodium hydride, DMF, RT, 12 h; (B) 3-(triphenylphosphoranylidene)pyrrolidine-2,5-dione, methanol, reflux, 2 h; (C) 10% Pd/C, hydrogen gas, ethanol, 12 h.

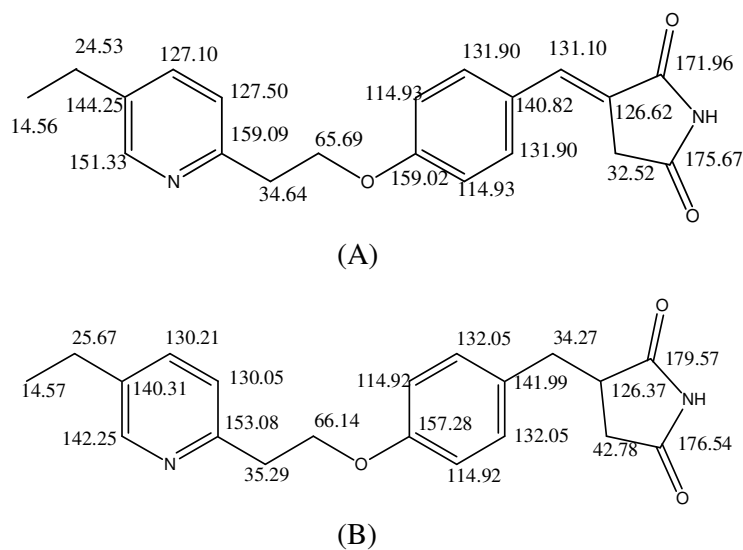


**Fig. 10**  $^{13}\text{C}$  NMR interpretation of (A) (3E)-3-[4-[2-(5-ethylpyridin-2-yl)ethoxy]benzylidene} pyrrolidine-2,5-dione and (B) PSN.

34.64, 65.69, 114.93, 126.62, 127.10, 127.50, 131.13, 131.90, 140.82, 144.25, 151.33 159.02, 150.09, 171.96, 175.67 (Fig. 10A). MS (ESI)  $m/z$  (M+H)<sup>+</sup> 337.2.

#### 2.4.3 Synthesis of (R,S)-3-{4-[2-(5-ethylpyridin-2-yl)ethoxy]benzyl}pyrrolidine-2,5-dione (PSN) [III (C)]

A solution of (3E)-3-{4-[2-(5-ethylpyridin-2-yl)ethoxy]benzylidene}pyrrolidine-2,5-dione (100 mg, 0.296 mmol) in ethanol (20 mL) was taken in a parr bottle and 50 mg of Pd/C (10%) was added to it. The compound was hydrogenated under hydrogen atmosphere (pressure 5 psi) at RT for 8 h. The mixture was filtered using celite and concentrated by evaporation under reduced pressure to give a red colour solid [III (C)] (Fig. 9). (0.98 g, 98% yield, 98.3% purity). <sup>1</sup>H NMR (CDCl<sub>3</sub>) δ: 1.32 (t, 3H, J=6 Hz, -CH<sub>3</sub>), 2.47 (d, 2H, J=6 Hz, -CH<sub>2</sub>-), 2.75 (m, 1H, -CH<), 2.88 (q, 2H, J=15 Hz, -CH<sub>2</sub>-), 3.13 (t, 2H, J=9 Hz, -CH<sub>2</sub>-), 3.57 (d, 2H, J=6 Hz, -CH<sub>2</sub>-), 4.41 (t, 2H, J=9 Hz, -OCH<sub>2</sub>-), 6.83 (d, 2H, J=9 Hz, -C<sub>6</sub>H<sub>4</sub>-), 7.05 (d, 2H, J=9 Hz, -C<sub>6</sub>H<sub>4</sub>-), 7.63 (d, 1H, J=9 Hz, -C<sub>5</sub>H<sub>3</sub>N-), 7.88 (s, 1H, -C<sub>5</sub>H<sub>3</sub>N-), δ: 7.95 (d, 1H, J=9 Hz, -C<sub>5</sub>H<sub>3</sub>N-), δ: 8.49 (s, 1H, >NH). <sup>13</sup>C NMR (CDCl<sub>3</sub>) 14.57, 25.67, 34.27, 35.29, 42.78, 66.14, 114.92, 126.37, 130.05, 130.21, 132.05, 140.31, 141.99, 142.54, 153.08, 157.28, 176.54, 176.57 (Fig. 10B). MS (ESI)  $m/z$  (M+H)<sup>+</sup> 339.2.

#### 2.5 Preparation of RSN (C<sub>19</sub>H<sub>21</sub>N<sub>3</sub>O<sub>3</sub>)

The synthetic routes of RSN are summarized in Fig. 11.

### 2.5.1 Synthesis of *tert*-butyl (2-hydroxyethyl)methylcarbamate [IV (A)]

A solution of di-*tert*-butyl dicarbonate (3.7 mL, 16 mmol) in chloroform (10 mL) was added dropwise to a solution of 2-(methylamino)ethanol (1.3 mL, 16 mmol) in chloroform (10 mL) at 0°C. The mixture was stirred for another 24 h at RT and concentrated to dryness. The residue was a colourless oil [IV (A)] (Fig. 11) which was not purified in this step (2.5 g, 89.3% yield). <sup>1</sup>H NMR (CDCl<sub>3</sub>) δ: 1.37 (9H, s, Me<sub>3</sub>C-), 2.79 (s, 3H, >N-CH<sub>3</sub>), 3.19 (t, 2H, J=6 Hz, -CH<sub>2</sub>-), 3.36 (br s, 1H, -OH), 3.45 (t, 2H, J=6 Hz, -OCH<sub>2</sub>-). MS (ESI) *m/z* (M+H)<sup>+</sup> 176.0.

### 2.5.2 Synthesis of *tert*-butyl [2-(4-formylphenoxy)ethyl]methylcarbamate [IV (B)]

*Tert*-butyl (2-hydroxyethyl)methylcarbamate (1 g, 6.21 mmol), 4-hydroxybenzaldehyde (760 mg, 6.21 mmol) and triphenylphosphine (895 mg, 6.82 mmol) were added together in dry THF (25 mL) and the mixture was stirred for 30 min at 0°C. Diisopropyl azodicarboxylate (0.7 mL, 6.82 mmol) was added dropwise to the mixture over 15 min at 0°C. It was stirred for 18 h at RT. THF was removed under reduced pressure and EtOAc (100 mL) was added to it. The EtOAc layer was washed with 1N sodium hydroxide (20 mL), water (25 mL) and brine (20 mL). The organic layer was dried using anhydrous sodium sulfate and concentrated. The product was purified by silica gel column chromatography (60–120 mesh) using *n*-hexane/EtOAc (4:1) to give the compound as a yellow liquid [IV (B)] (Fig.11) (0.5 g, 31.34% yield). <sup>1</sup>H NMR (CDCl<sub>3</sub>) δ: 1.43 (s, 9H, Me<sub>3</sub>C-), 2.96 (s, 3H, >N-CH<sub>3</sub>), 3.60 (t, 2H, J=9 Hz, -CH<sub>2</sub>-), 4.08 (t, 2H, J=9 Hz, -OCH<sub>2</sub>-), 6.96 (d, 2H, J=9 Hz, -C<sub>6</sub>H<sub>4</sub>-), 7.82 (d, 2H, J=9 Hz, -C<sub>6</sub>H<sub>4</sub>-), 9.85 (s, 1H, -CHO).

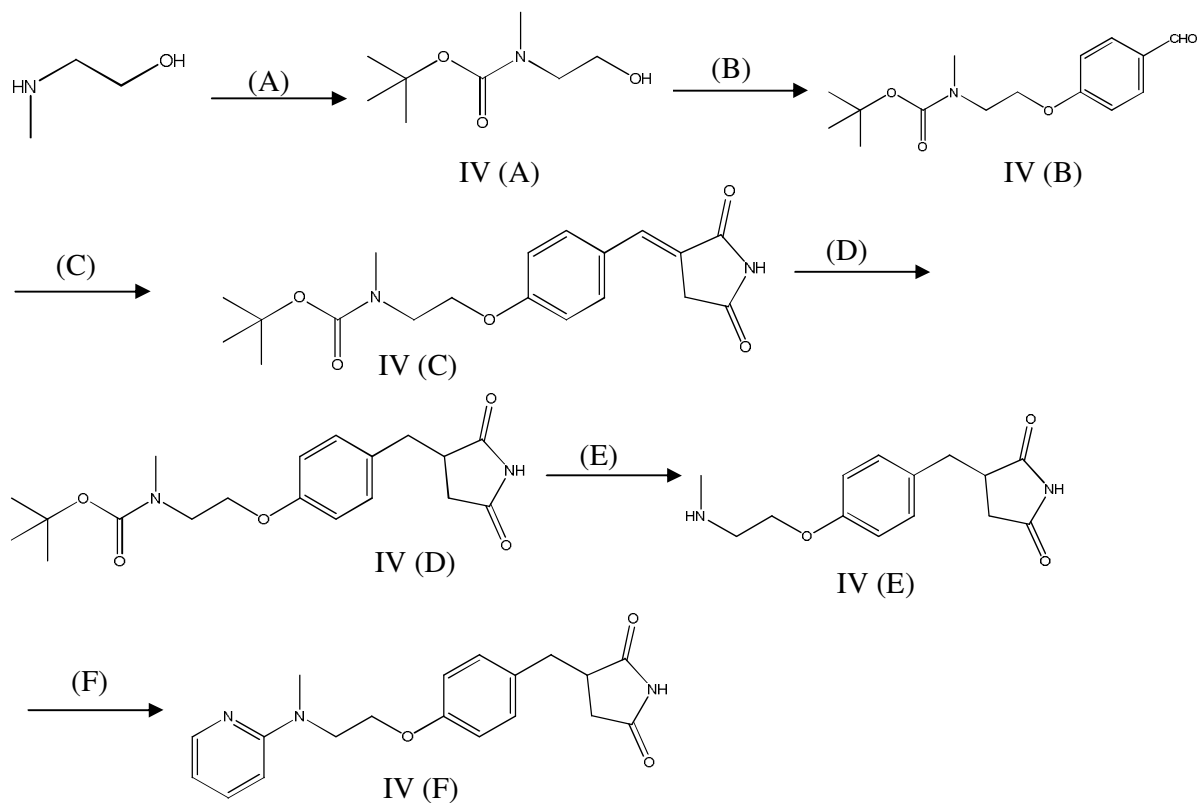


**Fig. 11** Synthesis of RSN. (A) Di-*tert*-butyl dicarbonate, chloroform, RT, 24 h; (B) 4-hydroxybenzaldehyde, triphenylphosphine, diisopropyl azodicarboxylate, dry THF, 0°C, RT, 18 h; (C) 3-(triphenylphosphoranylidene)pyrrolidine-2,5-dione, methanol, reflux, 2 h; (D) 10% Pd/C, hydrogen gas, ethanol, 12 h; (E) 0.5N HCl in dioxane, chloroform, RT, 2 h; (F) 2-chloropyridine, absolute ethanol, reflux, 24 h.

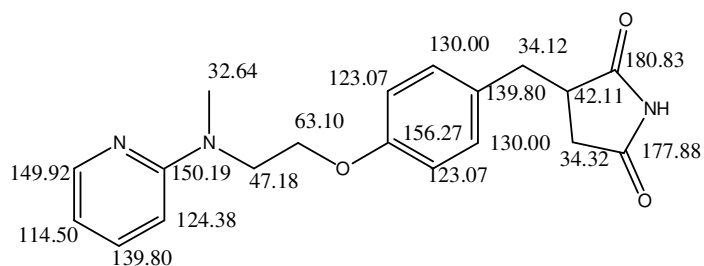


**Fig. 12** <sup>13</sup>C NMR interpretation RSN.



2.5.3 Synthesis of *tert*-butyl (2-{4-[(*E*)-(2,5-dioxopyrrolidin-3-ylidene)methyl]phenoxy}ethyl)methylcarbamate [IV (C)]

A mixture of 3-(triphenylphosphoranylidene)pyrrolidine-2,5-dione (255 mg, 0.717 mmol), *tert*-butyl [2-(4-formylphenoxy)ethyl]methylcarbamate (200 mg, 0.717 mmol) and methanol (20 mL) was heated under reflux for 1.5 h and then cooled at RT. The reaction mixture was kept at 4°C overnight to promote crystallization. The resulting crystal was filtered, washed with methanol (20 mL) and dried under vacuum at 40°C to give a white solid [IV (C)] (Fig. 11) (0.23 g, 92% yield). Melting point 242°C. <sup>1</sup>H NMR (DMSO-*d*<sub>6</sub>) δ: 1.39 (s, 9H, Me<sub>3</sub>C-), 2.96 (s, 3H, >N-CH<sub>3</sub>), 3.54 (t, 2H, J=9 Hz, -CH<sub>2</sub>-), 3.60 (s, 2H, -CH<sub>2</sub>-), 4.14 (t, 2H, J=9 Hz, -OCH<sub>2</sub>-), 7.04 (d, 2H, J=6 Hz, -C<sub>6</sub>H<sub>4</sub>-), 7.33 (s, 1H, -CH=), 7.58 (d, 2H, J=6 Hz, -C<sub>6</sub>H<sub>4</sub>-), 11.34 (s, 1H, -NH-). MS (ESI) *m/z* (M+H)<sup>+</sup> 361.1.

2.5.4 Synthesis of *tert*-butyl 2-(4-((2,5-dioxopyrrolidin-3-yl)methyl)phenoxy)ethyl(methyl)carbamate [IV (D)]

A solution of *tert*-butyl (2-{4-[(*E*)-(2,5-dioxopyrrolidin-3-ylidene)methyl]phenoxy}ethyl)methylcarbamate (200 mg, 0.055 mmol) in absolute ethanol (20 mL) was taken in a parr bottle and 50 mg of Pd/C (10%) was added to it. The compound was hydrogenated under hydrogen atmosphere (pressure 40 psi) at RT for 8 h. The mixture was filtered using celite and concentrated by evaporation under reduced pressure to give a white solid [IV (D)] (Fig. 11) (0.195 g, 97.5% yield). Melting point 202–203°C. <sup>1</sup>H NMR (CDCl<sub>3</sub>) δ: 1.44 (s, 9H, Me<sub>3</sub>C-), 2.70 (d, 2H, J=9 Hz, -CH<sub>2</sub>-), 2.85 (d, 2H, J=9 Hz, -CH<sub>2</sub>-), δ: 3.07 (s, 3H, >N-CH<sub>3</sub>), 3.43 (t, 2H, J=9 Hz, -CH<sub>2</sub>-), 3.50 (t, 2H, J=9 Hz, -OCH<sub>2</sub>-), 4.02 (m, 1H, -CH<), 6.82 (d, 2H, J=9 HZ, -C<sub>6</sub>H<sub>4</sub>-), 7.02 (d, 2H, J=9 HZ, -C<sub>6</sub>H<sub>4</sub>-). MS (ESI) *m/z* (M+H)<sup>+</sup> 363.1.

### 2.5.5 Synthesis of 3-{4-[2-(methylamino)ethoxy]benzyl}pyrrolidine-2,5-dione [IV (E)]

0.5 N hydrochloric acid in dioxane (10 ml) was added to a solution of *tert*-butyl 2-(4-((2,5-dioxopyrrolidin-3-yl)methyl)phenoxy) (195 mg) in chloroform (20 mL) under nitrogen atmosphere at 0°C. The mixture was stirred at RT for another 2 h. The chloroform layer was separated and evaporated to dryness to give the white colour solid compound [IV (E)] (Fig. 11) (0.13 g, 89% yield). Melting point 223°C. <sup>1</sup>H NMR (CDCl<sub>3</sub>) δ: 1.98 (s, 1H, -NH-), 2.06 (s, 3H, -CH<sub>3</sub>), 2.36 (d, 2H, J=6 Hz, -CH<sub>2</sub>-), 2.95 (d, 2H, J=6 Hz, -CH<sub>2</sub>-), 3.59 (t, 2H, J=9 Hz, >N-CH<sub>2</sub>-), 3.88 (t, 2H, J=9 Hz, -OCH<sub>2</sub>-), 4.32 (m, 1H, -CH<), 7.08 (d, 2H, J=9 Hz, -C<sub>6</sub>H<sub>4</sub>-), 7.56 (d, 2H, J=9 HZ, -C<sub>6</sub>H<sub>4</sub>-), 11.38 (s, 1H, -NH-). MS (ESI) *m/z* (M+H)<sup>+</sup> 263.1.

### 2.5.6 Synthesis of (R,S)-3-(4-{2-[methyl(pyridin-2-yl)amino]ethoxy}benzyl)pyrrolidine-2,5-dione [IV (F)]

2-Chloropyridine (0.2 mL, 1.7 mmol) was added to a stirred solution of 3-{4-[2-(methylamino)ethoxy]benzyl}pyrrolidine-2,5-dione (150 mg, 0.517 mmol) in anhydrous ethanol and it was refluxed for 24 h. The reaction mixture was cooled to RT and concentrated under reduced pressure. The reaction mixture was quenched with ammonium chloride (50 mL) and extracted with EtOAc (100 mL). The extracted organic layer was washed with water (30 mL), brine (50 mL) and dried by anhydrous sodium sulfate. The organic layer was concentrated under reduced pressure and the residue was purified by silica gel column chromatography (60-120 mesh) using n-hexane/EtOAc (1:1 v/v) as an eluent to give a white solid compound [IV (F)] (Fig. 11) (0.12 g, 53% yield, 99.7% purity). Melting point 234°C. <sup>1</sup>H NMR (DMSO-d<sub>6</sub>) δ: 2.62 (d, 2H, J=6 Hz, -CH<sub>2</sub>-), 3.02 (s, 3H, >N-CH<sub>3</sub>), 3.34 (d, 2H, J=6 Hz, -CH<sub>2</sub>-), 3.53 (m, 1H, -CH<), 4.14 (t, 2H, J=9 Hz, >N-CH<sub>2</sub>-), 4.24 (t, 2H, -OCH<sub>2</sub>-), 6.71

(d, 2H, J=9 Hz, -C<sub>6</sub>H<sub>4</sub>-), 7.15 (d, 1H, J=9 Hz, -C<sub>5</sub>H<sub>4</sub>N), 7.43 (d, 2H, J=9 Hz, -C<sub>6</sub>H<sub>4</sub>-), 7.53 (dd, 1H, J=9 Hz, -C<sub>5</sub>H<sub>4</sub>N), 7.85 (dd, 1H, J=9 Hz, -C<sub>5</sub>H<sub>4</sub>N), 8.14 (d, 1H, J=9 Hz, -C<sub>5</sub>H<sub>4</sub>N), 11.10 (s, 1H, >NH). <sup>13</sup>C NMR (DMSO-d<sub>6</sub>) 32.64, 34.12, 34.32, 42.11, 47.18, 63.10, 114.50, 123.07, 124.38, 130.00, 130.79, 139.80, 149.92, 150.19, 156.27, 177.88 & 180.83 (Fig. 12). MS (ESI) *m/z* (M+H)<sup>+</sup> 340.1.

## 2.6 Preparation of CSN (C<sub>19</sub>H<sub>25</sub>NO<sub>3</sub>)

The synthetic routes of CSN are summarized in Fig. 13.

### 2.6.1 Synthesis of (1-methylcyclohexyl)methanol [V (A)]

A solution of iodine (5.3 g, 21 mmol) in anhydrous THF (20 mL) was added dropwise to a stirred solution of sodium borohydride (1.5 g, 4.18 mmol) in anhydrous THF (10 mL) under nitrogen atmosphere at 0°C over 30 min. Next, 1-methylcyclohexanecarboxylic acid (2 g, 14.0 mmol) in THF (5 mL) was added to it and the mixture was stirred for another 4 h at RT. The reaction mixture was then cooled to 0°C and excess hydride was quenched by dry methanol (10 mL). The whole mixture was concentrated by evaporation under reduced pressure. 40 mL of 20% solution of potassium hydroxide was added to it and the mixture was extracted with ether (100 mL) two times. Each ether layer was washed with sodium thiosulfate solution and then with brine solution. The combined ether layer was dried under anhydrous sodium sulfate and concentrated under reduced pressure. The crude product was purified by silica gel column chromatography (60–120 mesh) using n-hexane/EtOAc (10:1 v/v). It was recrystallized by dichloromethane/methanol (10:1 v/v), filtered and dried under vacuum to give a white crystal [V (A)] (Fig. 13) (1.2 g, 66.67% yield). Melting point 172°C.

$^1\text{H}$  NMR (DMSO- $d_6$ )  $\delta$ : 1.04 (s, 3H,  $-\text{CH}_3$ ),  $\delta$ : 1.11 to 1.46 (m, 10H,  $-\text{C}_6\text{H}_{10}-$ ),  $\delta$ : 1.92 (s, 2H,  $-\text{CH}_2-$ ),  $\delta$ : 3.10 (s, 1H,  $-\text{OH}$ ). MS (ESI)  $m/z$  ( $\text{M}+\text{H}$ ) $^+$  128.7.

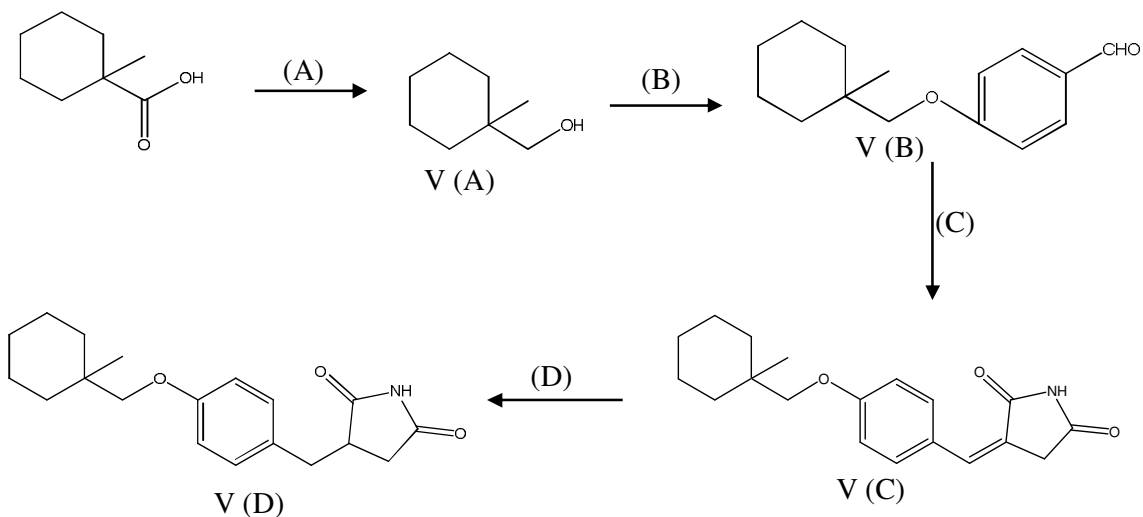


**Fig. 13** Synthesis of CSN. (A) Iodine, sodium borohydride, anhydrous THF, 0°C, RT; (B) 4-hydroxybenzaldehyde, triphenylphosphine, diisopropyl azodicarboxylate, dry THF, 0°C, RT, 18 h; (C) methanol, reflux, 2 h, 3-(triphenylphosphoranylidene)pyrrolidine-2,5-dione; (D) 10% Pd/C, hydrogen gas, ethanol, 12 h.

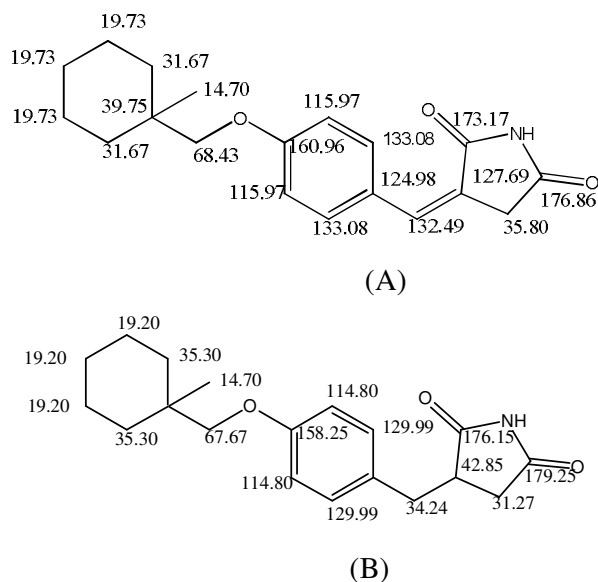


**Fig. 14**  $^{13}\text{C}$  NMR interpretation of (A) (3Z)-3-{4-[(1 methylcyclohexyl)methoxy]benzylidene}pyrrolidine-2,5-dione and (B) CSN.

### 2.6.2 Synthesis of 4-[(1-methylcyclohexyl)methoxy]benzaldehyde [V (B)]

4-Hydroxybenzaldehyde (1.14 g, 9.37 mmol) and triphenylphosphine (3.07 g, 11.7 mmol) were added to a solution of (1-methylcyclohexyl)methanol (1 g, 0.781 mmol) in dry THF at 0°C. Diisopropyl azodicarboxylate (2.30 mL, 11.71 mmol) was added dropwise to the mixture over 15 min at 0°C. It was stirred for 18 h at RT. THF was removed under reduced pressure and EtOAc (100 mL) was added to it. The EtOAc layer was washed with 1N sodium hydroxide (20 mL), water (25 mL) and brine (20 mL). Then the organic layer was dried by anhydrous sodium sulfate and concentrated. The product was purified by silica gel column chromatography (60-120 mesh) using n-hexane/EtOAc (12:1 v/v) to give a yellow liquid [V (B)] (Fig. 13) (0.5 g, 24.21% yield). <sup>1</sup>H NMR (DMSO-d<sub>6</sub>) δ: 1.04 (s, 3H, -CH<sub>3</sub>), δ: 1.16 to 1.44 (m, 10H, -C<sub>6</sub>H<sub>10</sub>-), 2.12 (m, 2H, -CH<sub>2</sub>O-), δ: 7.36 (d, 2H, J=6 Hz, -C<sub>6</sub>H<sub>4</sub>-), δ: 7.99 (d, 2H, J=6 Hz, -C<sub>6</sub>H<sub>4</sub>-), δ: 10.01 (s, 1H, -CHO). MS (ESI) *m/z* (M+H)<sup>+</sup> 233.1.

### 2.6.3 Synthesis of (3Z)-3-{4-[(1-methylcyclohexyl)methoxy]benzylidene}pyrrolidine-2,5-dione [V (C)]

A mixture of 3-(triphenylphosphoranylidene)pyrrolidine-2,5-dione (250 mg, 0.69 mmol), 4-[(1-methylcyclohexyl)methoxy]benzaldehyde (160 mg, 0.69 mmol) and methanol (20 mL) was heated under reflux for 1.5 h and then cooled at RT. The reaction mixture was kept at 4°C overnight to promote the crystal formation. The resulting crystal was filtered, washed with methanol (20 mL) and dried under vacuum at 40°C to give a white solid [V (C)] (Fig. 13) (0.31 g, 91% yield). Melting point 181°C. <sup>1</sup>H NMR (DMSO-d<sub>6</sub>) δ: 0.935 (m, 3H, -CH<sub>3</sub>), 1.45 (m, 2H, -C<sub>6</sub>H<sub>10</sub>-), 1.70 (m, 2H, -C<sub>6</sub>H<sub>10</sub>-), 2.08 (m, 6H, -C<sub>6</sub>H<sub>10</sub>-), 3.60 (s, 2H, -OCH<sub>2</sub>-), 4.02 (s, 2H, -CH<sub>2</sub>-), 7.01 (d, 2H, J=6 Hz, -C<sub>6</sub>H<sub>4</sub>-), 7.33 (s, 1H, -CH=), 7.55 (d, 2H,

J=9 Hz, -C<sub>6</sub>H<sub>4</sub>-), 11.33 (s, 1H, >NH). <sup>13</sup>C NMR (DMSO-d<sub>6</sub>) 14.70, 19.73, 31.67, 35.80, 39.75, 68.43, 115.97, 124.98, 127.69, 132.49, 133.08, 160.96, 173.17, 176.68 (Fig. 14A). MS (ESI) *m/z* (M+H)<sup>+</sup> 314.2.

#### 2.6.4 Synthesis of (R,S)-3-{4-[(1-methylcyclohexyl)methoxy]benzyl}pyrrolidine-2,5-dione [V (D)]

A solution of (3Z)-3-{4-[(1-methylcyclohexyl)methoxy]benzylidene}pyrrolidine-2,5-dione (100 mg, 0.31 mmol) in ethanol was taken in a parr bottle and 50 mg of Pd/C (10%) was added to it. The compound was hydrogenated under hydrogen atmosphere (pressure 40 psi) at RT for 8 h. The mixture was filtered using celite and concentrated by evaporation under reduced pressure to give a white solid [V (D)] (Fig. 13) (0.98 g, 98% yield, 99.8% purity). Melting point 142°C. <sup>1</sup>H NMR (DMSO-d<sub>6</sub>) δ: 1.25 (s, 3H, -CH<sub>3</sub>), 1.52-1.56 (m, 2H, -CH<sub>2</sub>-), 1.70-1.73 (m, 2H, -CH<sub>2</sub>-), 1.78-1.85 (m, 2H, -CH<sub>2</sub>-), 2.45-2.50 (m, 2H, -CH<sub>2</sub>-), 2.66-2.71 (m, 2H, -CH<sub>2</sub>-), 2.86-2.92 (m, 2H, -CH<sub>2</sub>-), 2.99-3.02 (m, 2H, -CH<sub>2</sub>-), 3.05 (s, 2H, -CH<sub>2</sub>-), 3.32-3.39 (m, 1H, -CH<), 6.84 (d, 2H, J=6 Hz, -C<sub>6</sub>H<sub>4</sub>-), 7.08 (d, 2H, J=6 Hz, -C<sub>6</sub>H<sub>4</sub>-). <sup>13</sup>C NMR (CDCl<sub>3</sub>) 14.70, 19.20, 31.27, 34.24, 35.30, 42.85, 67.67, 114.80, 129.99, 158.25, 176.15, 179.15 (Fig. 14B). MS (ESI) *m/z* (M+H)<sup>+</sup> 316.1.

#### 2.7 Discussion

In our present synthesis, we followed the same synthetic procedures for PRD analogues like TZD durg synthesis (page 21) except the last step. For the last step, PRD ring was converted to 3-(triphenylphosphoranylidene)pyrrolidine-2,5-dione first and this intermediate again reacted with corresponding aldehyde to get desired product .

A new chiral centre had been generated during synthesis for PRD analogues. The separation of compound from the racemic mixture was beyond our limit. We demonstrated that PRD analogues were racemic mixture (R,S) which were finally used for biological screening. The PRD analogues were successfully synthesized and characterized using NMR and MS. In the next chapter, RM profiling of the TZD drugs and the PRD analogues using both HLM and THLE-2 cells is discussed.

## Chapter 3

### RM profiling using HLM and THLE-2 cells

#### 3.1 Introduction

Toxicity induced via metabolic activation is being increasingly screened during the drug discovery process in recent years. A variety of analytical methods were developed and employed for the profiling and characterization of RMs. Screening of RM-protein covalent adducts using HLM and liver cells from animals and humans is commonly used for the determination of RMs of drug candidates. Specifically, numerous methods have been developed to detect reactive RM-GSH adducts *in vitro*. The early LC/MS/MS method employed the neutral loss (NL) experiment (129 amu) to screen for the RM-GSH adducts (Dieckhaus et al., 2005) where the fragment of mass 129 corresponds to the polyglutamic acid moiety of GSH. The structure of each screened RM-GSH adduct can be further elucidated using product ion scan (PIS) experiment (Dieckhaus et al., 2005). In some cases, the effectiveness of the NL scanning experiment varies among different classes of RM-GSH adducts because the NL fragmentation patterns are compound-dependent (Dieckhaus et al., 2005). To improve the sensitivity of the RM-GSH adduct screening by NL scan, stable-isotope labelled GSH was explored as the trapping agent (Mutlib et al., 2005). Alternatively, multiple reaction monitoring (MRM) could be utilized to screen the transition of RM-GSH adduct from the protonated ion (parent ion,  $[M+H]^+$ ) to the corresponding product ion  $[MH-129]^+$  (Soglia et al., 2004). In addition, a precursor ion scan experiment at  $m/z$  272 in the ESI- mode had been employed to detect the RM-GSH adducts in biological samples (Christine et al. 2005). More recently, new MS techniques such as QTRAP MS (Joanna et al., 2007; Li et al., 2009), orbitrap or fourier transform ion cyclotron resonance MS (Mingshe et



al., 2007) and new trapping agents such as  $\gamma$ -glutamylcysteine (Zhengyin et al., 2007), dansyl GSH (Jinping et al., 2009), quaternary ammonium GSH (Sogila et al., 2006) were used for the detection of RMs in biological samples *in vitro*.

In my project, NL scan at 129 amu and PIS experiments were performed for the profiling of RM-GSH adducts generated from the biotransformation of TZD antidiabetic drugs and their PRD analogues.

### 3.2 Materials

GSH, potassium monohydrogen phosphate, potassium dihydrogen phosphate, bovine serum albumin, 0.5% trypsin-ethylenediaminetetraacetic acid solution (trypsin-EDTA), phosphate buffer saline and fetal bovine serum were purchased from Sigma-Aldrich (Saint Louis, MO, USA). HLM and nicotinamide adenine-di-nucleotide phosphate hydrogen (NADPH) regenerating system (solutions A and B), fibronectin and collagen were purchased from BD Biosciences (Woburn, MA, USA). TGZ, PGZ, RGZ and CGZ were purchased from Cayman Chemical Company (Ann Arbor, MI, USA). Bronchial epithelial cell basal medium (BEBM) provided with supplements (bronchial epithelial cell growth medium, BEGM BulletKit, CC-3170) was purchased from Cambrex Corporation (Rutherford, NJ, USA). THLE-2 cell line was purchased from ATCC (Manassas, VA, USA). All other reagents and chemicals used for the experiments were of analytical grade.

### 3.3 Methods

#### 3.3.1 HLM incubation for RM profiling

50 mM stock solutions of all the test compounds (both the TZD and PRD analogues) were prepared individually in DMSO and diluted to a 5 mM working solution using methanol. For each compound, triplicate incubations ( $n = 3$ ) were performed at 37°C in 300  $\mu\text{L}$  of 50 mM of potassium phosphate buffer (both potassium monohydrogen phosphate and potassium dihydrogen phosphate,) containing 2 mg/mL microsomal proteins and NADPH regenerating system. After 5 min pre-incubation, the reaction was initiated by the addition of 30  $\mu\text{L}$  of 50 mM GSH and 3  $\mu\text{L}$  of the working solution of the substrate. The final reaction mixture contained 50  $\mu\text{M}$  of substrate, 1.55 mM  $\text{NADP}^+$ , 3.3 mM glucose-6-phosphate, 3.3 mM magnesium chloride, 0.4 U/mL glucose-6-phosphate dehydrogenase, 0.05 mM sodium citrate and 5 mM of GSH. The final organic solvent concentration was 0.2% v/v. At 0 and 60 min, 120 and 180  $\mu\text{L}$  of the incubation mixture was quenched, respectively, with two volumes of cold ACN. These samples were centrifuged at 13,000 rpm for 10 min at 20°C. The supernatant was removed and evaporated to dryness at 35°C for 2 h under gentle flow of nitrogen gas using the Turbovap LV (Caliper Life Science, Hopkinton, MA, USA). The dried samples were reconstituted with 30  $\mu\text{L}$  of ACN/water (50:50, v/v), vortex-mixed and centrifuged at 13,000 rpm for 2 min at 4°C. 3  $\mu\text{L}$  of the supernatant was subjected to UPLC/MS/MS analysis. Negative control experiments were also performed in the absence of GSH, NADPH regenerating system or the substrate.

### 3.3.2 THLE-2 cell culture

THLE-2 cells were cultured in plates pre-coated with collagen I (2.9 mg/mL), fibronectin (1 mg/mL) and bovine serum albumin (1 mg/mL) in BEBM according to ATCC guidelines. For all cell-based experiments, THLE-2 cells were maintained in the logarithmic growth phase in BEBM supplemented with 10% fetal bovine serum and BEGM BulletKit in

humidified air with 5% CO<sub>2</sub> at 37°C. Supplemented BEBM was termed as BEGM subsequently.

### 3.3.3 THLE-2 incubation for RM profiling

THLE-2 cells were seeded into a 6-well plate ( $1.0 \times 10^7$  cells per well). 100 µM of each substrate was added to the cells and the mixture was incubated in a humidified condition (95% air/5% CO<sub>2</sub>) at 37°C. The final concentration of each test compound and organic solvent were 50 µM and 0.3% v/v, respectively. After 24 h ( $t_{24}$ ), the reaction was terminated by addition of 2 mL of ice cold ACN/water (50:50 v/v). Initial time point samples ( $t_0$ ) were prepared by terminating the reaction immediately after adding the test compound to the THLE-2 cells with the same quenching solvent. These samples were centrifuged at 13,000 rpm at 4°C for 10 min and the supernatants were removed and evaporated to dryness at 35°C for 8 h under gentle flow of nitrogen gas using the Turbovap LV. They were each reconstituted with 50 µL of ACN/water (50:50 v/v), vortex-mixed and centrifuged for 13,000 rpm at 4°C for 2 min. 5 µL of the supernatant was subjected to UPLC/MS/MS analysis. Negative control experiments were also performed in the absence of THLE-2 cells or the substrates.

### 3.4 LC/MS/MS conditions

The LC/MS/MS system comprised an ACQUITY UPLC system (Waters, Milford, MA, USA) interfaced with a hybrid QTRAP MS equipped with TurboIonSpray ESI source (3200 QTRAP, Applied Biosystems, Foster City, CA, USA). The UPLC and QTRAP MS

systems were both controlled by the Analyst 1.4.2 software (Applied Biosystems). The column and autosampler temperatures were maintained at 60 and 4°C, respectively.

For the profiling of the RM-GSH adducts in HLM and THLE-2 cells, chromatographic separations were performed using an ACQUITY UPLC BEH C<sub>18</sub> 1.7 μm 100 × 2.1 mm i.d. column (Waters). The flow rate was 0.5 mL/min and the mobile phases consisted of solvent A (0.1% formic acid in water) and solvent B (0.1% formic acid in ACN). The elution conditions were: linear gradient of 5 to 95% solvent B (0 – 9.50 min), isocratic at 95% solvent B (9.50 – 10.50 min) and then isocratic at 5% solvent B (10.50 – 12.00 min). ESI+ mode was employed throughout the experiments. NL scan experiment at *m/z* 129 and PIS were performed to profile the RM-GSH conjugates. The optimized MS conditions are summarized in Table 2.

Parameters	Values
Curtain gas, psi	25.0
Ion spray voltage, V	4500.0
CAD gas	Medium
Gas 1, psi	40.0
Gas 2, psi	45.0
Interface heater	On
Temperature, °C	550.0
Declustering potential, V	80.0
Entrance potential, V	10.0
Collision cell entrance potential, V	25.0
Collision energy, V	4.0
Collision cell exit potential, V	1.0

**Table 2** Optimized MS parameters for the detection of RM-GSH adducts.

### 3.5 Results

#### 3.5.1 RM profiling of TGZ and TSN

LC/MS/MS analysis of TGZ incubated with HLM and THLE-2 cells revealed the presence of four RM-GSH adducts using NL scan of 129 amu. A representative RM-GSH adduct (RM1,  $[M+H]^+$  ion at  $m/z$  722, retention time 4.78 min) was absent in “0 min TGZ-HLM-GSH” and “0 h TGZ-THLE-2” samples but present in “60 min TGZ-HLM-GSH” and “24 h TGZ-THLE-2” incubations, respectively (Fig. 15C). RM1 was fragmented using PIS experiment and yielded product ions at  $m/z$  647  $[MH-75]^+$  and  $m/z$  593  $[MH-129]^+$  which shared characteristic fragmentation pattern of GSH-adducted conjugates. The PIS spectrum also contained an intense ion at  $m/z$  416  $[MH-306]^+$  that was derived via the retro-Michael cleavage of the RM-GSH adduct (Kassahun et al., 1994). Collectively, these characteristic fragmentation patterns supported that the RM1 was formed *in vitro*. In summary, RM1 is a RM-GSH adduct of TGZ where the disulfide bond formation occurred between the TZD ring-opened oxidized TGZ and sulfur moiety of GSH.

As shown in Fig. 15D, our experiments exhibited another RM-GSH adduct (RM2,  $[M+H]^+$  ion at  $m/z$  747, retention time 4.45 min) when the “60 min TGZ-HLM-GSH” and “24 h TGZ-THLE-2” incubations were analyzed. As expected, this peak was absent in the corresponding “0 min TGZ-HLM-GSH”, “0 h TGZ-THLE-2” and negative control samples. RM2 underwent fragmentation using PIS experiment and yielded product ions at  $m/z$  672  $[MH-75]^+$  and  $m/z$  618  $[MH-129]^+$ . Interestingly, the PIS spectrum also contained an intense peak at  $m/z$  308  $[GSH_2]^+$ . Collectively, the characteristic fragmentation patterns indicated clearly the formation of RM2 *in vitro*. RM2 is a RM-GSH adduct of TGZ where the conjugation with GSH occurred at the C-5 position of TZD ring. Similar observations were made for RM3 ( $[M+H]^+$  ion at  $m/z$  737, retention time 4.10 min) and RM4 ( $[M+H]^+$  ion at  $m/z$  781, retention time 3.20 min). RM3 yielded product ions at  $m/z$  662  $[MH-75]^+$  and  $m/z$  608  $[MH-129]^+$  (Fig. 15E) while RM4 produced product ions

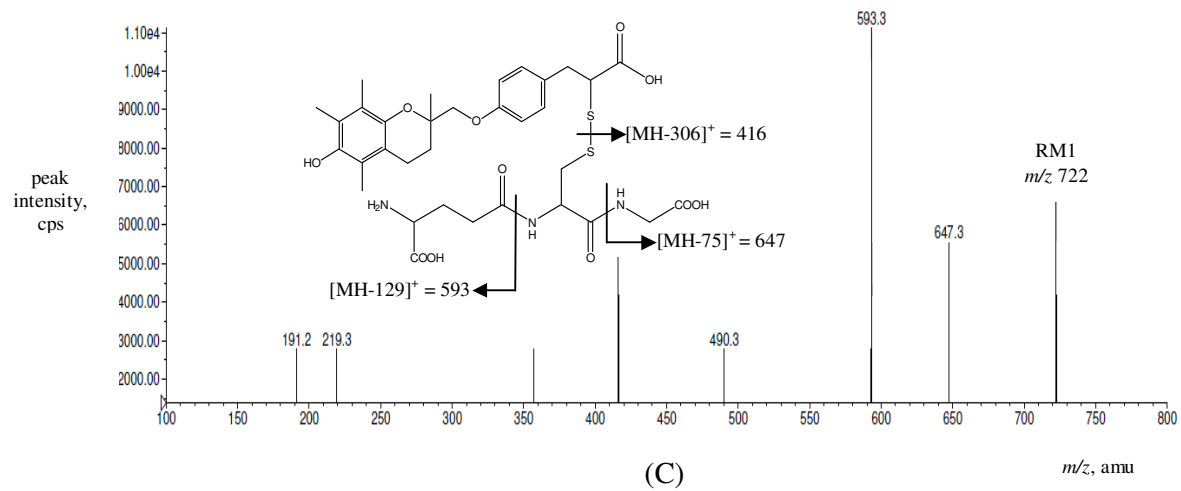
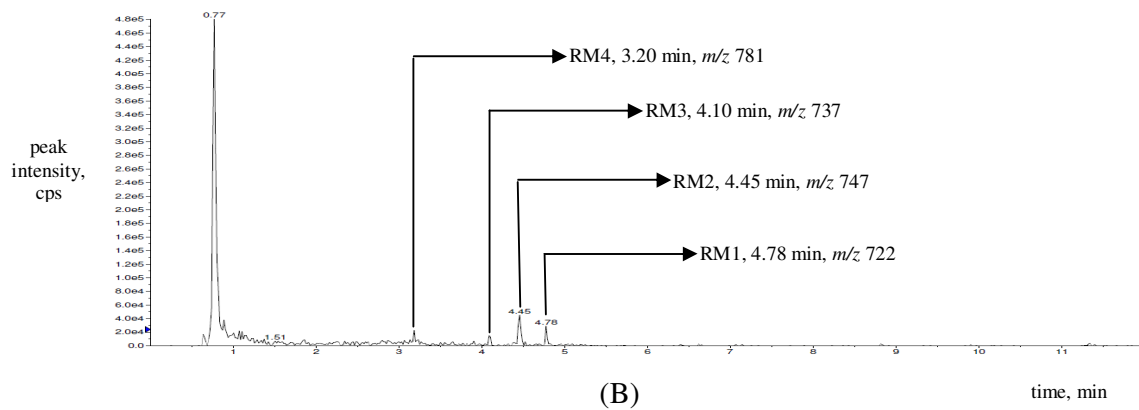
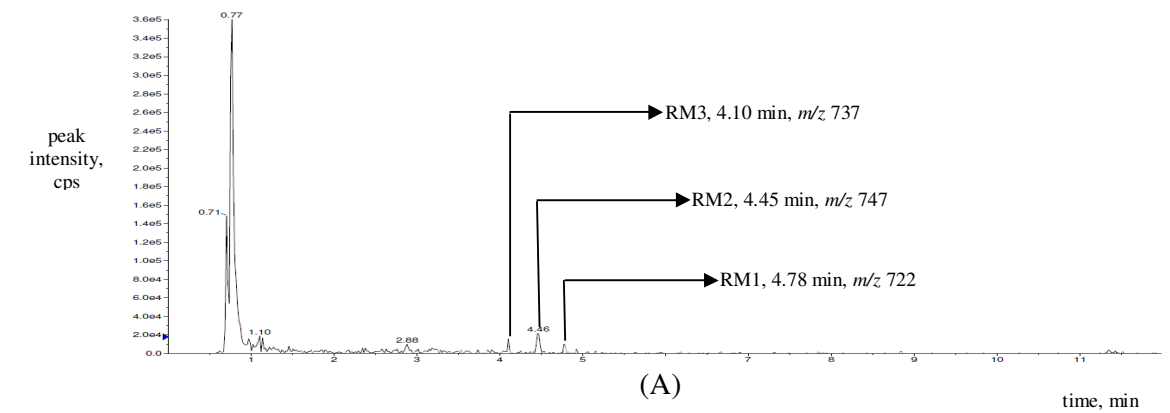


**Fig. 15** NL scan at 129 amu of (A) 24 h TGZ-THLE-2 sample and (B) 60 min TGZ-HLM-GSH sample. PIS of (C) RM1,  $m/z$  722.

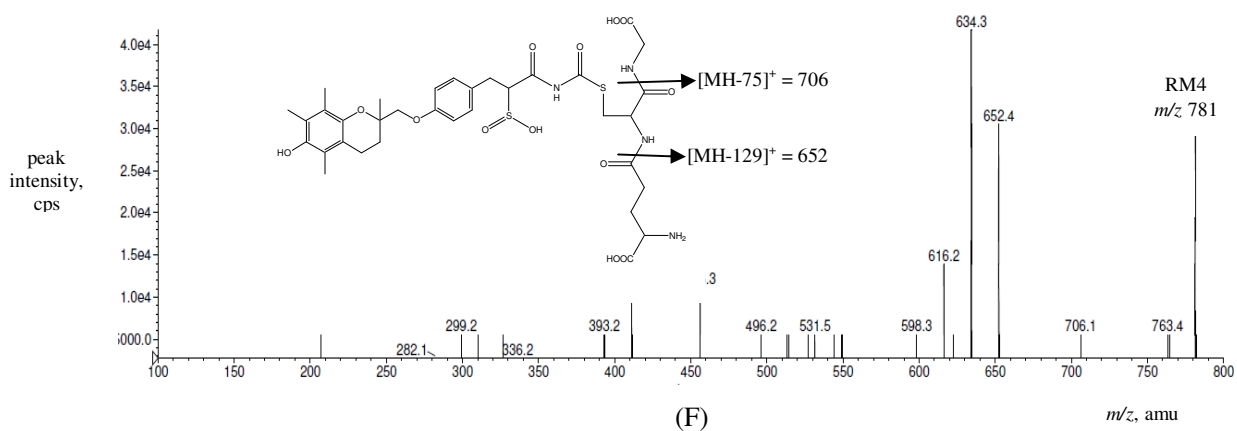
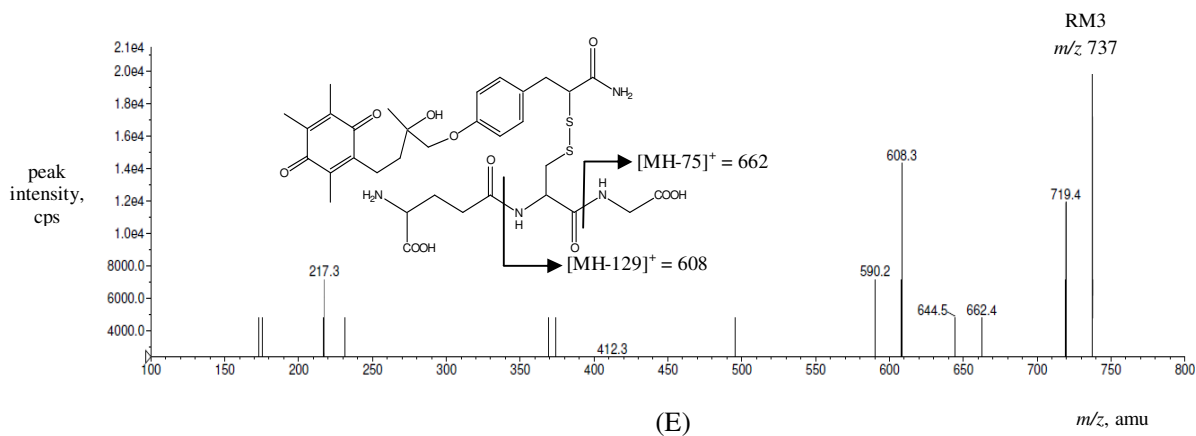
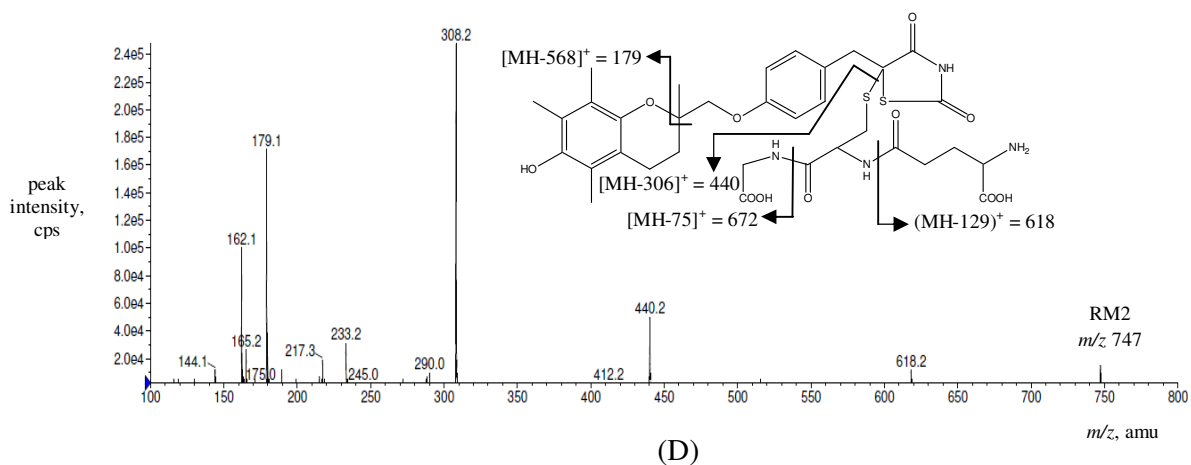


**Fig. 15 (continue)** PIS of (D) RM2, *m/z* 747, (E) RM3, *m/z* 737 and (F) RM4, *m/z* 781.

$m/z$  706 [MH-75]<sup>+</sup> and  $m/z$  652 [MH-129]<sup>+</sup> (Fig. 15F). It is worthwhile to note that RM4 was found only in HLM but not in THLE-2 incubation.

Among the identified RM-GSH adducts in our LC/MS/MS experiment, RM1 is the oxidized product of TZD ring which is similar to oxidized product of M1 of TGZ (Kassahun et al, 2001). The molecular weight of RM1 (721 Da) is one mass unit higher than M1. RM1 conjugate is related to carboxylic acid derivative of M1, formed by hydrolysis of the primary amide of the latter. RM2 is the direct adduct between C-5 position of TGZ ring and GSH (He et al. 2004). RM3 and RM4 are related to M4 and M2 of TGZ, respectively (Kassahun et al, 2001). RM3 is related to direct adduct between quinoid TGZ and GSH while RM4 is the indirect adduct between S-hydroxylated TGZ and GSH.

Importantly, no RM was detected when TSN was incubated with HLM and THLE-2 incubations. While it was possible for TSN to also form quinoid metabolite, we did not detect such metabolite in our experiment. This adverts to the possibility that PRD moiety, unlike TZD, is less prone to ring opening and attack by nucleophilic GSH. This observation suggested that the sulfur atom of the TZD ring of TGZ is responsible for the formation of RMs either directly or indirectly. TGZ had been shown to act as an inducer of CYP3A4 enzymes in human hepatocytes which played an important role in metabolic activation of this drug (Ramachandran et al., 1999). Due to the enhanced metabolic activation of TGZ by CYP3A4, more reactive intermediates might be generated in the liver. This had been suggested to be a potential cause of TGZ inducing hepatotoxicity.

### 3.5.2 RM profiling of PGZ and PSN

Using NL scan of 129 amu, LC/MS/MS analysis of PGZ incubated with HLM and THLE-2 cells incubations revealed the presence of two RM-GSH adducts. A representative



RM-GSH adduct (RM5,  $[M+H]^+$  ion at  $m/z$  636, retention time 2.43 min) was absent in “0 min PGZ-HLM-GSH” sample but present in “60 min PGZ-HLM-GSH” incubation (Fig. 16C). RM5 was also absent in “24 h PGZ-THLE-2” incubation. RM5 was fragmented using PIS experiment and yielded product ions at  $m/z$  507  $[MH-129]^+$  which shared characteristic fragmentation pattern of GSH-adducted conjugates. The PIS spectrum also contained an intense ion at  $m/z$  331  $[MH-306]^+$  that was derived via the retro-Michael cleavage of the RM-GSH adduct (Kassahun et al., 1994). Collectively, these characteristic fragmentation patterns supported that RM5 was formed *in vitro*. In summary, RM5 is a RM-GSH adduct of PGZ where the disulfide bond formation occurred between the TZD ring-opened PGZ and sulfur moiety of GSH.

As shown in Fig. 16D, another RM-GSH adduct (RM6,  $[M+H]^+$  ion at  $m/z$  637, retention time 2.13 min) was determined when the “60 min PGZ-HLM-GSH” and “24 h PGZ-THLE-2” incubations were screened. As expected, the same peak was absent in the corresponding “0 min PGZ-HLM-GSH” and “0 h PGZ-THLE-2” incubations and negative control samples. RM6 underwent fragmentation using PIS experiment and yielded product ions at  $m/z$  509  $[MH-129]^+$ . Collectively, the characteristic fragmentation patterns indicated clearly the formation of RM6 *in vitro*. RM6 was the oxidized product of RM5 where the amide moiety of RM5 was further oxidised to the corresponding carboxyl moiety in the incubation mixture.

These two identified RM-GSH adducts (RM5, in HLM and RM6, in both HLM and THLE-2 incubations) were consistent with previous published adducts of PGZ (Baughman et al., 2005).

No GSH adduct was detected when the same experiments were performed on PSN using both HLM and THLE-2 incubations.

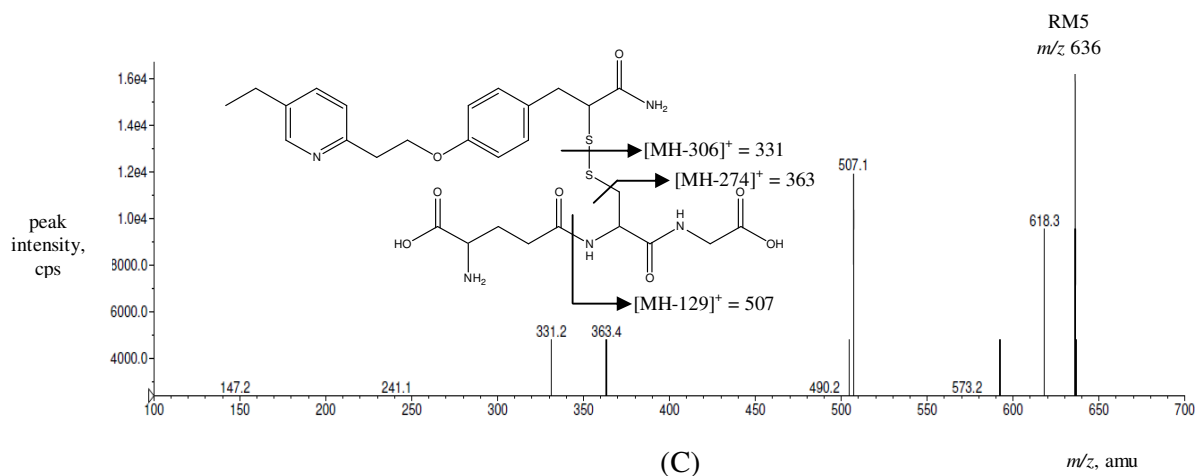
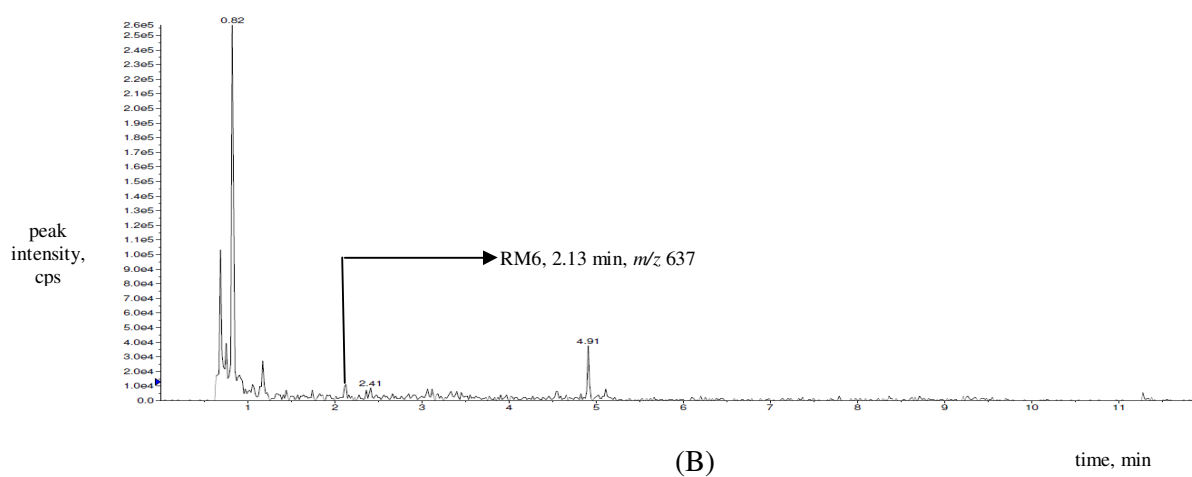
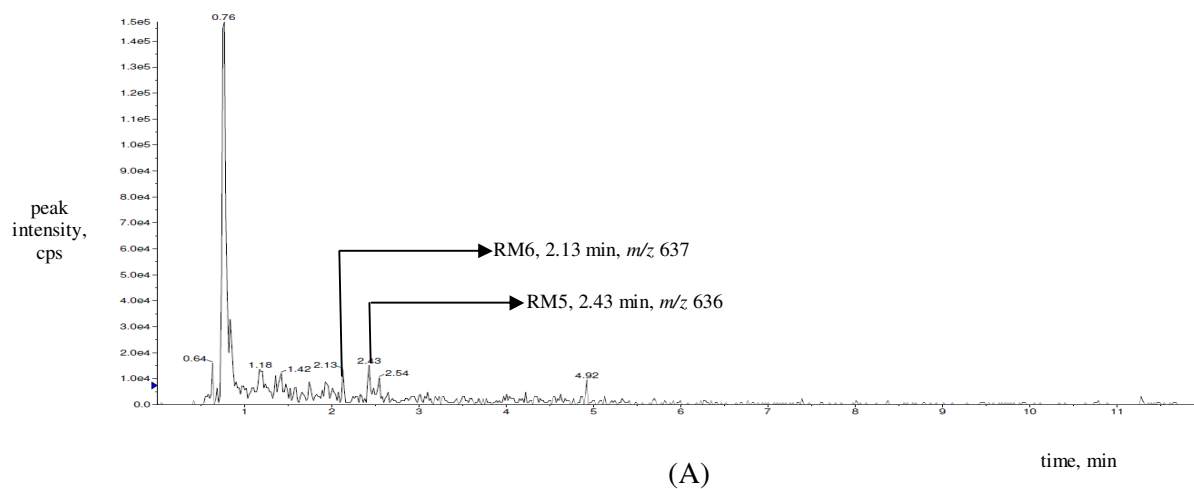


**Fig. 16** NL scan of at  $m/z$  129 amu of (A) 60 min PGZ-HLM-GSH sample and (B) 24 h PGZ-THLE-2 sample. PIS of (C) RM5,  $m/z$  636.

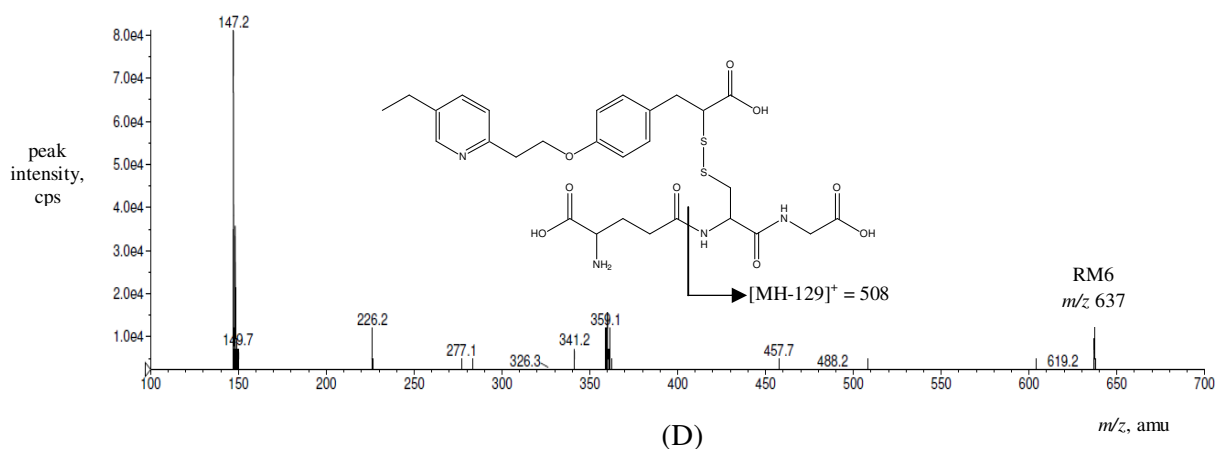


**Fig. 16 (continue)** PIS of (D) RM6,  $m/z$  637.

### 3.5.3 RM profiling of RGZ and RSN

LC/MS/MS analysis of RGZ incubated with HLM and THLE-2 cells incubations revealed the presence of two RM-GSH adducts using NL scan of 129 amu. A representative RM-GSH adduct (RM7,  $[M+H]^+$  ion at  $m/z$  637, retention time 2.06 min) was absent in “0 min RGZ-HLM-GSH” and “0 h RGZ-THLE-2” samples but present in both “60 min RGZ-HLM-GSH” and “24 h RGZ- THLE-2” incubations (Fig. 17C). RM7 was fragmented using PIS experiment and yielded product ions at  $m/z$  562  $[MH-75]^+$  and  $m/z$  508  $[MH-129]^+$  which shared characteristic fragmentation pattern of GSH-adducted conjugates. Collectively, these characteristic fragmentation patterns supported that the RM7 was formed *in vitro*. In summary, RM7 is a RM-GSH adduct of RGZ where the disulfide bond formation occurred between the TZD ring-opened oxidized RGZ and sulfur moiety of GSH.

As shown in Fig. 17D, our experiment yielded another RM-GSH adduct (RM8,  $[M+H]^+$  ion at  $m/z$  638, retention time 1.73 min) when the “60 min RGZ-HLM-GSH” and “24 h RGZ-THLE-2” incubations were analyzed. As expected, this peak was absent in the

corresponding “0 min RGZ-HLM-GSH”, “0 h RGZ-THLE-2” and negative control samples. RM8 underwent fragmentation using PIS experiment and yielded product ions at  $m/z$  563  $[MH-75]^+$  and  $m/z$  509  $[MH-129]^+$ . Collectively, the characteristic fragmentation patterns indicated clearly the formation of RM8 *in vitro*. RM8 is a RM-GSH adduct of RM7 where the amide moiety of RM7 was oxidised to the corresponding carboxyl moiety in the incubation mixture.

Our identified RM-GSH adducts (RM7 and RM8, in both HLM and THLE-2) were similar to previous published adducts of RGZ (Alvarez-Sánchez et al., 2006) confirming the reliability of our assay.

No GSH adduct was detected when the same experiments were performed on RSN using both HLM and THLE-2 incubations.

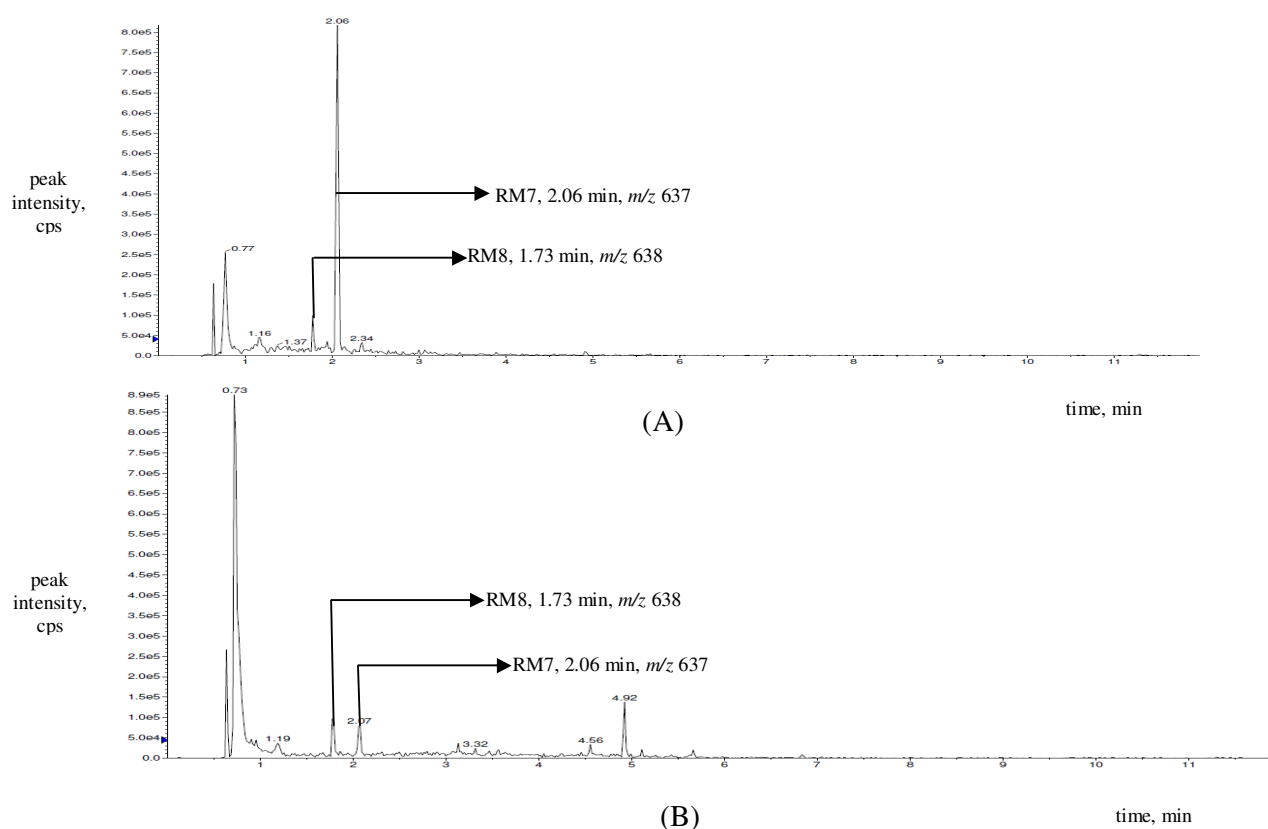


**Fig. 17** NL scan of at  $m/z$  129 amu of (A) 60 min RGZ-HLM-GSH and (B) 24 h RGZ-THLE-2 sample.

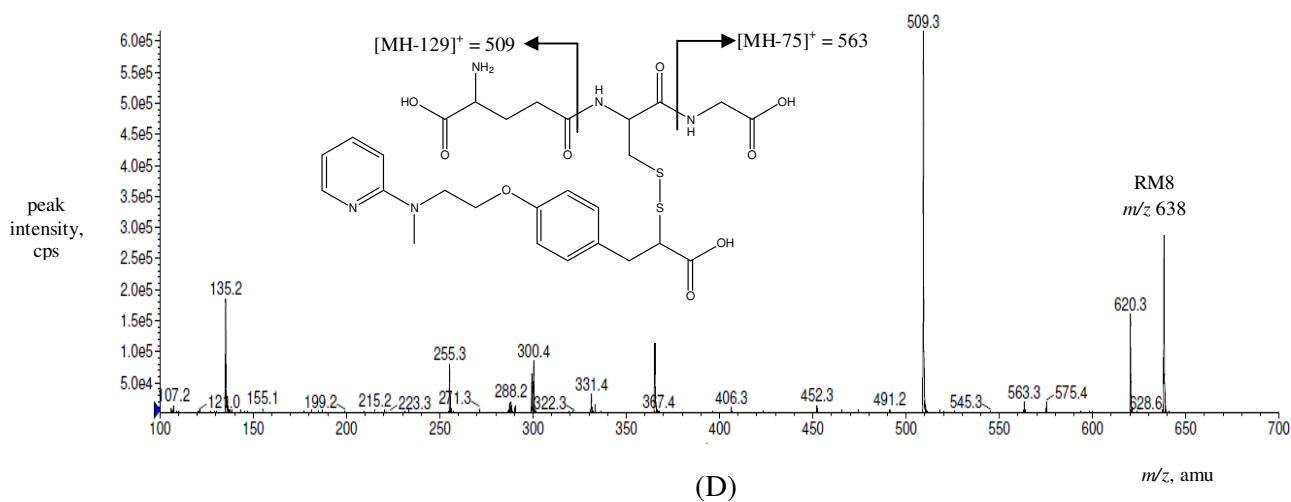
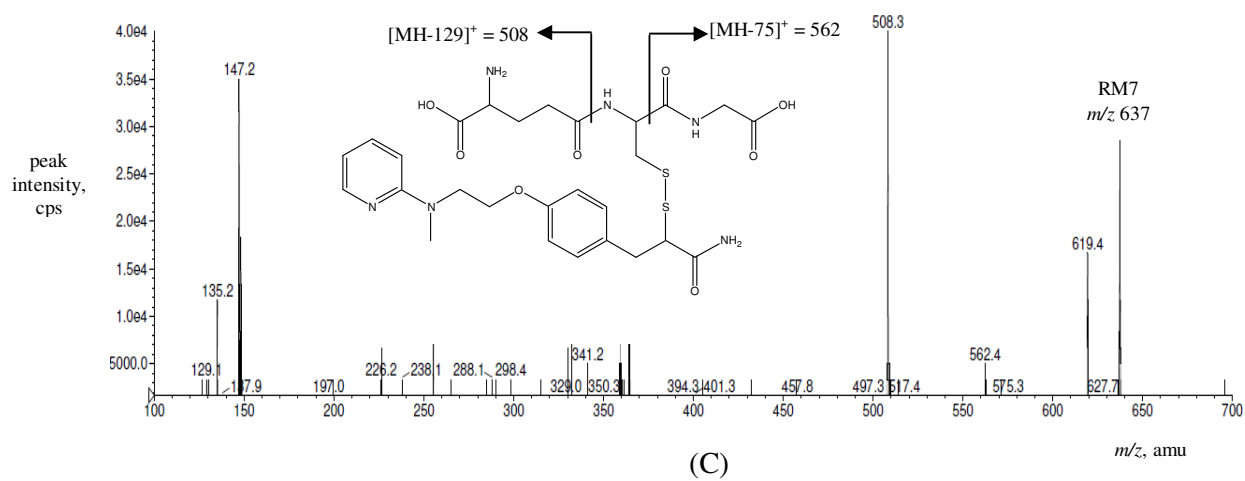


**Fig. 17 (continue)** PIS of (C) RM7,  $m/z$  637 and (D) RM8,  $m/z$  638.

### 3.5.4 RMs profiling using CGZ and CSN

No RM-GSH adduct was detected when the RM-GSH adduct screening experiments were performed on CGZ and CSN using both HLM and THLE-2 incubations.

### 3.6 Discussion

TGZ was withdrawn from market in 2000 due to its idiosyncratic liver toxicity (Chojkier, 2005) but the mechanism of toxicity remains unknown to clinicians. It is necessary to highlight that although many mechanisms had been proposed (Smith, 2003), the exact mechanism of toxicity remains elusive. Many unanswered questions remain for TGZ-induced toxicity and we want to ascertain the contribution of the sulfur moiety to the toxicity of TGZ. It is also necessary to investigate the role of sulfur moiety of TZD ring of other TZD antidiabetic drugs (RGZ, PGZ, and CGZ) in inducing hepatotoxicity. Therefore, we aimed to first screen and characterize the electrophilic RM generated by the TZD drugs and their analogues.

In this chapter, we used GSH to trap reactive electrophilic intermediates and identified RM-GSH adducts in HLM and THLE-2 cells. Consistently, we observed TZD-dependent bioactivation occurred for the TZD drugs in both enzymatic and cellular incubations using LC/MS/MS experiments. Our study revealed that both RGZ and PGZ were prone to form reactive intermediates, suggesting that these two compounds might be liable for toxicity in humans. This is consistent with the reports on clinical toxicity cases related to these two drugs. Unlike RGZ and PGZ, TGZ generated a quinone-related RM-GSH adduct, RM3, as a predominant product detected in both HLM and THLE-2 cells. The formation of this unique quinone reactive intermediate might account for potential oxidative stress-induced toxicity associated with TGZ in humans (Smith 2003). We confirmed the generation of RMs by the TZD drugs, however, a pertinent question arose if these RMs account for toxicity in humans?

To get the answer to the above question, we prepared the PRD analogues. When the PRD analogues were incubated with both HLM and THLE-2 cells, no clear RM-GSH adduct

was detected. One possible reason was that the PRD moiety, unlike TZD, was less prone to ring opening and attack by nucleophilic GSH. This observation suggests that the sulfur atom of the TZD ring is responsible for the formation of RMs either directly or indirectly. When the sulfur moiety of TZD ring was substituted by the methylene moiety of the PRD ring, we found that this structural modification circumvented RM formation. Therefore, such structural modification may become an important strategy to reduce the toxicity of the TZD class of antidiabetic drugs.

RM4 and RM5 were absent in “24 h TGZ-THLE-2” and “24 h PGZ-THLE-2” incubations. THLE-2 cells contain more CYP3A4 and less CYP2C8 enzymes (Andrea et al., 1993). Both TGZ and PGZ are mainly metabolized by both CYP3A4 and CYP2C8. RM4 and RM5 were not produced during incubation due to absence of CYP2C8 enzymes in THLE-2 cells.

We observed that TZD antidiabetic drugs formed TZD-ring opened oxidized reactive intermediates during both HLM and THLE-2 incubations. The questions arose whether these TZD drugs may produce any oxidative stress in THLE-2 cells. Therefore, to link the formation of RMs to the onset of toxicity, we further performed cell cytotoxicity assays using THLE-2 cells. In the next chapter, the cytotoxicity assays of the TZD and PRD analogues using metabolically-active THLE-2 cells are discussed.

## Chapter 4

### Cytotoxicity assays

#### 4.1 Introduction

Chapter four presents and discusses the cytotoxicity assays of TZD and PRD analogues using metabolically active THLE-2 cells. To make correlation between RMs formation and toxicity, we performed MTT cell viability, GSH and protein carbonyl (PC) assays. GSH and PC assays were performed to examine the mechanism of toxicity of TZD antidiabetic drugs.

MTT cell viability assay is used preliminarily to detect the cytotoxicity of compounds *in vitro*. Several methods had been used for the determination of cell viability. Among them, trypan blue staining is a simple way to evaluate cell membrane integrity and assume cell proliferation or death. However, the method is not sensitive and cannot be used for high throughput screening. Therefore, researchers perform the cell viability using trypan blue first and then using MTT. Yellow MTT is reduced to purple formazan in the mitochondria of living cells. The absorbance of this colour solution can be quantitated by measuring light at a certain wavelength (usually between 500 and 600 nm) via a spectrophotometer. This reduction takes place when mitochondrial reductase enzymes are active and can be directly related to the number of viable (living) cells. When the amount of purple formazan produced by cells treated with an agent is compared with the amount of formazan produced by untreated control cells, the effectiveness of the agent in causing the death of cells can be derived from the dose-response curve. An increase in the cell number results in an increase in the formation of MTT formazan and a corresponding increase in absorbance. The MTT method has a few limitations. The assay depends on physiological state of the cells and



variance in mitochondrial dehydrogenase activity in different cell types (Bigl et al., 2007). Nevertheless, the MTT assay is useful for the measurement of cell growth in response to mutagens, antigenic stimuli, growth factors and cytotoxicity studies. For MTT assay, percentage cell viability was calculated based on the equation:

$$\frac{Absorbance_{test} - Absorbance_{blank}}{Absorbance_{control} - Absorbance_{blank}} \times 100\%$$

To link RM formation to the mechanism of toxicity, a question arose whether the TZD antidiabetic drugs exert any direct effect on endogenous GSH depletion. Preliminary investigation revealed that TGZ-induced hepatotoxicity might be due to the formation of oxidized TZD ring-opened RMs. To confirm this observation, it is necessary to confirm whether the TZD drugs produce oxidative stress in normal human hepatocytes. In the thesis, we performed GSH depletion assay on all TZD drugs and their analogues using THLE-2 cells. GSH is a tripeptide comprising of L-cysteine, L-glutamic acid and glycine. It is an antioxidant which protects cells from reactive oxygen species (ROS) such as free radicals and peroxides (Prompela et al., 2003). GSH acts as nucleophile which binds to poisonous electrophile in our body. Thiol groups are kept in reduced state at a concentration of approximately ~5 mM in animal cells. GSH is converted to its oxidized form glutathione disulfide (GSSG) during oxidative stress. In fact, the ratio of GSH to GSSG within cells is used scientifically as a measurement of cellular toxicity (Pastore et al., 2003). The depletion of GSH has dual implications in the biochemical system. The depletion of GSH is either effected via adduct formation to RM-GSH conjugates or via oxidation to GSSG suggesting oxidative stress.

While several methods are available for the determination GSH in biological samples, oxidation of GSH remains a major problem during sample preparation. Therefore, the blocking of thiol group using various agents such as N-ethylmaleimide (NEM), iodoacetic

acid and 2-vinyl pyridine has been explored to prevent GSH oxidation (Roman et al., 2007). A variety of HPLC methods with ultraviolet (UV) detection had been developed for the detection of GSH in the biological samples (Farris and Reed, 1987; Katrusiak et al., 2001). The main drawback of HPLC-UV method is its poor limit of detection. While HPLC with fluorescence detection is more sensitive than the HPLC-UV method, it requires sample derivatization and is relatively more tedious (Cereser et al., 2001). Recently, LC/MS/MS had been developed for the determination of GSH or GSH conjugates from biological systems (Ranieri et al., 2006). In our study, we performed GSH assay using LC/MS/MS (ESI+ mode and MRM transition) with NEM as derivatizing agent. The decreased GSH synthesis may be a possibility causing GSH depletion in our LC/MS/MS experiments.

The implication of GSH depletion is related to both oxidative stress and its binding to RM. Therefore, a more specific assay for oxidative stress may be necessary to help relate or differentiate between the two possibilities. Therefore, PC assay was performed to elucidate the mechanism of toxicity. Reactive oxygen species (ROS) are formed during normal metabolism and in various pathological conditions. They cause cellular damage by the oxidation of amino acid residues on proteins and form PC. PC is the most widely used marker of oxidative modification of proteins. There are several methodologies available for the quantitation of PC in the biological system. Among them, 2,4-dinitrophenylhydrazine is the common reagent for the determination of PC which forms the corresponding hydrazone in the incubation mixture and can be analyzed spectrophotometrically (Levine et al., 1990; Chevion et al., 2000). In our study, we performed PC assay spectrophotometrically using 2,4-dinitrophenylhydrazine as derivatizing reagent.

Before performing the MTT, GSH and PC assays, it was necessary to investigate the stability of each TZD and PRD analogues in BEGM to correlate the toxicity and oxidative stress end-points with the expected level of each parent compound. Hence, we first performed

stability studies of the TZD and PRD analogues at varying concentrations (1 and 50  $\mu\text{M}$ ) in BEGM at 37°C up to 72 h.

## *4.2 Materials*

GSH, GSSG, MTT, trichloroacetic acid (TCA), NEM, guanidine hydrochloride, 2,4-dinitrophenylhydrazine, trypan blue, tocopherol acetate (TA) were purchased from Sigma-Aldrich (Saint Louis, MO, USA). Ethylenediaminetetraacetic acid disodium salt dihydrate ( $\text{Na}_2\text{EDTA}\cdot 2\text{H}_2\text{O}$ ) with > 98% purity was obtained from Duchefa Biochemie B. V. (Haarlem, The Netherlands). All other reagents and chemicals used for the experiments were of analytical grade.

## *4.3 Methods*

### *4.3.1 Stability studies of TZD and PRD analogues*

#### *4.3.1.1 BEGM incubation conditions*

Stability studies of TZD and PRD analogues at 1.0 and 50.0  $\mu\text{M}$  were performed using BEGM at 37°C up to 72 h. At various time points (0, 24, 48 and 72 h), 1 mL methanol was added to 1 mL of the incubation mixture. Subsequently, each sample was centrifuged at 13,000 rpm for 5 min and the supernatant was removed and evaporated to dryness at 40°C for 8 to 10 h under a gentle flow of nitrogen gas using the Turbovap LV. Each dried residue was reconstituted with 50  $\mu\text{L}$  of methanol, vortex-mixed and centrifuged at 13,000 rpm for 2 min.

5  $\mu$ L of the supernatant was subjected to UPLC/MS/MS analysis. Triplicate analyses were performed at each time point.

#### 4.3.1.2 LC/MS/MS conditions

For the stability studies using LC/MS/MS, LC experimental setup was similar to that we used for the profiling of RM-GSH conjugates. MRM in ESI+ and ESI- mode were employed throughout the experiment for stability studies. The MS conditions are summarized in Tables 3 and 4 for TZD and PRD analogues, respectively. For stability studies, all chromatographic peak area integrations were performed using the Analyst Software v 1.4.2 (Applied Biosystems) and analyzed using GraphPad Prism 4 (San Diego, CA, USA).

MRM transitions were performed in ESI- mode at  $m/z$  440.0 $\rightarrow$ 397.0,  $m/z$  356.0 $\rightarrow$ 313.0 and  $m/z$  332.0 $\rightarrow$ 289.0 for TGZ, RGZ and CGZ, respectively. MRM transition was performed in ESI+ mode at  $m/z$  357.0 $\rightarrow$ 134.0 for PGZ.

MRM transitions were performed in ESI+ mode at  $m/z$  339.0 $\rightarrow$ 134.0,  $m/z$  340.0 $\rightarrow$ 263.0 and  $m/z$  316.0 $\rightarrow$ 106.0 for PSN, RSN and CSN, respectively while MRM transition was performed in ESI- mode at  $m/z$  422.0 $\rightarrow$ 203.0 for TSN.

The common MS parameters for the TZD and PRD analogues were as follows: curtain gas (CUR); 10 psi, ion spray voltage; -4500 V, collision gas (CAD); medium, ion source gas (GS<sub>1</sub>); 40 psi, ion source gas (GS<sub>2</sub>); 45 psi, interface heater; On, temperature; 500°C, scan time; 250 ms.

Parameters	Values			
	TGZ	PGZ	RGZ	CGZ
Declustering Potential, V	-49.0	52.0	-50.0	-57.0
Entrance potential, V	-5.6	7.0	-3.0	-2.0
Collision energy, V	-30.0	40.0	-35.2	-29.0
Collision cell exit potential, V	-4.0	2.4	-3.0	-2.0

**Table 3** Optimized MS parameters for stability studies of the TZD analogues.

Parameters	Values			
	TSN	PSN	RSN	CSN
Declustering Potential, V	-80.0	56.0	20.0	57.0
Entrance potential, V	-4.0	40.0	1.0	8.0
Collision energy, V	-42.0	38.0	35.0	32.5
Collision cell exit potential, V	-2.0	2.0	3.8	3.3

**Table 4** Optimized MS parameters for stability studies of the PRD analogues.

#### 4.3.2 MTT viability assay

MTT viability assay was performed as described previously (Marcsek et al., 2007). Briefly, THLE-2 cells were seeded into 96-well plate ( $1.0 \times 10^4$  cells per well). After 24 h, the medium was removed and 200  $\mu$ L of varying concentrations of TZD and PRD analogues (1 to 150  $\mu$ M) in media was added to each well and the samples were incubated in a humidified condition 5% CO<sub>2</sub> at 37°C. After 72 h, MTT solution (1 mg/mL, 50  $\mu$ L) was added to each well and incubated for another 4 h. After which, the media and excess MTT were removed and 150  $\mu$ L of DMSO was added. The absorbance at 570 nm was recorded using the Infinite M200 microplate reader controlled by Magellan and i-control softwares (Tecan Group Ltd.,

Mannedorf, Switzerland). Samples containing media with and without cells were also analyzed and labelled as 'control' and 'blank', respectively. Another assay was performed by spiking 20  $\mu\text{M}$  of TA (antioxidant) at varying concentrations of analytes (1–150  $\mu\text{M}$ ) in THLE-2 cells (Patrick et al., 2005). Independently, we performed the cytotoxicity assay of TA (1, 10, 50 and 100  $\mu\text{M}$  concentrations) in THLE-2 cells in the absence of analytes. All the experiments were performed in triplicates. The final organic solvent concentration was 0.3% (v/v). Cell survival (% of control) was calculated relative to untreated control cells. Data were analyzed by GraphPad Prism 4 and represented as the mean  $\pm$  S.D. of triplicate experiments to determine the  $\text{EC}_{50}$  of the respective compounds. Statistical differences were analyzed using one-way analysis of variance (one-way ANOVA) and paired T-test and  $P < 0.05$  represented the statistically significant data.

#### 4.3.3 *GSH depletion assay*

##### 4.3.3.1 *Preparation of calibration curve*

The details of our GSH assay using NEM as a derivatizing agent to prevent auto-oxidation of GSH had been previously published (New and Chan, 2008). To prevent auto-oxidation of GSH during sample preparation, a derivatizing solution (solution A) was prepared freshly by mixing NEM and  $\text{Na}_2\text{EDTA}\cdot 2\text{H}_2\text{O}$  in water/methanol (3:2 v/v) and adjusting the pH of the solution to 7.4 with solid sodium bicarbonate. The final concentrations of NEM and  $\text{Na}_2\text{EDTA}\cdot 2\text{H}_2\text{O}$  in solution A were 250 mM and 1.5 mg/mL, respectively. Under these conditions, the oxidation of GSH will be terminated by the formation of a stable GSH derivative, GSH-NEM.

50 mM stock solution of GSH was prepared freshly in water and its calibrated concentrations were prepared via serial dilutions of this stock solution using water. 200  $\mu\text{L}$  each of the calibrants was added to 50  $\mu\text{L}$  of solution A in a 1.5 mL microcentrifuge tube and vortex-mixed at high speed for 20 s. Then 50  $\mu\text{L}$  of TCA was added and the mixture was centrifuged at 13,000 rpm for 5 min at 4°C. 300  $\mu\text{L}$  of the supernatant was collected into a clean tube and subjected to LLE using 2 mL of dichloromethane. The mixture was vortexed at high speed for 1 min and subsequently centrifuged at 13,000 rpm for 8 min at 4°C. 300  $\mu\text{L}$  of the supernatant was collected into a clean tube and evaporated to dryness for 2 h at 35°C under nitrogen using the Turbovap LV. The residue was reconstituted with 100  $\mu\text{L}$  of water, vortex-mixed and centrifuged at 13,000 rpm for 5 min. 3  $\mu\text{L}$  of supernatant was injected for UPLC/MS/MS analysis. The concentrations of the GSH-NEM calibrants were 0.001, 0.01, 0.05, 0.1, 0.5, 1.0 and 10.0  $\mu\text{M}$ . Quality control (QC) samples were also prepared at concentrations of 0.003, 0.05 and 8.0  $\mu\text{M}$ , representing low, medium and high QC samples (LQC, MQC and HQC), respectively. Triplicate samples were prepared at each concentration.

#### *4.3.3.2 GSH depletion assay using THLE-2 cells*

THLE-2 cells were seeded into 24-well plate ( $2.0 \times 10^4$  cells/well). After 24 h, 1 mL of varying concentrations of TZD and PRD analogues in BEGM (1, 10, 25, 50, 75, 100, 125 and 150  $\mu\text{M}$ ) was added to each well and incubated in a humidified condition 5%  $\text{CO}_2$  at 37°C. After 72 h incubation, cells were washed with phosphate buffer saline and trypsinized using 0.05% trypsin-EDTA. Subsequently, the excess trypsin was inactivated with BEGM. The suspended cells were then transferred into clean tubes, centrifuged at 13,000 rpm for 2 min

and the supernatant removed. After which, 200  $\mu$ L of water was added to the cell samples and 50  $\mu$ L of solution A (mixture of NEM [250 mM] and Na<sub>2</sub>EDTA•2H<sub>2</sub>O [1.5 mg/mL] in water/methanol [3:2], pH 7.4) was added to it. The mixture was vortex-mixed at high speed for 20 s. Then 50  $\mu$ L of TCA (10%) was added and the mixture was centrifuged at 13,000 rpm for 5 min at 4°C. The supernatant was transferred into clean tubes and subjected to NEM derivatization and extraction as previously published (New and Chan, 2008). Total protein content of cell suspension was measured at 72 h using the Pierce Micro BCA™ (Bicinchoninic acid) Protein Assay Kit.

#### 4.3.3.3 LC/MS/MS conditions

In the measurement of GSH depletion assay, an ACQUITY UPLC HSS T3 1.8  $\mu$ m 100  $\times$  2.1 mm i.d. column (Waters) was used to achieve chromatographic separation. The mobile phases and optimized elution conditions utilized were published previously (New and Chan, 2008) (Table 5). ESI+ mode and MRM were employed throughout the experiments. The MRM transition for GSH-NEM was  $m/z$  433.0 $\rightarrow$ 304 and the MS conditions are summarized in Table 6. For GSH depletion assay, all chromatographic peak area integrations were performed using the Analyst Software v 1.4.2 and analyzed using GraphPad Prism 4. Statistical differences were analyzed using one-way ANOVA and paired T-test. P<0.05 represented statistical significance between the test groups.



Time (min)	% B	Curve
0.00	0.1	-
2.00	2.0	9
3.50	30.0	3
3.51	95.0	6
4.79	95.0	6
4.80	0.1	6
6.00	0.1	6

**Table 5** Optimized LC conditions for GSH depletion assay (New and Chan, 2008).

Parameters	Values
Curtain gas, psi	15.0
Ion spray voltage, V	5000.0
CAD gas	Medium
Gas 1, psi	40.0
Gas 2, psi	45.0
Interface heater	On
Temperature, °C	500.0
Declustering potential, V	29.55
Entrance potential, V	5.43
Collision cell entrance potential, V	15.00
Collision energy, V	18.00
Collision cell exit potential, V	2.00
Scan time, ms	250

**Table 6** Optimized MS parameters for GSH depletion assay.

#### 4.3.3.4 PC assay

PC assay was performed as described previously (Reznick and Packer, 1994). In brief, THLE-2 cells were seeded at  $5.0 \times 10^4$  cells/well into 6-well plate which was previously coated with the fibronectin-collagen medium. After 24 h, 2 mL of varying concentrations of TZD and PRD analogues in BEGM (1 to 50  $\mu$ M) were added to each well and incubated at 37°C in a humidified condition at 5% CO<sub>2</sub>. After 48 h, each medium was removed and the cells were washed with phosphate buffer saline. The cells were removed from the surface of the plates using 0.05% trypsin-EDTA and the excess trypsin was deactivated by adding BEGM. Media containing cells were transferred into clean tubes and centrifuged at 13,000 rpm for 2 min. The supernatant was removed, the cell pellet was reconstituted with 300  $\mu$ L of water and vortexed for 1 min. 150  $\mu$ L of cell suspension was aliquoted into a clean tube and precipitated using 500  $\mu$ L of 10% TCA solution. The tubes were centrifuged subsequently at 13,000 rpm for 2 min and the supernatant was removed. Each cell pellet was incubated with 500  $\mu$ L of 0.2% 2,4-dinitrophenylhydrazine for 1 h with constant vortexing at every 5 min interval. 50  $\mu$ L of 100% TCA solution was added, vortexed and centrifuged at 13,000 rpm for 5 min. All the supernatant was removed and the cell pellet was washed with 500  $\mu$ L of ethanol: EtOAc (1:1 v/v) mixture three times. Finally, the cell pellet was dissolved in 600  $\mu$ L of 6 M guanidine hydrochloride and 300  $\mu$ L was transferred to a 96-well plate and absorbance was measured at 360 nm using the Infinite M200 microplate reader. The remaining 150  $\mu$ L of cell suspension was used for measuring total protein content using the Pierce Micro BCA™ (Bicinchoninic acid) Protein Assay Kit. PC content ( $\mu$ M) per  $\mu$ g of protein was calculated at varying concentration of the test compounds. All data were analyzed by GraphPad Prism 4. Statistical differences were analyzed using one-way ANOVA and paired T-test. P<0.05 represented statistical significance between groups. All the experiments were performed in triplicates for every compound.

## 4.4 Results

### 4.4.1 Stability studies

Stability studies of TZD antidiabetic drugs and synthesized PRD analogues were performed using BEGM at 37°C up to 72 h. The results of stability studies are described below. The stability ranges were  $100 \pm 15\%$  up to 72 h for the TZD and PRD analogues.

#### 4.4.1.1 Stability studies of TGZ and TSN

The retention time of TGZ and TSN were 6.44 (Fig. 18A) and 8.11 (Fig. 18B) min, respectively. Our stability study demonstrated that TGZ and TSN at both 1.0 and 50.0  $\mu\text{M}$  were stable up to 72 h in BEGM at 37°C.

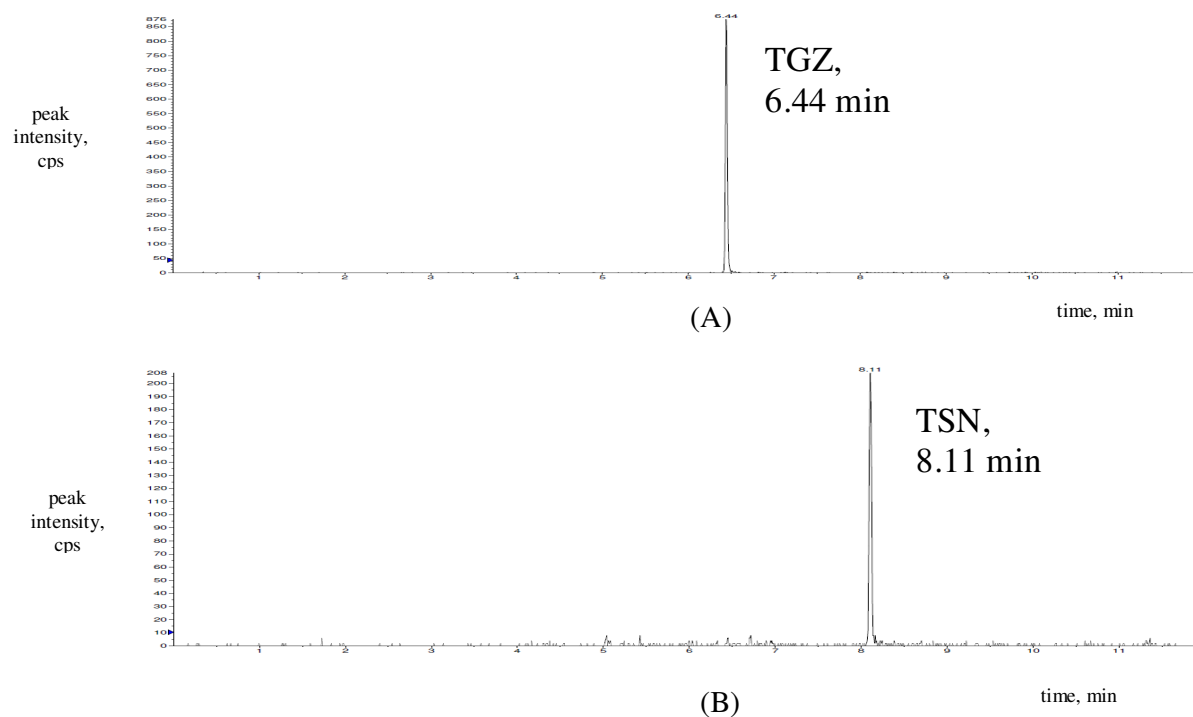


**Fig. 18** Representative LC/MS/MS chromatograms of (A) TGZ (6.44 min), (B) TSN (8.11 min) in BEGM.

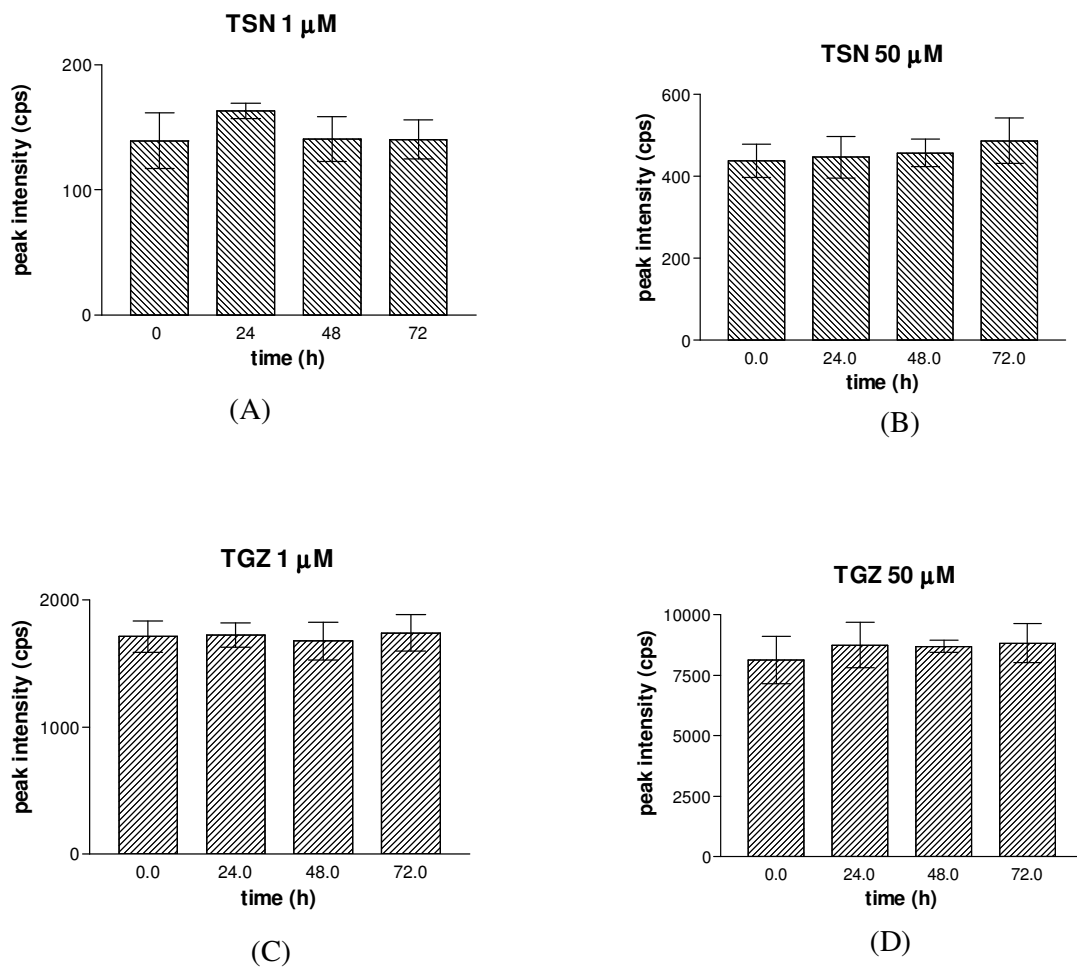


**Fig. 19** Stability profiles of TSN at (A) 1 and (B) 50  $\mu$ M, TGZ at (C) 1 and (D) 50  $\mu$ M in BEGM at 37°C up to 72 h (average $\pm$ SD, n=3).

Our stability studies showed that TSN was stable at 1  $\mu$ M (101.43%) (Fig. 19A) and 50  $\mu$ M (111.28%) (Fig. 19B) while TGZ was stable at 1  $\mu$ M (101.67%) (Fig. 19C) and 50  $\mu$ M (108.68%) (Fig. 19D) up to 72 h incubation.

#### 4.4.1.2 Stability studies of PGZ and PSN

The retention time of PGZ and PSN were 3.13 (Fig. 20A) and 2.66 (Fig. 20B) min, respectively. Our stability study demonstrated that PGZ and PSN at both 1.0 and 50.0  $\mu\text{M}$  were stable up to 72 h in BEGM at 37°C.

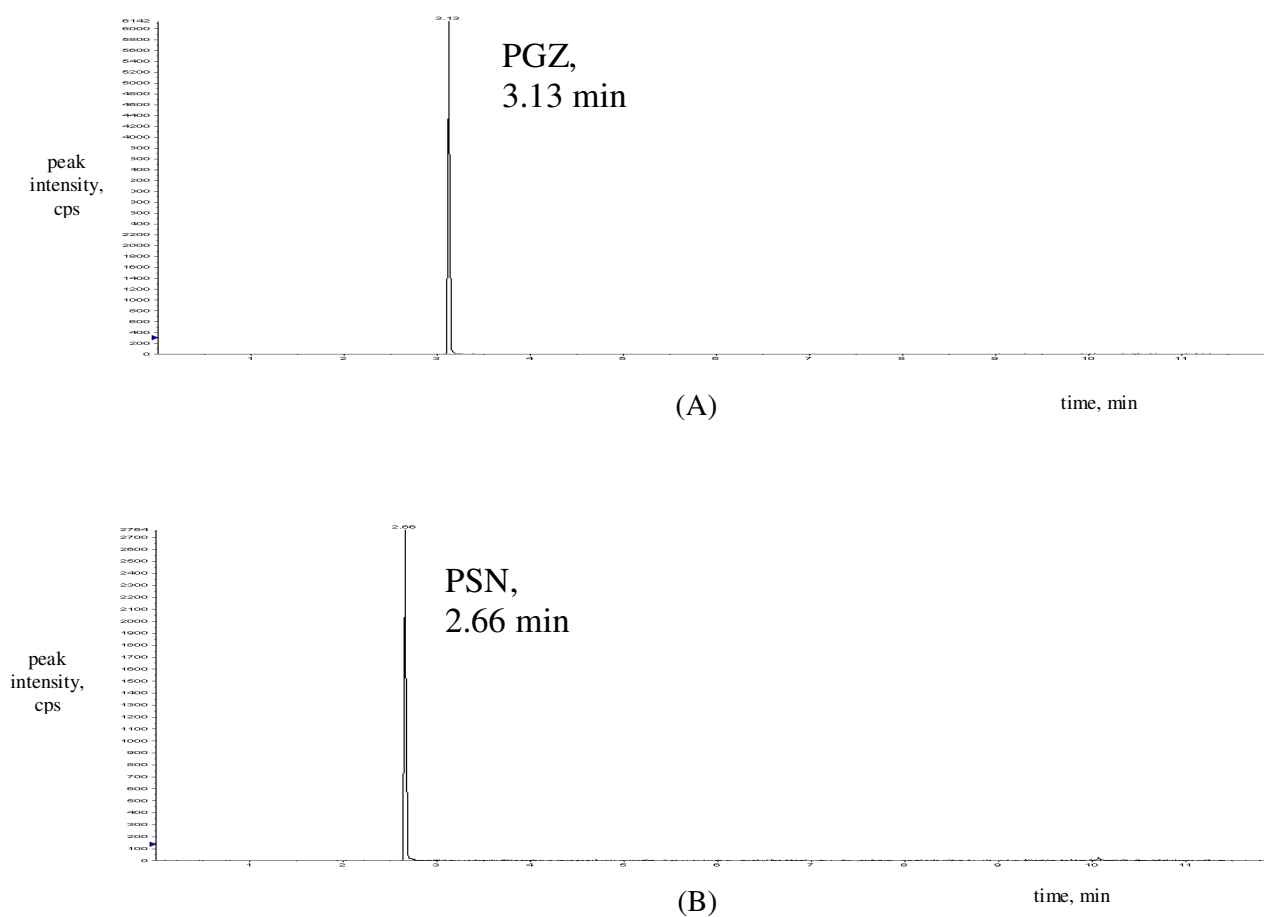


**Fig. 20** Representative LC/MS/MS chromatograms of (A) PGZ (3.13 min), (B) PSN (2.66 min) in BEGM.

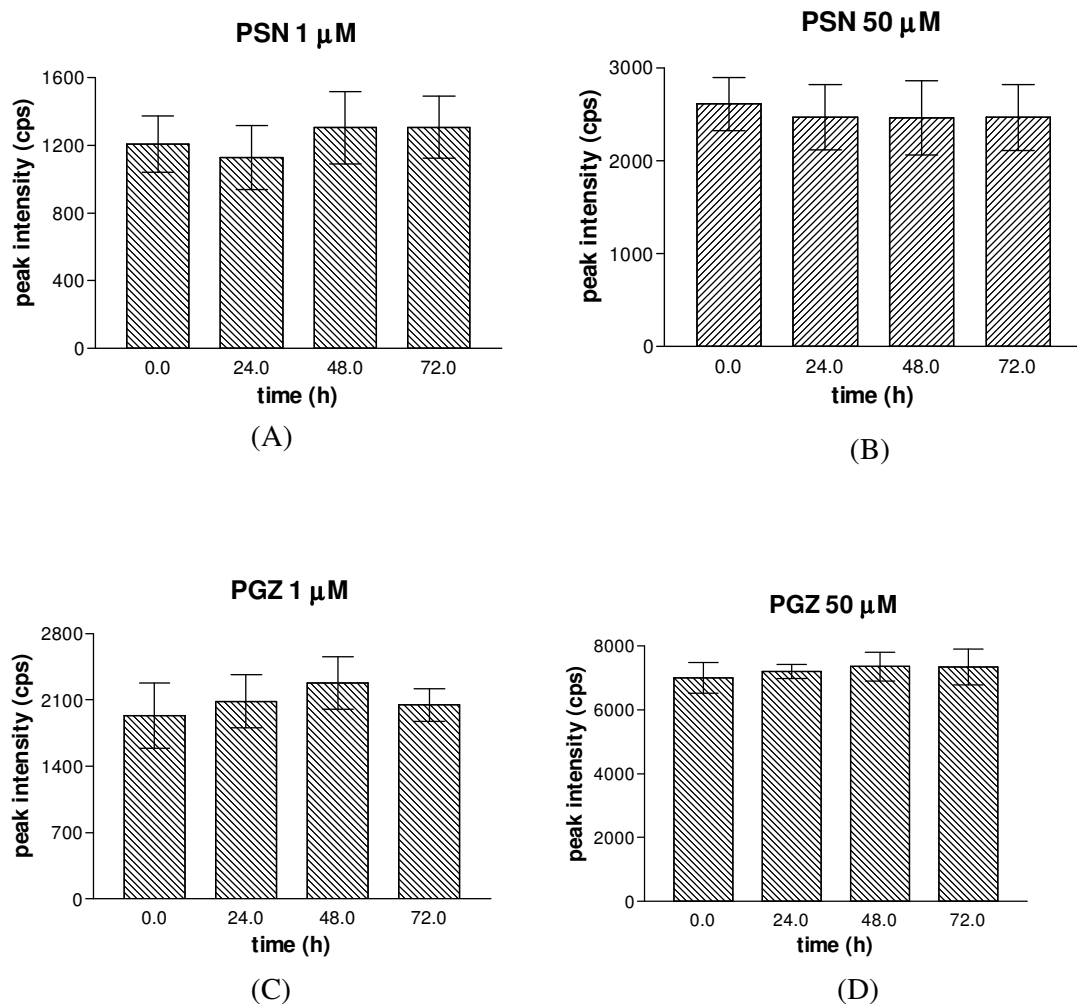


**Fig. 21** Stability studies of PSN at (A) 1 and (B) 50  $\mu\text{M}$ , PGZ at (C) 1 and (D) 50  $\mu\text{M}$  in BEGM at 37°C up to 72 h (average $\pm$ SD, n=3).

Our stability studies showed that PSN was stable at 1  $\mu\text{M}$  (108.26%) (Fig. 21A) and 50  $\mu\text{M}$  (94.53%) (Fig. 21B) while PGZ was stable at 1  $\mu\text{M}$  (106.04%) (Fig. 21C) and 50  $\mu\text{M}$  (104.91%) (Fig. 21D) up to 72 h incubation.

#### 4.4.1.3 Stability studies of RGZ and RSN

The retention time of RGZ and RSN were 2.59 (Fig. 22A) and 5.39 (Fig. 22B) min, respectively. Our stability study demonstrated that RGZ and RSN at both 1.0 and 50.0  $\mu\text{M}$  were stable up to 72 h in BEGM at 37°C.

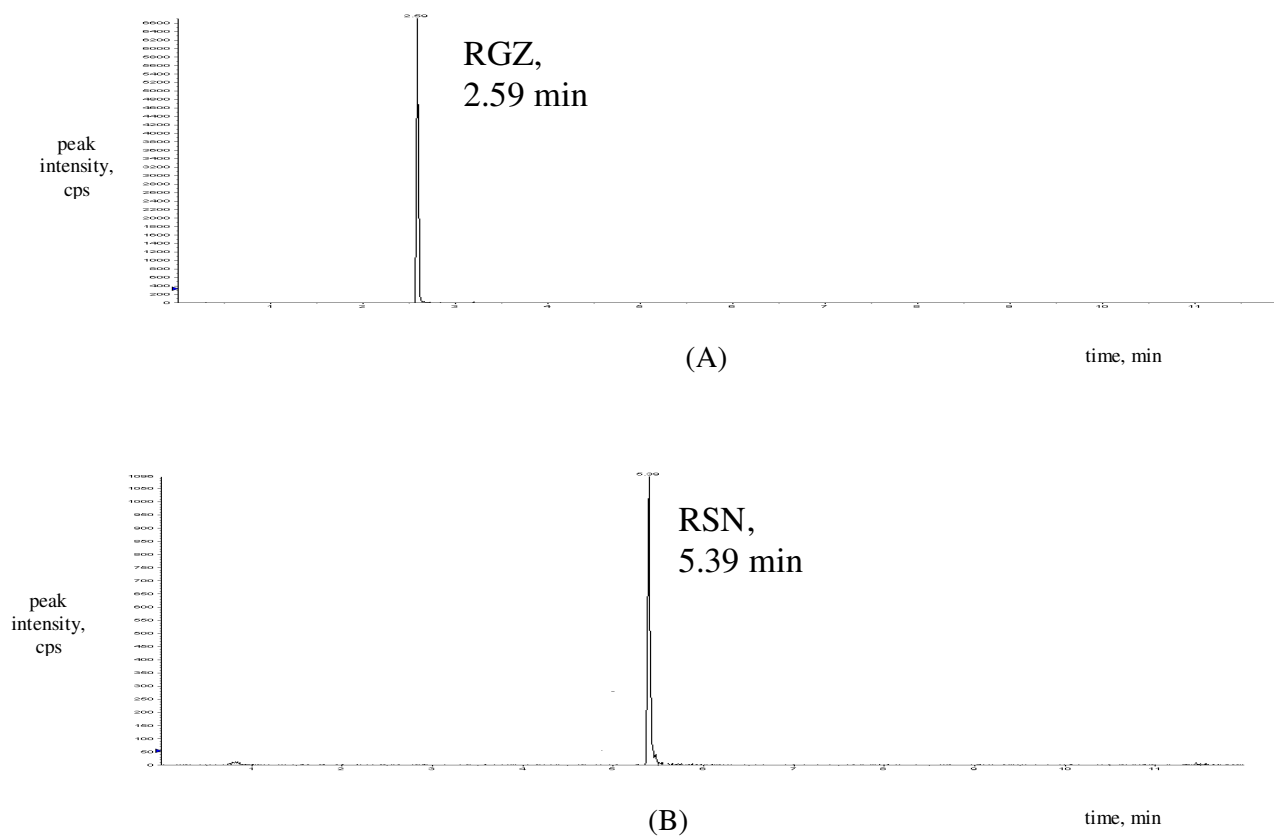


**Fig. 22** Representative LC/MS/MS chromatograms of (A) RGZ (2.59 min), (B) RSN (5.39 min) in BEGM.

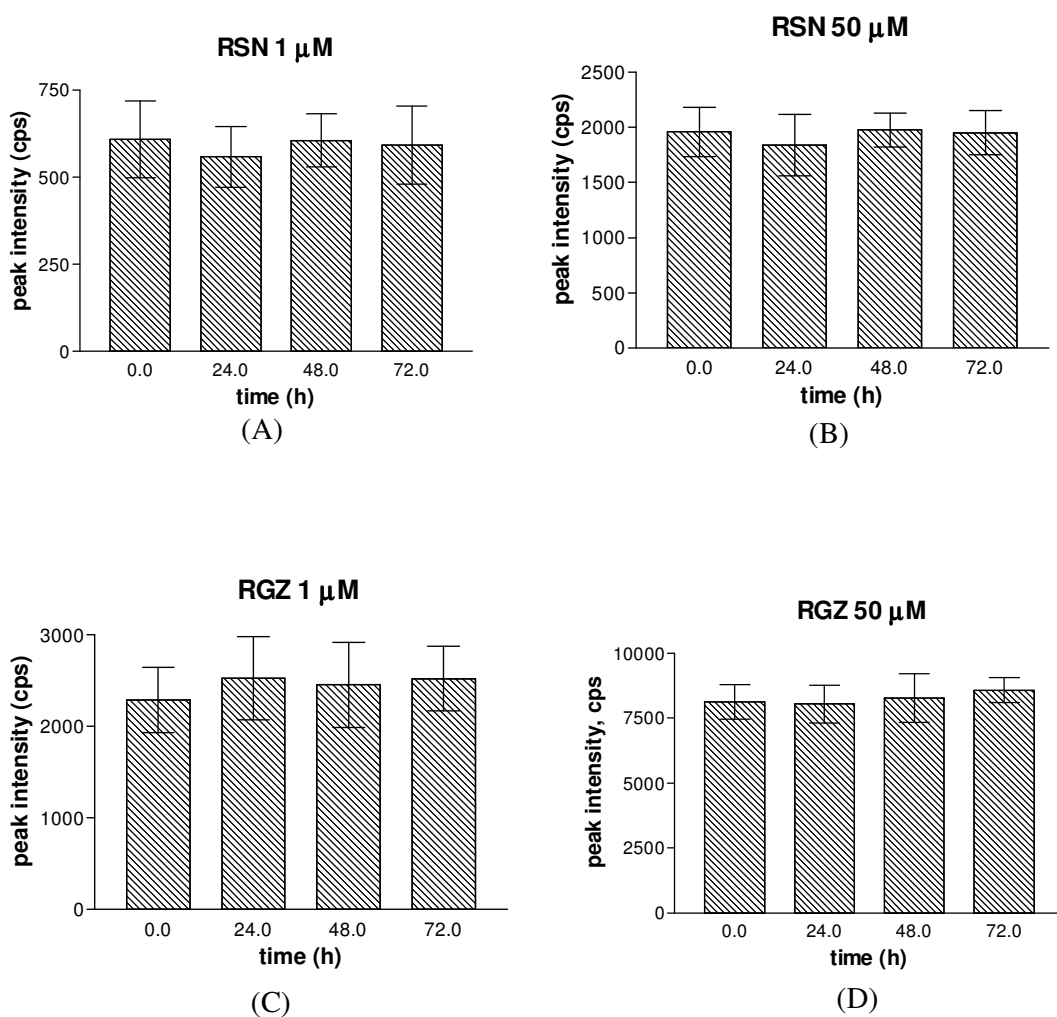


**Fig. 23** Stability studies of RSN at (A) 1 and (B) 50  $\mu\text{M}$ , RGZ at (C) 1 and (D) 50  $\mu\text{M}$  in BEGM at 37°C up to 72 h.

Our stability studies showed that RSN was stable at 1  $\mu\text{M}$  (97.26%) (Fig. 23A) and 50  $\mu\text{M}$  (99.65%) (Fig. 23B) while RGZ was stable at 1  $\mu\text{M}$  (110.48%) (Fig. 23C) and 50  $\mu\text{M}$  (105.61%) (Fig. 23D) up to 72 h incubation (average $\pm$ SD, n=3).



#### 4.4.1.4 Stability studies of CGZ and CSN

The retention time of CGZ and CSN were 7.65 (Fig. 24A) and 7.31 (Fig. 24B) min, respectively. Our stability study demonstrated that CGZ and CSN at both 1.0 and 50.0  $\mu\text{M}$  were stable up to 72 h in BEGM at 37°C.

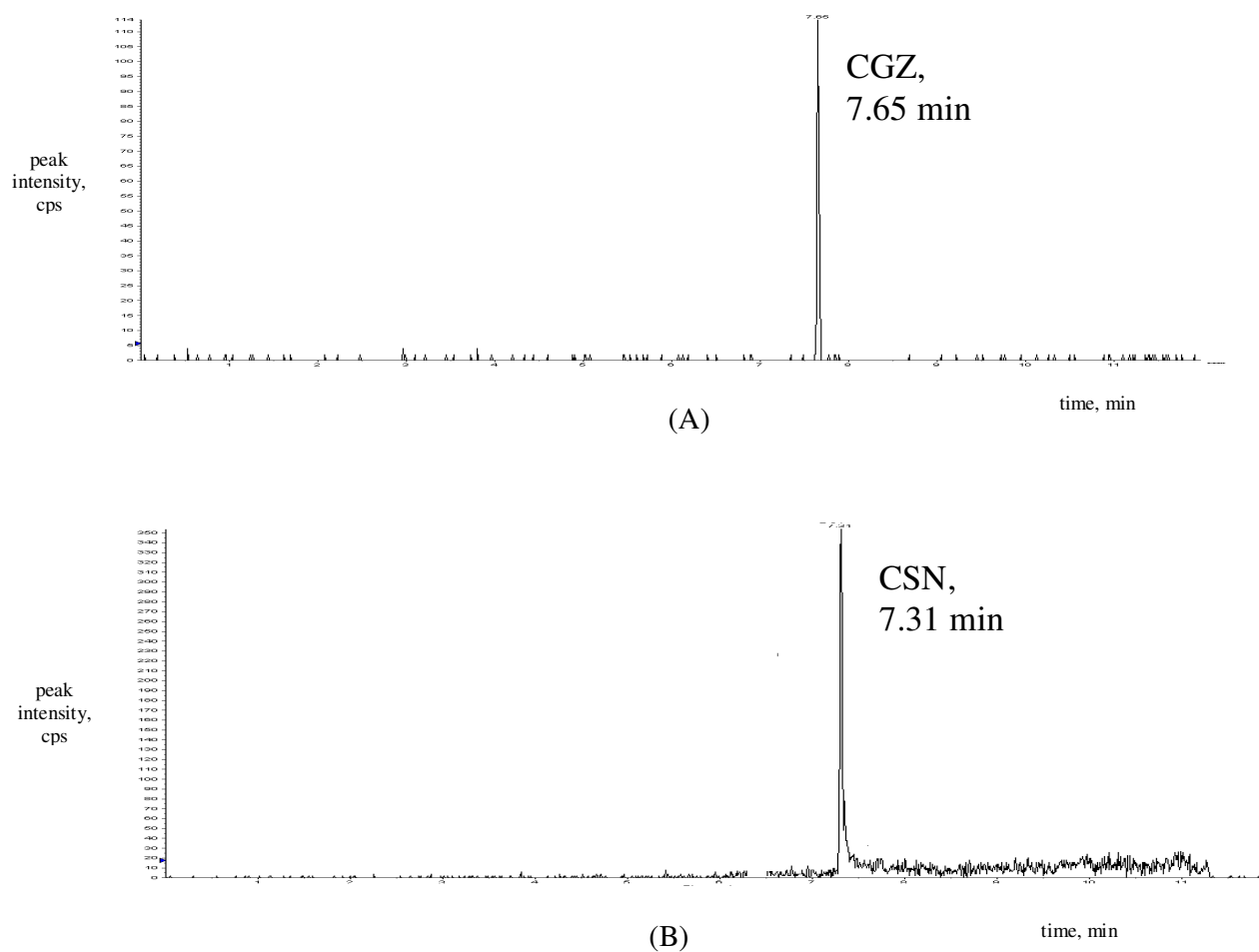


**Fig. 24** Representative LC/MS/MS chromatograms of (A) CGZ (7.65 min) and (D) CSN (7.31 min) in BEGM.

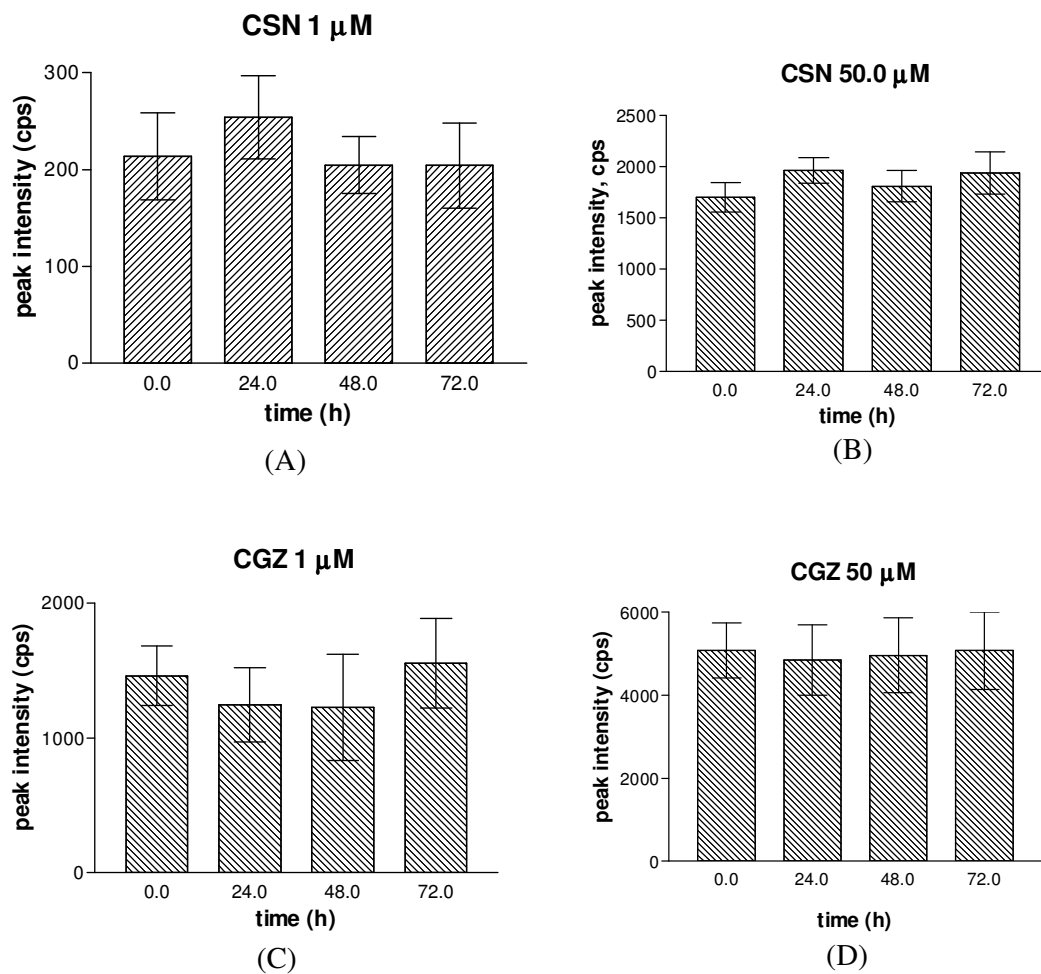


**Fig. 25** Stability studies of CSN at (A) 1 and (B) 50  $\mu$ M, CGZ at (C) 1 and (D) 50  $\mu$ M in BEGM at 37°C up to 72 h (average $\pm$ SD, n=3).

Our stability studies showed that CSN was stable at 1  $\mu$ M (95.32%) (Fig. 25A), and 50  $\mu$ M (113.86%) (Fig. 25B) while CGZ was stable at 1  $\mu$ M (106.49%) (Fig. 25C) and 50  $\mu$ M (99.94%) (Fig. 25D) up to 72 h incubation.

#### 4.4.2 MTT viability assay

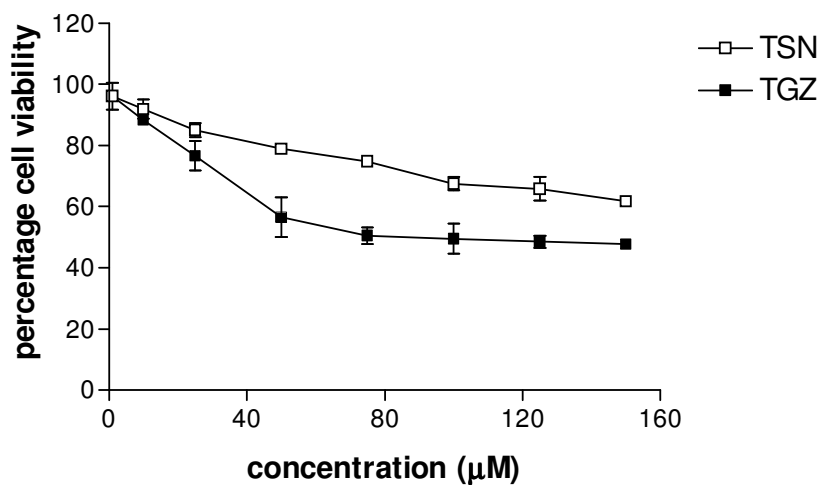
MTT viability assays of the TZD and PRD analogues were performed using THLE-2 cells. The final results regarding MTT assays are described below.

##### 4.4.2.1 MTT viability assay of TGZ and TSN

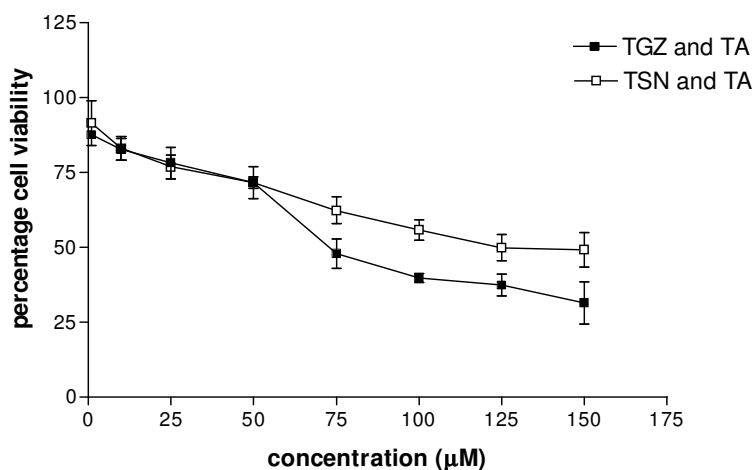
THLE-2 cells were treated with TGZ and TSN at varying concentrations for 72 h. As shown in Fig. 26A, the cell viability of THLE-2 was decreased with increasing concentration of both compounds. Minimal toxicity was observed at 1  $\mu\text{M}$  for both compounds and viability was similar up to 10  $\mu\text{M}$  (90% cell viability). However, the cytotoxic effect was more pronounced for TGZ than TSN from 25  $\mu\text{M}$ , with viability reducing to 50% at 75  $\mu\text{M}$  of TGZ. The calculated  $\text{EC}_{50}$  for TGZ and TSN were  $41.12 \pm 4.3 \mu\text{M}$  and  $138.5 \pm 7.3 \mu\text{M}$ , respectively. Statistical differences were demonstrated between control and test compounds (one-way ANOVA,  $P < 0.05$ ) and between TGZ and TSN (paired T-test,  $P < 0.05$ ) at and above 25 and 50  $\mu\text{M}$  concentration, respectively. Our results further demonstrated that TGZ was more toxic than TSN above 50  $\mu\text{M}$  when TA (antioxidant) was co-incubated at 20  $\mu\text{M}$  level (Fig. 26B). Statistical differences were observed between TGZ and TSN in terms of percentage cell viability at and above 100  $\mu\text{M}$  (paired T-test,  $P < 0.05$ ). The viability of THLE-2 cells was not affected by the presence of TA up to a concentration of 100  $\mu\text{M}$  (data not shown).

##### 4.4.2.2 MTT viability assay of PGZ and PSN

THLE-2 cells were treated with PGZ and PSN at varying concentrations (1–150  $\mu\text{M}$ ) for 72 h. As shown in Fig. 27A, cell viability of the hepatocytes was dose-dependent for both

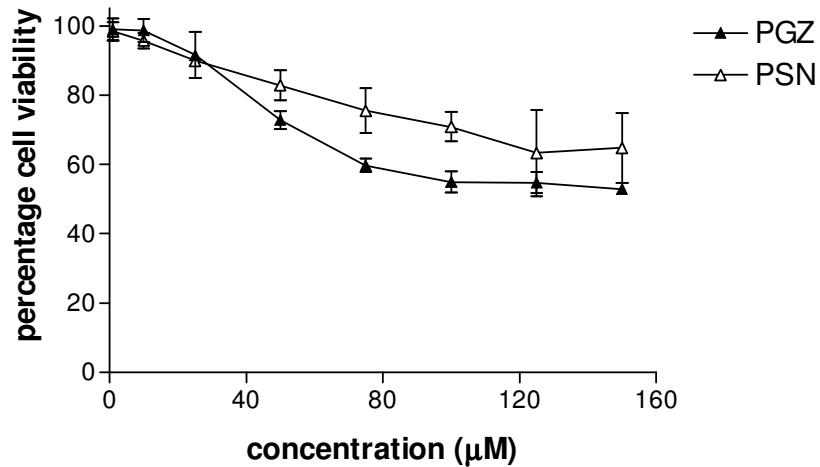


(A)

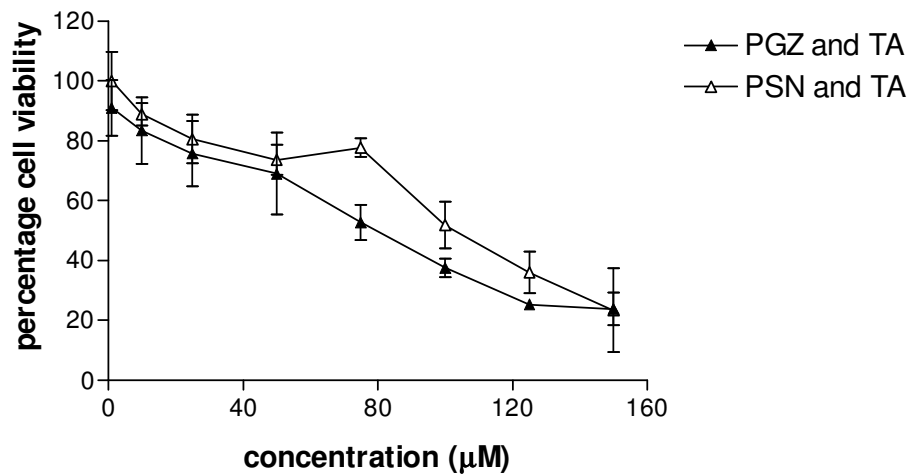


(B)

**Fig. 26** (A) Percentage MTT cell viabilities of THLE-2 cells at varying concentrations of TGZ and TSN. Statistical differences were demonstrated between control and test compounds (one-way ANOVA,  $P < 0.05$ ) and between TGZ and TSN (paired T-test,  $P < 0.05$ ) at and above 25 and 50  $\mu\text{M}$  concentration, respectively. (B) Percentage MTT cell viabilities of THLE-2 cells at varying concentrations of TGZ and TSN co-incubated with 20  $\mu\text{M}$  TA. Statistical differences were observed between TGZ and TSN in terms of percentage cell viability at and above 100  $\mu\text{M}$  (paired T-test,  $P < 0.05$ ).



(A)



(B)

**Fig. 27** (A) Percentage MTT cell viabilities of THLE-2 cells at varying concentrations of PGZ and PSN. Statistical differences were demonstrated between control and test compounds (one-way ANOVA,  $P < 0.05$ ) at and above 50  $\mu\text{M}$  concentration. Statistical differences were also observed between PGZ and PSN (paired T-test,  $P < 0.05$ ) at 50, 75 and 100  $\mu\text{M}$ . (B) Percentage MTT cell viabilities of THLE-2 cells at varying concentrations of PGZ and PSN co-incubated with 20  $\mu\text{M}$  TA. Statistical differences were observed between PGZ and PSN in terms of percentage cell viability at 75, 100 and 125  $\mu\text{M}$  (paired T-test,  $P < 0.05$ ).

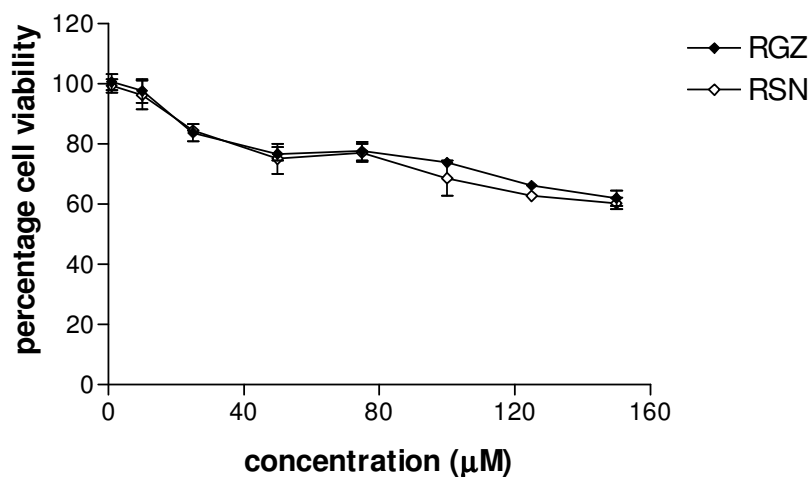
PGZ and PSN where an increase in dose of each test compound was associated with a consistent decline in cell viability. It was shown that when each compound was incubated

with THLE-2 cells, toxicity was observed from 10  $\mu\text{M}$  with respect to control in both cases. However, the observed toxic effect of PGZ was greater than PSN after 10  $\mu\text{M}$ . The THLE-2 cell viability was 50% at 75  $\mu\text{M}$  of PGZ and remained unchanged up to 150  $\mu\text{M}$ . On the other hand, cell viability was 70% at 75  $\mu\text{M}$  of PSN and remained 60 % at and above 100  $\mu\text{M}$  of PSN. The calculated  $\text{EC}_{50}$  for PGZ and PSN were  $77.12 \pm 10.04$  and  $107.22 \pm 20.51$   $\mu\text{M}$ , respectively. Statistical differences were demonstrated between control and test compounds (one-way ANOVA,  $P < 0.05$ ) at and above 50  $\mu\text{M}$  concentration. Statistical differences were also observed between PGZ and PSN (paired T-test,  $P < 0.05$ ) at 50, 75 and 100  $\mu\text{M}$ . To determine whether the increased cytotoxicity of PGZ was linked to oxidative stress, we co-incubated both treatments with the antioxidant, TA. The results further demonstrated that PGZ was more toxic than PSN above 75  $\mu\text{M}$  when the compounds were co-incubated with TA at 20  $\mu\text{M}$  level (Fig. 27B). Statistical differences were observed between PGZ and PSN in terms of percentage cell viability at 75, 100, 125  $\mu\text{M}$  (paired T-test,  $P < 0.05$ ). By comparing Fig. 27A and 27B, it was clear that PGZ produced less toxicity in the presence of TA as compared to PGZ alone. There were no significant differences observed between PSN alone and PSN co-incubation with TA up to 100  $\mu\text{M}$ . This result might be due to the relatively lower oxidative stress effect caused by PSN in THLE-2 cells.

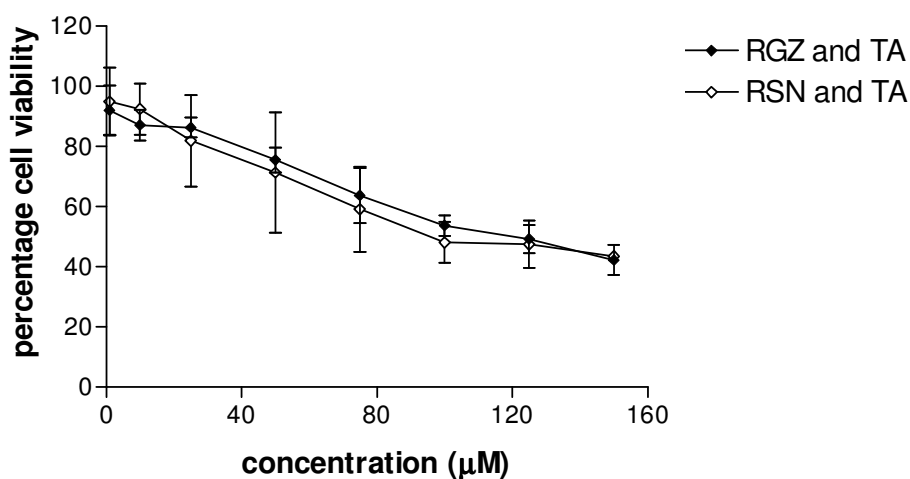
#### 4.4.2.3 MTT viability assay of RGZ and RSN

THLE-2 cells were treated with RGZ and RSN at various concentrations (1–150  $\mu\text{M}$ ) for 72 h. It was shown that the cell viabilities were decreased according to the increase of incubated concentrations of both compounds. Both compounds showed significant decrease in viability at and above 25  $\mu\text{M}$  with respect to control whereas there was no significant statistical difference observed between them up to 150  $\mu\text{M}$  (Fig. 28A). Statistical differences

were demonstrated between control and test compounds (one-way ANOVA,  $P < 0.05$ ) at and above 25  $\mu\text{M}$  concentration. There were no significant differences observed when the compounds were co-incubated with TA at 20  $\mu\text{M}$  concentration (Fig. 28B).



(A)



(B)

**Fig. 28** (A) Percentage MTT cell viabilities of THLE-2 cells at varying concentrations of RGZ and RSN. Statistical differences were demonstrated between control and test compounds (one-way ANOVA,  $P < 0.05$ ) at and above 25  $\mu\text{M}$  concentration. (B) Percentage MTT cell viabilities of THLE-2 cells at varying concentrations of RGZ and RSN co-incubated with 20  $\mu\text{M}$  TA.

#### 4.4.2.4 MTT viability assay of CGZ and CSN

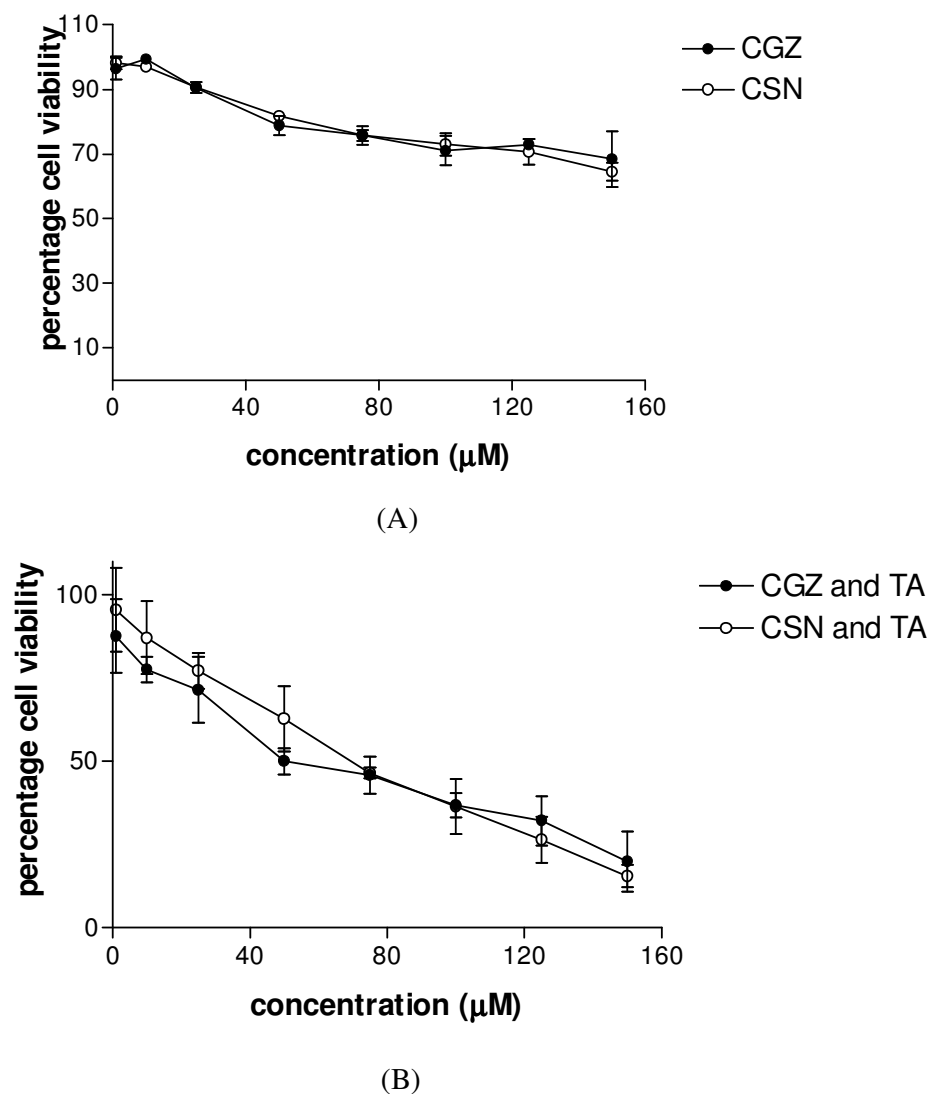


**Fig. 29** (A) Percentage MTT cell viabilities of THLE-2 cells at varying concentrations of CGZ and CSN. Statistical differences were demonstrated between control and test compounds (one-way ANOVA,  $P < 0.05$ ) at and above 25  $\mu\text{M}$  concentration. (B) Percentage MTT cell viabilities of THLE-2 cells at varying concentrations of CGZ and CSN co-incubated with 20  $\mu\text{M}$  TA.

THLE-2 cells were treated with CGZ and CSN at various concentrations (1–150  $\mu\text{M}$ ) for 72 h. It was shown that the cell viabilities were decreased according to the increase of



incubated concentrations for both these compounds. Both compounds showed significant decrease in viability at and above 25  $\mu\text{M}$  with respect to control whereas there was no significant statistical difference observed between them up to 150  $\mu\text{M}$  (Fig. 29A). Statistical differences were demonstrated between control and test compounds (one-way ANOVA,  $P < 0.05$ ) at and above 25  $\mu\text{M}$  concentration. There were no significant differences observed when the compounds were co-incubated with TA at 20  $\mu\text{M}$  concentration (Fig. 29B).

#### 4.4.3 GSH depletion assay

Determination of GSH-NEM was performed in THLE-2 cells after 72 h incubation with the TZD and PRD analogues at varying concentrations (1–150  $\mu\text{M}$ ). A linear regression performed over a range of 0.001 to 10  $\mu\text{M}$  yielded a correlation coefficient ( $r^2$ ) of 0.9985 to 0.9999. The accuracy of the assay was found to be within 80 to 108%. The percentage recoveries of the GSH-NEM complex in QC samples were 60 to 80%. The retention time for GSH-NEM complex was 3.13 min (Fig. 30). The GSH depletion capacities of TZD and PRD analogues are described below.

##### 4.4.3.1 GSH depletion assay of TGZ and TSN

The GSH depletion ( $\mu\text{M}$ ) per  $\mu\text{g}$  of protein was measured at varying concentrations of TGZ and TSN after 72 h. TGZ depleted more GSH than TSN after 50  $\mu\text{M}$ . According to Fig. 31, it was seen that TGZ depleted more GSH than TSN from 1 to 150  $\mu\text{M}$ . The GSH-NEM concentration of  $2.0 \times 10^4$  cells/well was  $\sim 9$  to 2  $\mu\text{M}$  per  $\mu\text{g}$  of protein in case of TGZ whereas GSH-NEM concentration was higher  $\sim 9$  to 4  $\mu\text{M}$  per  $\mu\text{g}$  of protein for TSN from 1 to 150  $\mu\text{M}$  concentrations. Statistical differences were demonstrated between control and test

compounds (one-way ANOVA,  $P < 0.05$ ) and between TGZ and TSN (paired T-test,  $P < 0.05$ ) at and above 25 and 75  $\mu\text{M}$ , respectively.

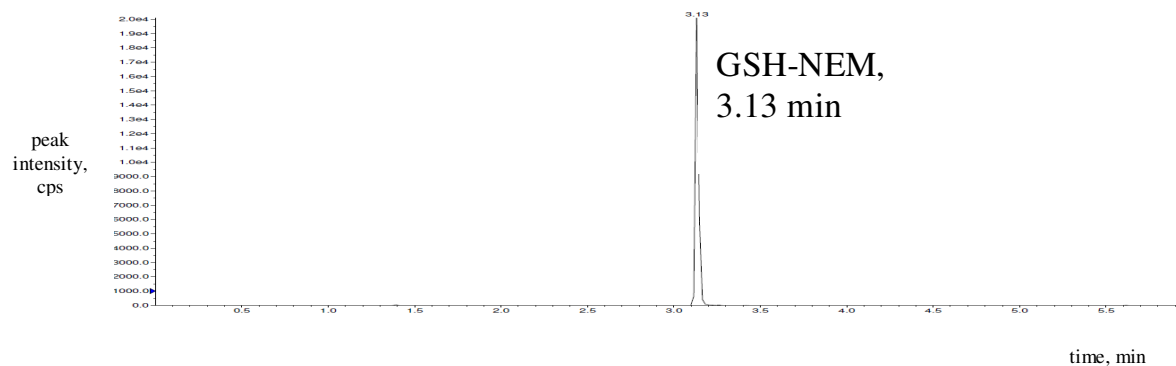


**Fig. 30** Representative LC/MS/MS chromatogram of GSH-NEM complex (3.13 min).

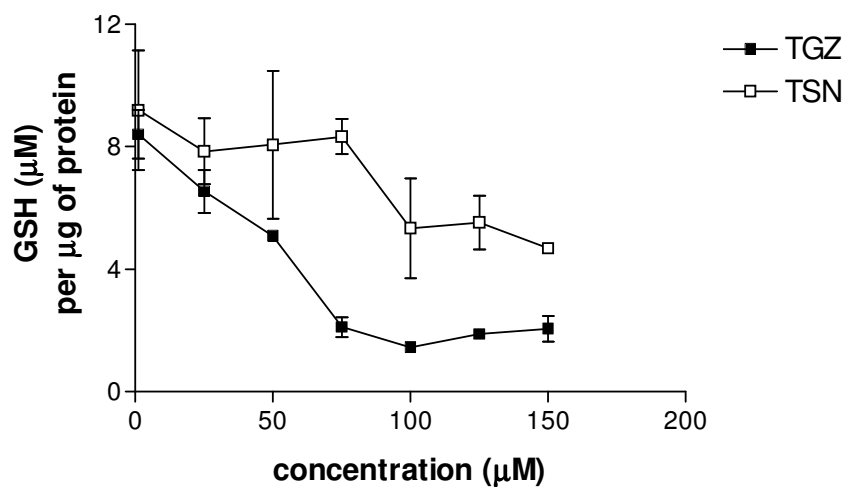


**Fig. 31** GSH depletion in THLE-2 cells at varying concentrations of TGZ and TSN. Statistical differences were demonstrated between control and test compounds (one-way ANOVA,  $P < 0.05$ ) and between TGZ and TSN (paired T-test,  $P < 0.05$ ) at and above 25 and 75  $\mu\text{M}$ , respectively.

#### 4.4.3.2 GSH depletion assay of PGZ and PSN

Determination of GSH-NEM adducts was performed in THLE-2 cells after 72 h incubation with PGZ and PSN (Fig. 32). PGZ depleted more GSH than PSN after 25  $\mu\text{M}$  concentration. The total GSH-NEM concentration was  $\sim 7$  to 1  $\mu\text{M}$  per  $\mu\text{g}$  of protein for PGZ whereas it was  $\sim 7$  to 2.5  $\mu\text{M}$  per  $\mu\text{g}$  of protein for PSN from 1 to 150  $\mu\text{M}$ . Statistical differences were demonstrated between control and test compounds (one-way ANOVA,  $P < 0.05$ ) at and above 25  $\mu\text{M}$ . Statistical differences were also observed between PGZ and PSN (paired T-test,  $P < 0.05$ ) from 25 to 100  $\mu\text{M}$ .

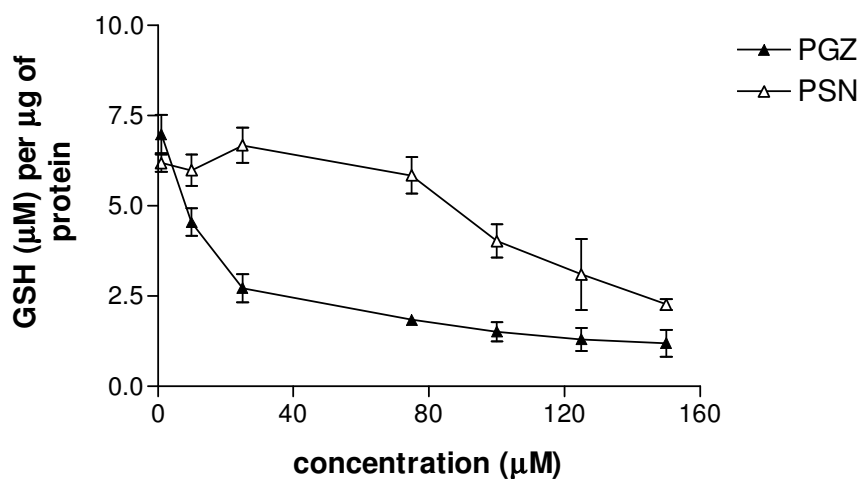


**Fig. 32** GSH depletion in THLE-2 cells at varying concentrations of PGZ and PSN. Statistical differences were demonstrated between control and test compounds (one-way ANOVA,  $P < 0.05$ ) at and above 25  $\mu\text{M}$ . Statistical differences were also observed between TGZ and TSN (paired T-test,  $P < 0.05$ ) from 25 to 100  $\mu\text{M}$ .

#### 4.4.3.3 GSH depletion assay of RGZ and RSN

Determination of GSH-NEM adducts was performed in THLE-2 cells after 72 h incubation with RGZ and RSN (Fig. 33). RGZ depleted more GSH than RSN at concentration greater than 25  $\mu\text{M}$ . RSN showed no toxicity up to 100  $\mu\text{M}$  with respect to control. The concentration of GSH-NEM was  $\sim 6$  to 5  $\mu\text{M}$  per  $\mu\text{g}$  of protein for RSN whereas its concentration was  $\sim 6$  to 1.5  $\mu\text{M}$  per  $\mu\text{g}$  of protein for RGZ from 1 to 150  $\mu\text{M}$ . Statistical differences were demonstrated between control and test compounds (one-way ANOVA,  $P < 0.05$ ) and between RGZ and RSN (paired T-test,  $P < 0.05$ ) at and above 100 and 25  $\mu\text{M}$ , respectively.

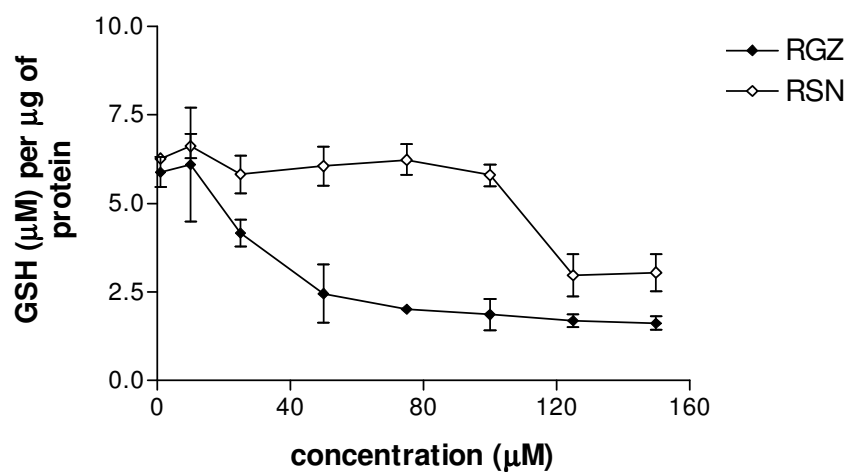


**Fig. 33** GSH depletion in THLE-2 cells at varying concentrations of RGZ and RSN. Statistical differences were demonstrated between control and test compounds (one-way ANOVA,  $P < 0.05$ ) and between RGZ and RSN (paired T-test,  $P < 0.05$ ) at and above 100 and 25  $\mu\text{M}$ , respectively.

#### 4.4.3.4 GSH depletion assay of CGZ and CSN

The GSH depletion ( $\mu\text{M}$ ) per  $\mu\text{g}$  of protein was measured at varying concentrations of CGZ and CSN after 72 h (Fig. 34). CGZ depleted more GSH than CSN after 25  $\mu\text{M}$ . There were no differences in terms of GSH depletion observed after 75  $\mu\text{M}$  concentration for both CGZ and CSN. Statistical differences were demonstrated between control and test compounds (one-way ANOVA,  $P < 0.05$ ) at and above 25  $\mu\text{M}$ . Statistical differences were observed between CGZ and CSN at 10, 25 and 50  $\mu\text{M}$  (paired T-test,  $P < 0.05$ ).

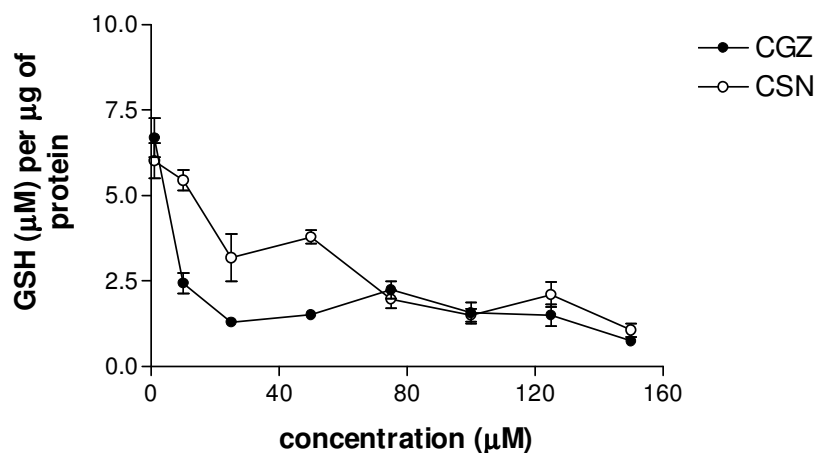


**Fig. 34** GSH depletion in THLE-2 cells at varying concentrations of CGZ and CSN. Statistical differences were demonstrated between control and test compounds (one-way ANOVA,  $P < 0.05$ ) at and above 25  $\mu\text{M}$ . Statistical differences were observed between CGZ and CSN at 10, 25 and 50  $\mu\text{M}$  (paired T-test,  $P < 0.05$ ).

#### 4.4.4 PC assay

Finally, we performed PC assay to elucidate the mechanism of toxicity of the TZD and PRD analogues using 2,4-dinitrophenylhydrazine as a derivatizing reagent. The results related to the PC assay are described below.

#### 4.4.4.1 PC assay of TGZ and TSN

Determination of PC was performed in THLE-2 cells after 48 h incubation of TGZ and TSN. For each compound, PC ( $\mu\text{M}$ ) per  $\mu\text{g}$  of protein of THLE-2 cells was increased from 10  $\mu\text{M}$  of each test compound with respect to control. Significant difference in PC of THLE-2 cells was observed at 50  $\mu\text{M}$  between TGZ and TSN (Fig. 35). Statistical differences were demonstrated between control and test compounds (one-way ANOVA,  $P < 0.05$ ) and between TGZ and TSN (paired T-test,  $P < 0.05$ ) at 50  $\mu\text{M}$ .

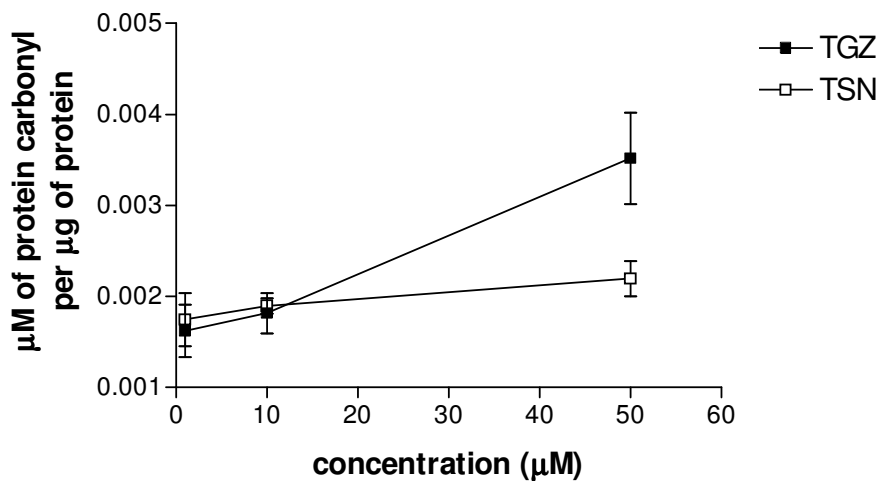


**Fig. 35** PC assay of THLE-2 cells at varying concentrations of TGZ and TSN. Statistical differences were demonstrated between control and test compounds (one-way ANOVA,  $P < 0.05$ ) and between TGZ and TSN (paired T-test,  $P < 0.05$ ) at 50  $\mu\text{M}$ .

#### 4.4.4.2 PC assay of PGZ and PSN

For each compound, PC ( $\mu\text{M}$ ) per  $\mu\text{g}$  of protein of THLE-2 cells was increased from 10  $\mu\text{M}$  of each test compound with respect to control. Statistical differences were observed between PGZ and PSN at 1 and 50  $\mu\text{M}$  (paired T-test,  $P < 0.05$ ) (Fig. 36). Statistical

differences were demonstrated between control and test compounds (one-way ANOVA,  $P < 0.05$ ) at 50  $\mu\text{M}$ .

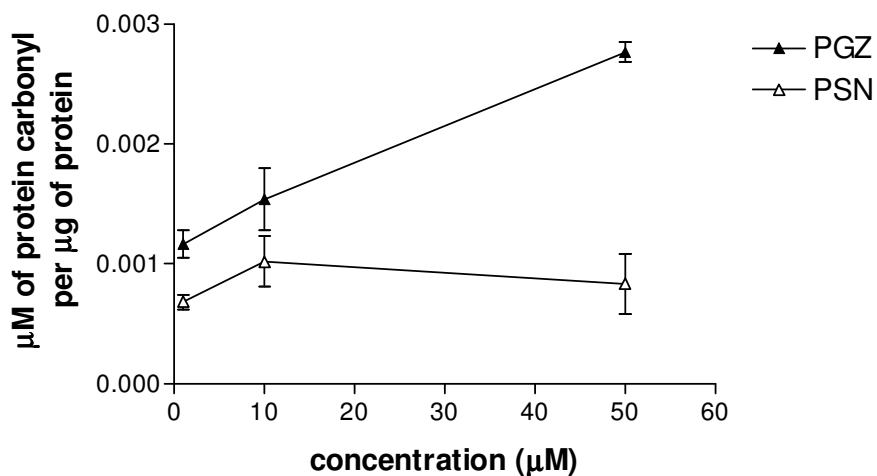


**Fig. 36** PC assay of THLE-2 cells at varying concentrations of PGZ and PSN. Statistical differences were demonstrated between control and test compounds (one-way ANOVA,  $P < 0.05$ ) at 50  $\mu\text{M}$ . Statistical differences were observed between PGZ and PSN at 1 and 50  $\mu\text{M}$  (paired T-test,  $P < 0.05$ ).

#### 4.4.4.3 PC assay of RGZ and RSN

Determination of PC was performed in THLE-2 cells after 48 h incubation of RGZ and RSN. Statistical difference was demonstrated between RGZ and RSN (paired T-test,  $P < 0.05$ ) at 50  $\mu\text{M}$  (Fig. 37).

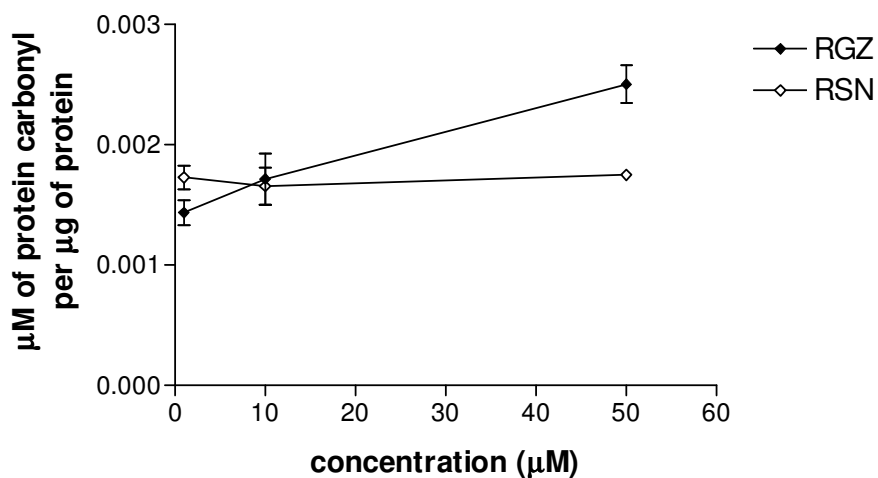


**Fig. 37** PC assay of THLE-2 cells at varying concentrations of RGZ and RSN. Statistical difference was demonstrated between RGZ and RSN (paired T-test,  $P < 0.05$ ) at 50  $\mu\text{M}$ .

#### 4.4.4.4 PC assay of CGZ and CSN

Determination of PC was performed in THLE-2 cells after 48 h incubation of CGZ and CSN. For each compound, PC ( $\mu\text{M}$ ) per  $\mu\text{g}$  of protein of THLE-2 cells was increased from 10  $\mu\text{M}$  with respect to control. Statistical difference was observed between CGZ and CSN at 10  $\mu\text{M}$  (paired T-test,  $P < 0.05$ ) (Fig. 38) but no difference was observed at 50  $\mu\text{M}$ . Statistical differences were demonstrated between control and test compounds (one-way ANOVA,  $P < 0.05$ ) at 50  $\mu\text{M}$ .



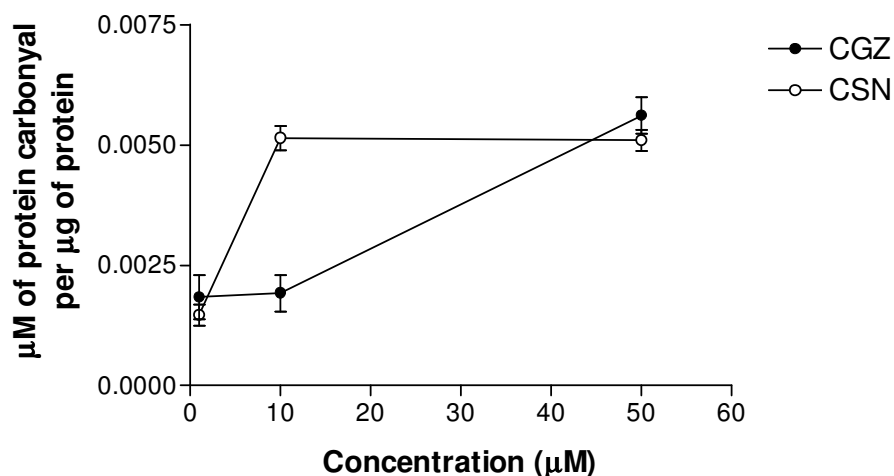


**Fig. 38** PC assay of THLE-2 cells at varying concentrations of CGZ and CSN. Statistical differences were demonstrated between control and test compounds (one-way ANOVA,  $P < 0.05$ ) at 50  $\mu\text{M}$ . Statistical differences were observed between CGZ and CSN at 10  $\mu\text{M}$  (paired T-test,  $P < 0.05$ ).

#### 4.5 Discussion

Effective usage of the TGZ as an antidiabetic agent is limited due to severe liver toxicity. Preliminary evidence suggested that the sulfur moiety of the TZD ring might contribute as both a toxicophore and pharmacophore. However, a more detailed characterization is required to determine the relative contribution of the sulfur moiety to toxicity, so as to optimize the clinical usage of existing TZD drugs. In this chapter, we attempt to address this issue by comparing the toxic effects of the TZD and PRD analogues.

First, we performed independent stability study on each TZD and PRD analogues in BEGM up to 72 h. While some succinimide derivatives may be chemically unstable in aqueous solution, our data confirmed that the PRD analogues were stable up to 72 h in BEGM. It was demonstrated that the TZD analogues were also stable up to 72 h in BEGM.

The establishment of the chemical stability of the TZD and PRD analogues in BEGM at 37°C was important to support the result and conclusion of all the subsequent experiments.

To link the formation of RMs to the onset of toxicity, we performed MTT cell viability assay of both TZD and PRD analogues on the same human hepatocyte cell line, THLE-2, that is metabolically-active (Andrea et al., 1993). We had previously demonstrated the generation of RMs in THLE-2 cells by the TZD analogues. Consistently, the results in this chapter indicated that TGZ and PGZ were more toxic in THLE-2 cells than TSN and PSN. Collectively, this was an indirect indication that the sulfur moiety of TGZ and PGZ might be partially responsible for liver toxicity in humans. On the other hand, there were no significant differences observed between RGZ and RSN, CGZ and CSN in terms of cell viability.

The next question arose whether TZD analogues exerted any oxidative stress in the biological system. To address this question, we further performed MTT assay by co-incubating 20  $\mu$ M TA (antioxidant) with both the TZD and PRD analogues at various concentrations in THLE-2 cells. By comparing Fig. 25A and 25B, it was clear that TGZ produced less toxicity in the presence of TA as compared to TGZ alone. The viabilities of THLE-2 cells were 50 and 75% in the absence and presence of TA at 50  $\mu$ M of TGZ, respectively. This might be due to the antioxidant effect of TA which acted as a scavenger for potential free radical oxygen species in cells. However, the effect was reversed at higher concentrations. On the other hand, the cell viability of THLE-2 cells, when incubated with TSN, was clearly less altered in the presence and absence of TA.

In another experiment, the results further demonstrated that PGZ was more toxic than PSN above 75  $\mu$ M when the compounds were co-incubated with TA at 20  $\mu$ M (Fig. 26B). By comparing Fig. 26A and 26B, it was clear that PGZ produced less toxicity in the presence of TA as compared to PGZ alone. There was no significant difference observed between PSN

alone and PSN co-incubated with TA up to 100  $\mu$ M. This result was possibly due to the comparatively lower oxidative stress effect of PSN on THLE-2 cells.

Our MTT and RM profiling data collectively suggested that TGZ and PGZ exerted oxidative stress on the THLE-2 cells via reactive intermediate formation. On the other hand, no significant statistical differences were observed between the other TZD and PRD analogues (RGZ and RSN, CGZ and CSN) in the presence or absence of antioxidant. This was not unexpected as was previously mentioned that there were no significant differences observed between RGZ and RSN, CGZ and CSN in terms of THLE-2 cell viability.

To further correlate RM formation and toxicity, we performed GSH depletion assay using NEM as a derivatizing reagent. Our GSH depletion assay demonstrated that the TZD analogues depleted more GSH than the PRD analogues as expected. Using this biochemical measurement, we further explained the greater toxicity generated by the TZD analogues as compared to their PRD counterparts. Depletion of GSH could either be due to a direct effect from the adduction of GSH by reactive intermediates or an indirect effect of oxidative stress (perhaps due to mitochondrial dysfunction) resulting in more oxidized GSSG formation. While the GSH experiments performed here could not differentiate between these two possibilities, our early finding from the MTT assay using TA suggested that TGZ and PGZ exerted greater oxidative stress to the human hepatocytes than TSN and PSN. Similarly, RGZ and CGZ depleted more GSH as compared to RSN and CSN, respectively, in our GSH depletion assay. Collectively, our GSH depletion assay demonstrated that the TZD analogues possessed greater GSH depletion capacities than the PRD analogues in THLE-2 cells and explained why the TZD analogues produced more toxicity than their PRD counterparts. To further confirm the occurrence of oxidative stress, we performed PC assay which demonstrated that the TZD analogues generated greater oxidative stress than the PRD

analogues. Collectively, oxidative stress appeared to be one likely cause of TZD antidiabetic drugs in inducing liver toxicity via reactive intermediate formation.

In the following chapter, we shall explore the pharmacological testing of the TZD and PRD analogues with regards to PPAR<sub>γ</sub> binding and ap2 gene expression.

## Chapter 5

### PPAR<sub>γ</sub> binding and ap2 gene expression assays

#### 5.1 Introduction

The sulfur moiety of the TZD ring is an important pharmacophore for the PPAR<sub>γ</sub> ligand. This moiety is also partially responsible for hepatotoxicity in humans as confirmed in the prevailing chapters of my thesis. Therefore, it becomes important to elucidate whether the substitution of the sulfur moiety with the methylene moiety has any direct effect on the binding and activation of the PPAR<sub>γ</sub>. The PPAR<sub>γ</sub> is a transcription factor which is expressed during glucose and lipid metabolism (Zhang et al., 1992; Kliewer et al., 1992). The PPAR<sub>γ</sub>-TZD agonist has no direct effect on insulin formation and secretion. They reduce blood glucose and triglyceride levels by partially binding to PPAR<sub>γ</sub> in adipocytes (Grossman et al., 1997). It was demonstrated that the ap2 gene was expressed in 3T3-L1 cells, a cell line that had similar morphological and biochemical pattern like human adipocytes (Kliewer et al., 1992). PGZ and RGZ were shown to increase the expression of the aP2 gene in adipocytes which was a region of the PPAR<sub>γ</sub> binding site (Lehmann et al., 1995; Forman et al., 1995).

In this chapter, we aimed to compare the PPAR<sub>γ</sub> binding affinities of both the TZD and the PRD analogues. Finally, we performed the aP2 gene expression assay which served as a robust indicator of pharmacological activity of the PRD analogues.

#### 5.2 Materials

Polarscreen<sup>TM</sup> PPAR<sub>γ</sub> competitor red assay kit (with PPAR<sub>γ</sub>-LBD) and superscript<sup>®</sup> III reverse transcriptase assay kit were purchased from Invitrogen Pte Ltd, Singapore. 3T3-L1

cell line was purchased from ATCC (Manassas, VA, USA). Microcon YM-30 centrifugal filters was purchased from Millipore, Singapore. Methyl tert-butyl ether (MTBE), insulin, gentamicin, triazole reagent, dichloromethane (cell culture grade) were purchased from Sigma-Aldrich (Saint Louis, MO, USA). Dullbecco's modified eagle's media (DMEM) was purchased from the National University Medical Store, Singapore. Ribonuclease free water, betaine, 10× hot start buffer, magnesium sulfate buffer and hot start DNA polymerase were purchased from 1<sup>st</sup> Base, Singapore. RNeasy mini kit was purchased from Qiagen, Singapore. Sybr<sup>®</sup> green master mix was purchased from Applied Biosystems (Foster city, USA).

### *5.3 Methods*

#### *5.3.1 PPAR<sub>γ</sub> binding assay*

##### *5.3.1.1 PPAR<sub>γ</sub> incubation conditions*

PPAR<sub>γ</sub> binding assay was performed using Polarscreen<sup>™</sup> PPAR<sub>γ</sub> competitor red assay kit. In brief, 50 μL of various concentrations of the substrates (both TZD and PRD analogues) and 50 μL of PPAR<sub>γ</sub>-LBD were transferred into 384-well plates (black) and co-incubated in the dark at 37°C. After 24 h, the free unbound drug was extracted using the Microcon YM-30 centrifugal filters (Millipore) via centrifugation at 14,000 rpm for 15 min. 90 μL each of the filtrate was transferred into a clean 1.5 mL microcentrifuge tube and 1 mL of MTBE was added. This mixture was vortexed at high speed for 1 min followed by centrifugation at 13,000 rpm for 5 min. The MTBE layer was removed and evaporated to dryness at 35°C for 1 h under a gentle flow of nitrogen gas using Turbovap LV. The dried residue was reconstituted with 50 μL of methanol, vortex-mixed and centrifuged at 13,000

rpm for 2 min. 5  $\mu$ L of the supernatant was subjected to UPLC/MS/MS analysis. 0 h ( $t_0$ ) sample was prepared by adding compounds and PPAR $_{\gamma}$ -LBD and immediately removing it for filtration via centrifugation. All samples were prepared in triplicates.

#### *5.3.1.1 LC/MS/MS conditions*

For PPAR $_{\gamma}$  binding assay, the LC experimental setup was similar to that we used for the profiling of RM-GSH conjugates (Chapter 3). MRM transitions of the TZD and PRD analogues (similar to that of the stability studies) were performed in the ESI- and ESI+ mode for the PPAR $_{\gamma}$  binding assays (Chapter 4). The MS conditions are summarized in Tables 3 and 4. For the PPAR $_{\gamma}$  assays, all chromatographic peak area integrations were performed using the Analyst Software version 1.4.2 and analyzed statistically using GraphPad Prism 4. Statistical differences were analyzed using paired T-test and  $P < 0.05$  represented statistically significant data.

#### *5.3.2 aP2 gene expression assay*

##### *5.3.2.1 3T3-L1 cells*

3T3-L1 cells were maintained in the logarithmic growth phase in DMEM supplemented with 10% fetal bovine serum and 25  $\mu$ g/mL gentamicin, in humidified air with 5% CO $_2$  at 37°C (according to ATCC guidelines).  $1 \times 10^6$  cells/well were seeded in a 10 cm petridish and pre-incubated with 5  $\mu$ g/mL of insulin in DMEM for 24 h. The medium was aspirated on the following day and 10 mL of 50  $\mu$ M of each test compound in DMEM spiked with 5  $\mu$ g/mL of insulin was added and incubated for another 4 days. The medium was

replaced every alternate day. Cells containing media with insulin but without test compound was employed as control. At the end of the incubation period, the cells were washed with ice-cold phosphate buffer saline and collected by scraping. Cell pellets were collected by centrifuging at 6000 rpm for 1 min at 4°C. Total ribonucleic acid (RNA) were isolated for ap2 gene expression assay.

#### 5.3.2.2 RNA isolation, PCR and qRT-PCR

Total RNA was isolated from the 3T3-L1 cultured cells by using TriZol reagent and RNeasy mini kit. Complementary de-oxyribonucleic acid (cDNA) was prepared from this total RNA according to the protocol of reverse transcript system using superscript<sup>®</sup> III reverse transcriptase assay kit for RT-PCR.

qRT-PCR was performed using the ABI system (7500 series, Applied Biosystems, Foster City, USA) and syber<sup>®</sup> green PCR master mix. The total volume of reaction mixture was 20 µL which contained 2 µL forward and reverse primer in each case (10 µM), 4 µL of cDNA (1:10 dilution using ribonuclease free water), 2 µL of ribonuclease free water and 10 µL of master mix. The cycle program for qRT-PCR was 50°C for 2 min, 95°C for 10 min, 95°C for 15 sec (repeat 40 times), 60°C for 1 min, 95°C for 0.15 sec (repeat 1 sec), 60°C for 1 min and 95°C for 0.15 min. The amount of messenger RNA (mRNA) for each ap2 gene was normalized according to the amount of mRNA encoding β-actin and calculated in terms of ΔCt values. ΔCt values were normalized with non-treated control samples for all compounds.

$$\Delta Ct = Ct_{\text{gene of interest}} - Ct_{\text{reference gene } (\beta\text{-actin})}$$



The reference mRNA was stable throughout the experiment. Relative changes in the expression level of one specific gene were calculated in terms of ( $\Delta\Delta Ct$ ) and then presented as  $2^{-\Delta\Delta Ct}$  (Rebeca et al., 2008).

$$\Delta\Delta Ct = \Delta Ct_{\text{test}} - \Delta Ct_{\text{control}}$$

The primer sequences were as follows:  $\beta$ -actin, 5'-GATCTGGCACCACCTTCT-3' (forward) and 5'-GGGGTGTGTAAGGTCTCAA-3' (reverse); ap2, 5'-CAACCTGTGTGATGCCTTTGTG-3' (forward) and 5'-CTCTCCCTTTGGCTCATGCC-3' (reverse) (Choi et al., 2009).

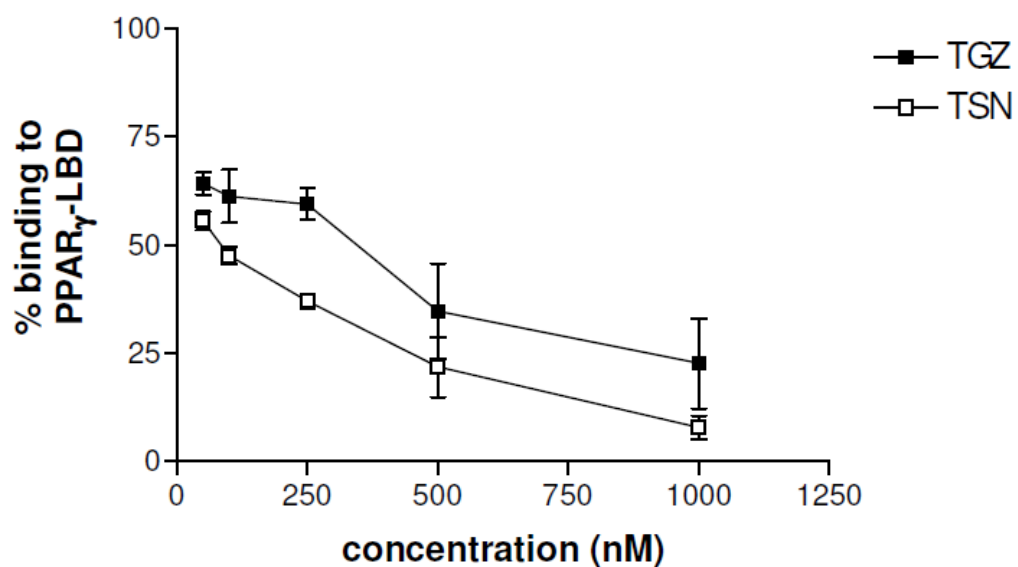
For the ap2 gene expression assay, the generated data were analyzed using the 7500 system SDS Software version 1.2.3 (Applied Biosystems, Foster City, CA, USA) and analyzed statistically using GraphPad Prism 4. Statistical differences were analyzed using paired T-test and  $P < 0.05$  represented statistically significant data.

## 5.4 Results

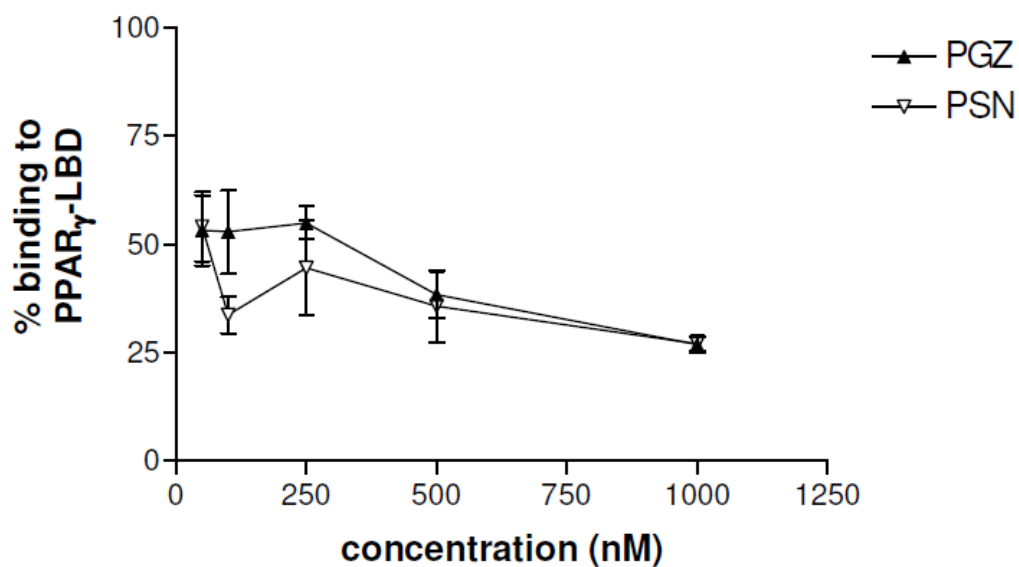
### 5.4.1 PPAR $\gamma$ binding assay

PPAR $\gamma$  binding assay was performed to evaluate the binding affinities of both the TZD and PRD analogues using LC/MS/MS. Determination of both compounds in PPAR $\gamma$ -LBD samples were performed at 0 and 24 h. PPAR $\gamma$ -LBD-drug stable complex was formed in the incubated mixture such that the free drug concentration in the incubated mixture decreased over time. The % binding to PPAR $\gamma$ -LBD was calculated based on the following equation:

$$\frac{\text{Peakarea}(0h) - \text{Peakarea}(24h)}{\text{Peakarea}(0h)} \times 100\%$$

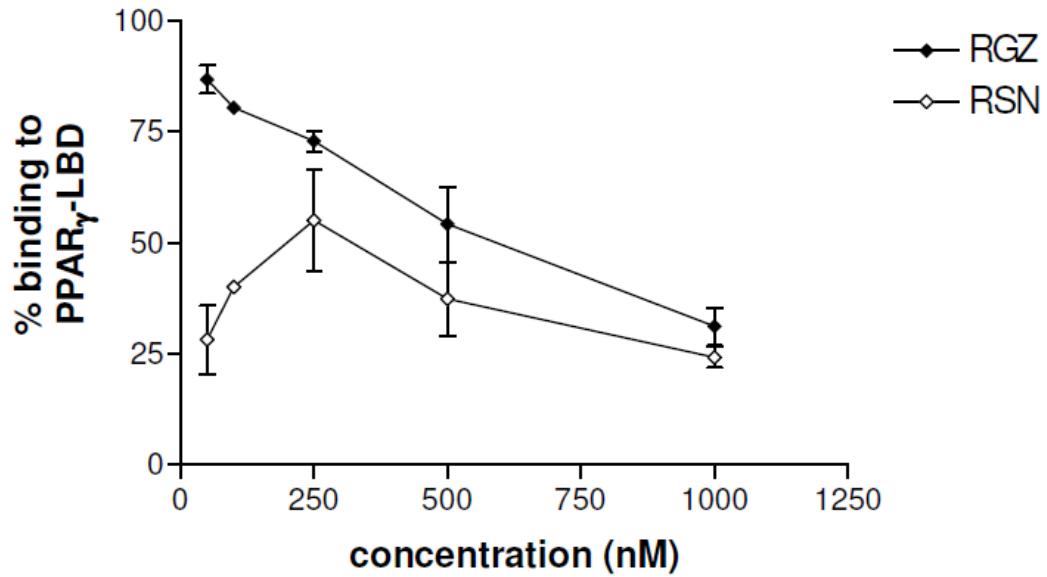


(A)

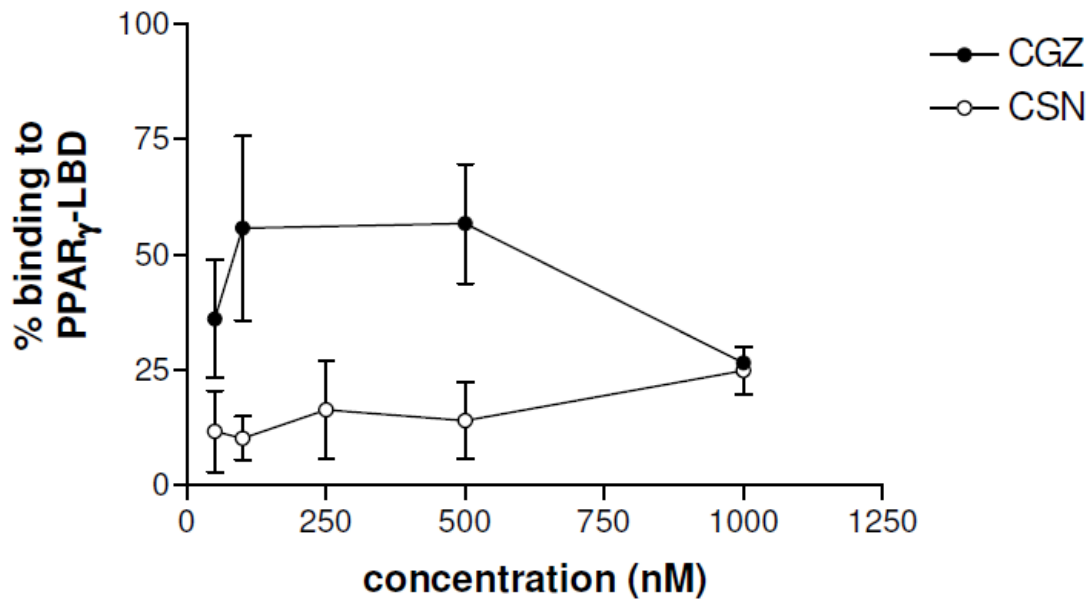


(B)

**Fig. 39** (A) Percentage binding to PPAR<sub>γ</sub>-LBD at varying concentrations of TGZ and TSN. Statistical differences were observed between TGZ and TSN in terms of percentage binding to PPAR<sub>γ</sub>-LBD at and above 50 nM (paired T-test, P<0.05). (B) Percentage binding to PPAR<sub>γ</sub>-LBD at varying concentrations of PGZ and PSN. Statistical differences were observed between PGZ and PSN in terms of percentage binding to PPAR<sub>γ</sub>-LBD at 100 nM (paired T-test, P<0.05).



(A)



(B)

**Fig. 40** (A) Percentage binding to PPAR<sub>γ</sub>-LBD at varying concentrations of RGZ and RSN. Statistical differences were observed between RGZ and RSN in terms of percentage binding to PPAR<sub>γ</sub>-LBD at 50 and 100 nM (paired T-test, P<0.05). (B) Percentage binding to PPAR<sub>γ</sub>-LBD at varying concentrations of CGZ and CSN. Statistical differences were observed between CGZ and CSN in terms of percentage binding to PPAR<sub>γ</sub>-LBD at 500.0 nM (paired T-test, P<0.05).

As shown in Fig. 39A, TGZ showed higher % binding than TSN at and above 100 nM. Statistical differences were observed between TGZ and TSN in terms of % binding to PPAR<sub>γ</sub>-LBD to PPAR<sub>γ</sub> at and above 50 nM (paired T-test, P<0.05).

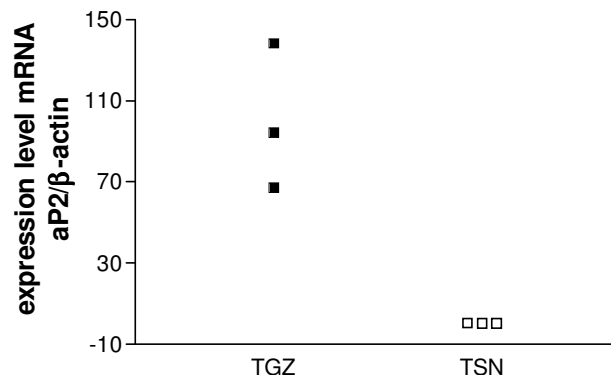
According to Fig. 39B, it was shown that PGZ had higher % binding than PSN at 100 and 250 nM. Statistical differences were observed between PGZ and PSN in terms of % binding to PPAR<sub>γ</sub>-LBD at 100 nM (paired T-test, P<0.05).

RGZ had higher % binding than RSN at and above 50 nM (Fig. 40A). Statistical differences were observed between RGZ and RSN in terms of % binding to PPAR<sub>γ</sub>-LBD at 50 and 100 nM (paired T-test, P<0.05). According to Fig. 40B, it was shown that CGZ had % higher binding than CSN at and above 250 nM. Statistical differences were observed between CGZ and CSN in terms of % binding to PPAR<sub>γ</sub>-LBD at 500 nM (paired T-test, P<0.05).

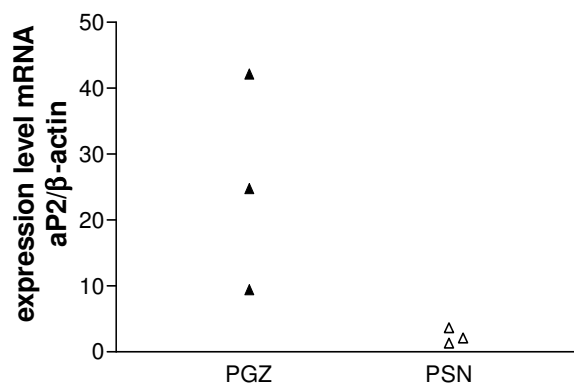
#### 5.4.2 *aP2 gene expression assay*

The *aP2* gene expression of the TZD analogues was higher than the PRD analogues at 50 μM concentration in 3T3-L1 cells (Fig. 41 and 42). Although the differences in mRNA expressions of the *aP2* gene between the TZD and PRD analogues, except TGZ and TSN (P<0.05), were not statistically significant (P>0.05), it was clear from our results (Fig. 41 and 42) that the mean mRNA expression levels between these two chemical classes were distinctively different. Consistently, the TZD analogues led to a greater expression of the *aP2* gene compared to the PRD analogues. A similar trend was observed between TGZ and TSN as well (Table 7).

Importantly, we confirmed that the PRD analogues could bind to the PPAR<sub>γ</sub> ligand to exert its pharmacological activity indicated by the expression of *aP2* gene



(A)



(B)

**Fig. 41** (A) Relative amount of mRNA expression of aP2 gene at 50  $\mu$ M concentration of TGZ and TSN. Statistical differences were observed between TGZ and TSN at 50  $\mu$ M (paired T-test,  $P < 0.05$ ). (B) Relative amount of mRNA expression of aP2 gene at 50  $\mu$ M of PGZ and PSN.

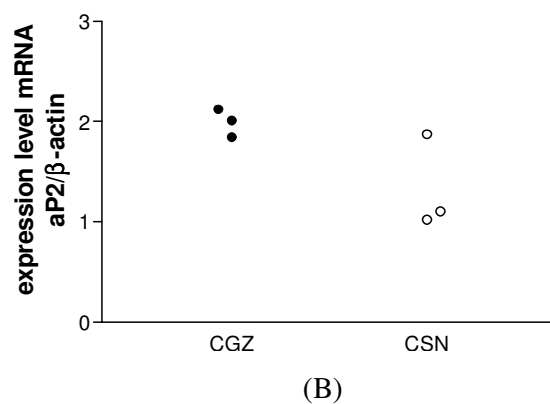
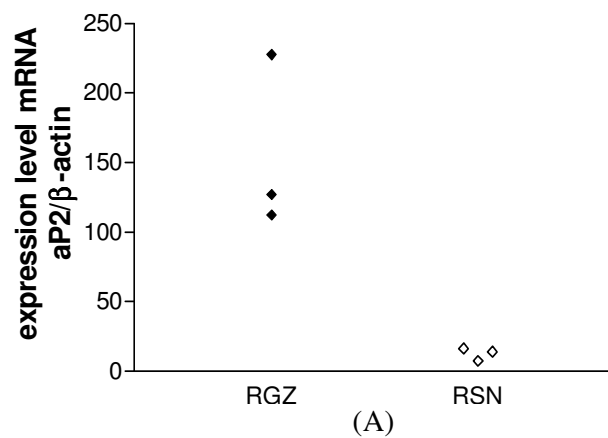


**Fig. 42** Relative amount of mRNA expression of aP2 gene at 50  $\mu$ M concentration of (A) RGZ and RSN, and (B) CGZ and CSN.

### 5.5 Discussion

Given that the sulfur moiety contributes to both adduct formation and toxicity, it becomes important to elucidate if the bioisosteric substitution also affect the pharmacological effect of the TZD class of antidiabetic drugs. The TZD class of antidiabetic drugs elicits their antidiabetic activity by binding partially to the PPAR $\gamma$ . In general, the TZD analogues showed

TZD analogues	Expression level mRNA (aP2/ $\beta$ -actin)	PRD analogues	Expression level mRNA (aP2/ $\beta$ -actin)
TGZ	138.14	TSN	0.29
	94.35		0.45
	67.18		0.18
PGZ	42.20	PSN	3.63
	9.38		2.05
	24.76		1.25
RGZ	227.54	RSN	16.33
	127.11		14.13
	112.20		7.36
CGZ	2.120	CSN	1.10
	1.840		1.87
	2.010		1.02

**Table 7** Expression level of mRNA in 3T3-L1 cells (aP2/ $\beta$ -actin)

higher % binding to PPAR $_{\gamma}$ -LBD than the PRD analogues, supporting that sulfur moiety is a key component of the pharmacophore for PPAR $_{\gamma}$  binding (Khanna et al. 2005).

It had been established that RGZ has greater % binding to PPAR $_{\gamma}$ -LBD as compared to other glitazones. This validated our assay and ensured that the other % binding were credible. Our data confirmed that while the PRD analogues lack the sulfur moiety, they could still bind to PPAR $_{\gamma}$ . In order to confirm if the binding to the PPAR $_{\gamma}$  by the PRD analogues lead to biological activity, aP2 gene expression of each TZD and PRD analogues was further measured and compared using qRT-PCR.

The aP2 gene expression assay confirmed again that RGZ yielded the highest aP2 gene expression among the other glitazones. In parallel, RSN also showed the highest aP2 gene expression as compared to the other PRD analogues (Table 7). Both the PPAR<sub>γ</sub> binding and the aP2 gene expression experiments confirmed that the pyridine ring of each RGZ and RSN molecule is an essential pharmacophore that binds and activates the PPAR<sub>γ</sub> ligand in addition to the five-membered TZD ring (Khanna et al., 2005; Ramachandran et al., 2004). This possibly accounted for the stronger binding affinities and aP2 gene expressions of both RGZ and RSN as compared to other glitazones and succinimides.

More importantly, we determined that the PRD analogues could also bind to the PPAR<sub>γ</sub> and stimulate aP2 gene expression. This suggested the potential of the PRD analogues to elicit *in vivo* antidiabetic pharmacological activity. In particular, RSN retained aP2 gene expression activity that was comparable to TGZ and PGZ. In summary, our findings ascertained the role of the sulfur moiety in eliciting both pharmacological and toxicological activity. Nevertheless, other pharmacophoric features besides the TZD ring can partially restore PPAR<sub>γ</sub> binding (as seen with RSN) to confer the pharmacological effects. Hence, the substitution of the TZD ring by PRD ring is a viable strategy to develop safer PPAR<sub>γ</sub> agonists in the future.



## Chapter 6

### Toxic effect of TGZS in THLE-2 cells

#### 6.1 Introduction

TGZS is the major metabolite of TGZ in human plasma (70%) after its oral administration (Loi et al., 1997; Loi et al., 1999). TGZS is mainly excreted through bile. The proposed mechanism of TGZS toxicity is via the inhibition of BSEP (Funk et al., 2001) (Chapter 1).

Although TGZS has been demonstrated to inhibit BSEP, its direct toxic effect on human liver cells has not been investigated. It is important to ascertain this property of TGZS as it is a major metabolite of TGZ and its mechanism of direct hepatocyte toxicity remains unclear. While it had been determined that TGZS showed no cytotoxicity in human hepatoma cell lines such as HepG2, HLE, HLF and HuH-7 cells (Yamamoto et al., 2001), its effect on physiologically-relevant normal human hepatocytes has not been established. In this study, TGZ and chemically-synthesized TGZS were evaluated for their *in vitro* toxicity using metabolically-active normal human hepatocytes, THLE-2 cells (Andrea et al., 1993; Saha et al., 2010).

#### 6.2 Preparation of TGZS ( $C_{24}H_{27}NO_8S_2$ )

##### 6.2.1 Synthesis of methyl-6-hydroxy-2,5,7,8-tetramethylchroman-2-carboxylate [II (A)]

The synthesis of 6-hydroxy-2,5,7,8-tetramethylchroman-2-carboxylate [II (A)] was performed by the method which had been described previously (Chapter 2).

### 6.2.2 Synthesis of (R,S)-2-(hydroxymethyl)-2,5,7,8-tetramethylchroman-6-ol [II (B)]

The synthesis of (R,S)-2-(hydroxymethyl)-2,5,7,8-tetramethylchroman-6-ol [II (B)] was performed by the method which had been described previously (Chapter 2).

### 6.2.3 Synthesis of [6-(tert-butyl-dimethyl-silyloxy)-2,5,7,8-tetramethyl-chroman-2-yl]-methanol [VI (A)]

A mixture of (R,S)-2-(hydroxymethyl)-2,5,7,8-tetramethylchroman-6-ol [II (B)] (2.4 g, 10.16 mmol), imidazole (0.898 g, 13.20 mmol) and tert-butyldimethylsilyl chloride (3.81 g, 25.40 mmol) in anhydrous DMF (5 mL) were stirred at RT for 36 h under nitrogen atmosphere. Consequently, the mixture was quenched by ice cold water (40 mL) and the mixture was extracted with dichloromethane (40 mL, twice). The organic layer was washed with brine, dried over anhydrous sodium sulfate and concentrated by evaporation under reduced pressure. The concentrate thus obtained was purified by column chromatography on silica gel (60-120 mesh) using a mixture of n-hexane/EtOAc (20:1 v/v) as eluent to give a colourless viscous oil [VI (A)] (Fig. 43) (2.2 g, 61% yield). <sup>1</sup>H NMR: (CDCl<sub>3</sub>) δ: 0.12 (s, 6H, [-Si(-CH<sub>3</sub>)<sub>2</sub>]), 1.05 (s, 9H, [-C(-CH<sub>3</sub>)<sub>3</sub>]), 1.22 (s, 3H, -CH<sub>3</sub>), 1.99-2.06 (m, 2H, -CH<sub>2</sub>-), 2.07 (s, 6H, -CH<sub>3</sub>), 2.11 (s, 3H, -CH<sub>3</sub>), 2.63 (t, 2H, J= 6 Hz, -CH<sub>2</sub>-), 3.61 (m, 2H, -CH<sub>2</sub>-). <sup>13</sup>C NMR: (CDCl<sub>3</sub>) δ: 3.33, 3.39, 11.98, 13.39, 14.29, 18.57, 20.34, 20.42, 26.06, 27.81, 69.34, 75.01, 117.39, 122.59, 123.71, 126.09, 144.55, 145.23 (Fig. 44A). MS (ESI+) *m/z* (M+H)<sup>+</sup> 351.2.

### 6.2.4 Synthesis of 4-(6-hydroxy-2,5,7,8-tetramethyl-chroman-2-ylmethoxy)-benzaldehyde [VI (B)]

Sodium hydride (60% in mineral oil, 0.288 g, 12.0 mmol) and [6-(tert-butyl-dimethylsilyloxy)-2,5,7,8-tetramethyl-chroman-2-yl]-methanol (2.1 g, 6.0 mmol) in anhydrous DMF (20 mL) was stirred for 30 min under nitrogen atmosphere at RT. Subsequently, 4-fluorobenzaldehyde (1.3 mL, 12.0 mmol) was added slowly dropwise to the reaction mixture under nitrogen atmosphere at RT. After stirring at the same temperature for overnight, the reaction mixture was quenched with aqueous ammonium chloride (20 mL). Ice-water (30 mL) was added to the reaction mixture and the resultant mixture was extracted with EtOAc (50 mL, two times). The organic layer was washed with water and brine, dried over anhydrous sodium sulfate and concentrated by evaporation under reduced pressure. The concentrate thus obtained was purified by column chromatography on silica gel (60-120 mesh) using a mixture of n-hexane/EtOAc (4:1 v/v) as eluent to give a yellow liquid [VI (B)] (Fig. 43) (0.45 g, 22.05% yield). <sup>1</sup>H NMR: (CDCl<sub>3</sub>) δ: 0.85 to 0.94 (m, 2H, -CH<sub>2</sub>-), 1.28 (s, 3H, -CH<sub>3</sub>), 1.96 (s, 3H, -CH<sub>3</sub>), 1.98 (s, 3H, -CH<sub>3</sub>), 2.12 (s, 3H, -CH<sub>3</sub>), 2.69 (t, 2H, J= 6 Hz, -CH<sub>2</sub>-), 3.63 (m, 2H, -OCH<sub>2</sub>-), 6.85 (d, 2H, J= 9 Hz, -C<sub>6</sub>H<sub>4</sub>-), 7.77 (d, 2H, J= 9 Hz, -C<sub>6</sub>H<sub>4</sub>-), 9.84 (s, 1H, -CHO). MS (ESI+) *m/z* (M+H)<sup>+</sup> 341.1.

#### 6.2.5 Synthesis of (R,S)-5-[4-(6-hydroxy-2,5,7,8-tetramethyl-chroman-2-ylmethoxy)-benzyl]-thiazolidine-2,4-dione [VI (C), TGZ]

A mixture of 4-(6-hydroxy-2,5,7,8-tetramethyl-chroman-2-ylmethoxy)-benzaldehyde (420 mg, 1.23 mmol) and TZD (128 mg, 1.10 mmol) in anhydrous ethanol (20 mL) were heated under reflux for 24 h in presence of few drops of 2-aminoethanol and then cooled to RT. The reaction mixture was concentrated by evaporation under reduced pressure. A solid compound was obtained and 25 mL hexane was added to dissolve excess aldehyde. The solid

compound was filtered, dissolved in excess ethanol and a reduction step was performed without further purification. The above-mentioned ethanol was taken in a parr bottle and 50 mg of Pd/C (10%) was added to it. The compound was hydrogenated under hydrogen atmosphere (pressure 40 psi) at RT for 8 h. The mixture was filtered using celite and concentrated by evaporation under reduced pressure to give a white solid. The compound was further purified by column chromatography on silica gel (60-120 mesh) using a mixture of n-hexane/EtOAc (10:1 v/v) as eluent to give a white solid [VI (C)] (Fig. 43) (0.256 g, 47.05% yield). Melting point 182°C (Literature value 184°C) (Lee et al., 2005). <sup>1</sup>H NMR: (DMSO-d<sub>6</sub>) δ: 1.28 (s, 3H, -CH<sub>3</sub>), 1.77-1.83 (m, 1H, -CH<sub>2</sub>-), 1.97 (s, 3H, -CH<sub>3</sub>), 2.02 (s, 3H, -CH<sub>3</sub>), 2.04 (s, 3H, -CH<sub>3</sub>), 2.05-2.08 (m, 1H, -CH<sub>2</sub>-), 2.56 (t, 2H, J = 6 Hz, -CH<sub>2</sub>-), 3.00-3.08 (m, 1H, -OCH<sub>2</sub>-), 3.25-3.30 (m, 1H, -OCH<sub>2</sub>-), 3.93 (d, 2H, J = 12 Hz, -CH<sub>2</sub>-), 4.83 (t, 1H, J = 6 Hz, -CH=), 6.88 (d, 2H, J = 9 Hz, -C<sub>6</sub>H<sub>4</sub>-), 7.11 (d, 2H, J = 9 Hz, -C<sub>6</sub>H<sub>4</sub>-), 7.42 (s, 1H, -OH), 11.99 (s, 1H, -NH). <sup>13</sup>C NMR: (DMSO-d<sub>6</sub>) δ: 12.83, 13.78, 20.80, 22.79, 29.31, 37.29, 39.72, 54.06, 73.49, 74.78, 115.67, 117.76, 121.36, 122.12, 123.77, 129.81, 131.35, 145.14, 146.44, 158.91, 172.73, 176.74 (Fig. 44B). MS (ESI-) *m/z* (M-H)<sup>-</sup> 440.1.

#### 6.2.6 Synthesis of (R,S)-sulphuric acid mono-{2-[4-(2,4-diox-thiazolidin-5-ylmethyl)-phoxymethyl]-2,5,7,8-tetramethyl-chorman-6-yl} ester [VI (D), TGZS]

A mixture of TGZ (0.25 g, 0.56 mmol), sulphur trioxide-N-triethylamine complex (0.135 g, 0.84 mmol) and potassium carbonate (0.234 g, 1.70 mmol) in 50 mL anhydrous DMF was agitated for 1 h at RT in argon atmosphere. The reaction mixture was placed in water bath (40°C) for 2 h, after which TGZS was precipitated out and stuck to the surface of glass. DMF layer was decanted out and precipitated TGZS was recrystallized with methanol (5 mL) and dried under vacuum at 40°C to give as a yellow solid [VI (D)] (Fig. 43) (0.008 g,

2.7% yield, 99.2% purity). Melting point 189°C. <sup>1</sup>H NMR: (DMSO-d<sub>6</sub>) δ: 1.28 (s, 3H, -CH<sub>3</sub>), 1.77-1.83 (m, 1H, -CH<sub>2</sub>-), 1.97 (s, 3H, -CH<sub>3</sub>), 2.02 (s, 3H, -CH<sub>3</sub>), 2.04 (s, 3H, -CH<sub>3</sub>), 2.05-2.08 (m, 1H, -CH<sub>2</sub>-), 2.09 (s, 1H, -SO<sub>3</sub>H), 2.56 (t, 2H, J = 6 Hz, -CH<sub>2</sub>-), 3.00-3.08 (m, 1H, -OCH<sub>2</sub>-), 3.25-3.30 (m, 1H, -OCH<sub>2</sub>-), 3.93 (d, 2H, J = 12 Hz, -CH<sub>2</sub>-), 4.83 (t, 1H, J = 6 Hz, -CH=), 6.88 (d, 2H, J = 9 Hz, -C<sub>6</sub>H<sub>4</sub>-), 7.11 (d, 2H, J = 9 Hz, -C<sub>6</sub>H<sub>4</sub>-), 11.99 (s, 1H, -NH). <sup>13</sup>C NMR: (DMSO-d<sub>6</sub>) δ: 12.85, 13.78, 20.80, 22.77, 29.30, 31.72, 37.27, 54.06, 73.45, 74.78, 115.66, 117.77, 121.36, 122.12, 123.77, 129.80, 131.36, 145.14, 146.42, 158.90, 172.77, 176.79 (Fig. 44C). MS (ESI-) *m/z* (M-H)<sup>-</sup> 520.1.

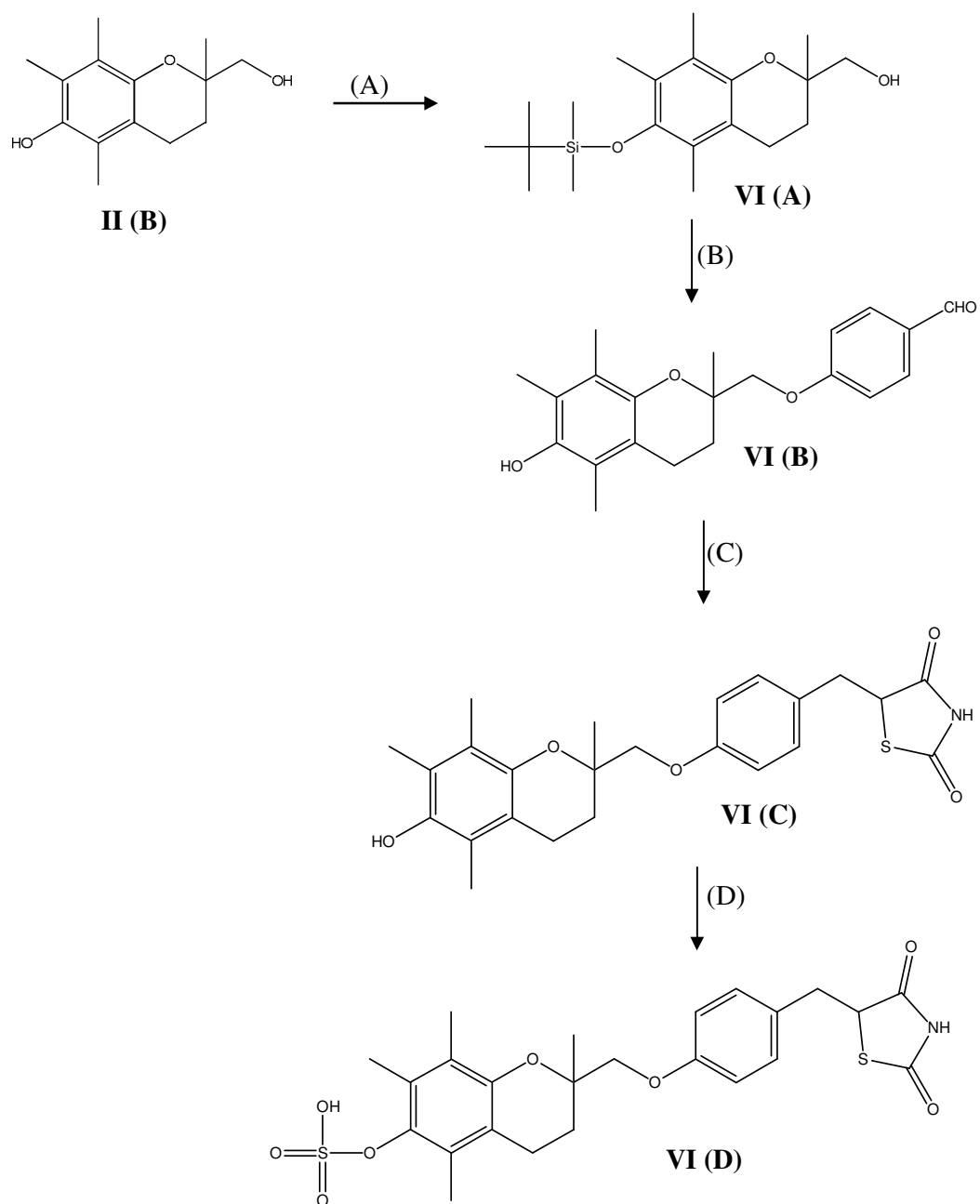


**Fig. 43** Synthesis of TGZS. (A) Tert-butyldimethylsilyl chloride, imidazole, anhydrous DMF, RT, 36 h; (B) sodium hydride, anhydrous DMF, 4-fluorobenzaldehyde, RT, 12 h; (C) TZD, 2-aminoethanol, reflux, 24 h and then 10% Pd/C, H<sub>2</sub> gas, EtOH, 12 h; (D) sulphur trioxide-N-triethylamine complex, potassium carbonate, anhydrous DMF, RT for 1h then 40°C for 2 h.

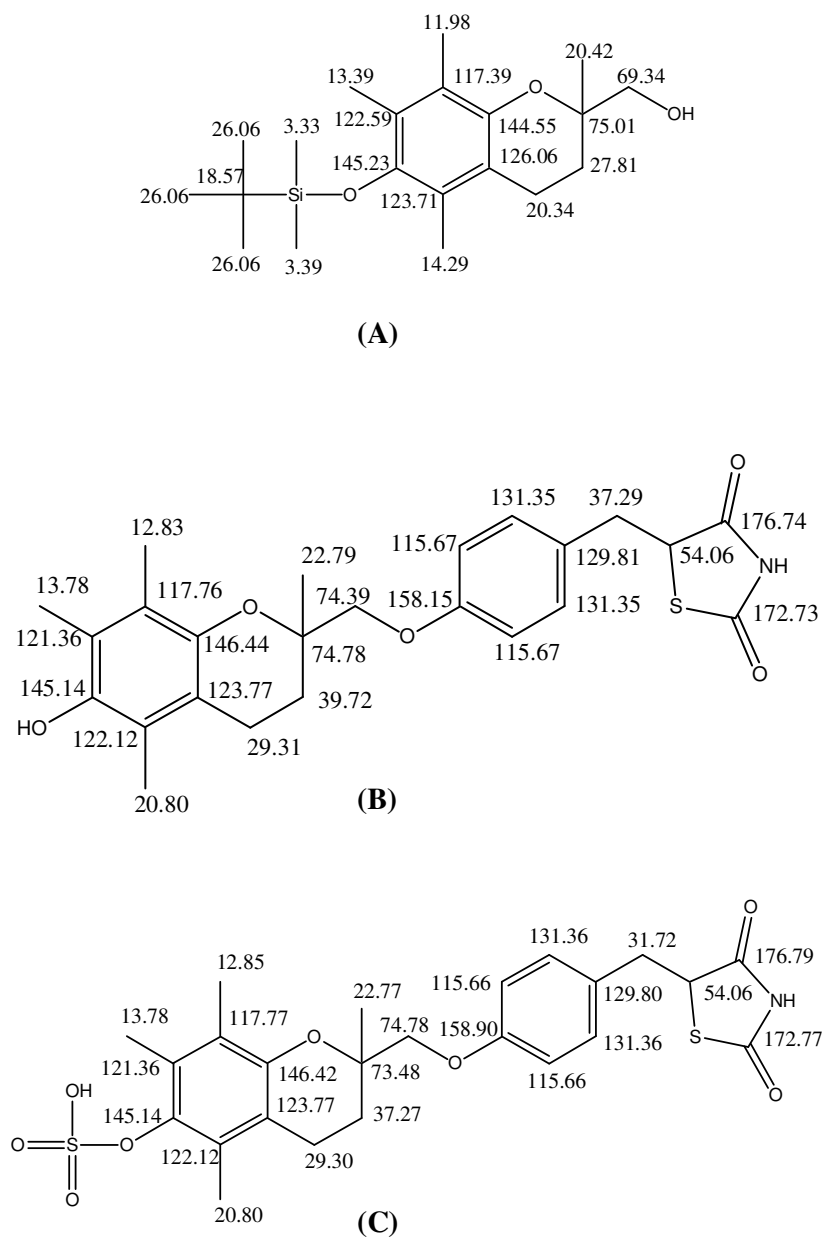


**Fig. 44**  $^{13}\text{C}$  NMR interpretation (A) 6-(tert-butyl-dimethyl-silyloxy)-2,5,7,8-tetramethyl-chroman-2-yl]-methanol; (B) TGZ and (C) TGZS.

## 6.3 Methods

### 6.3.1 Sulfotransferase enzyme inhibition assay

#### 6.3.1.1 THLE-2 cells incubation

THLE-2 cells were seeded into a 6-well plate ( $1.0 \times 10^7$  cells/well). 100  $\mu\text{M}$  of either TGZ alone or TGZ and quercetin (QR) in combination were added to the cells and the mixtures were incubated under a humidified condition with 5%  $\text{CO}_2$  at  $37^\circ\text{C}$ . QR is a phenol sulfotransferase enzyme inhibitor and its concentration used in each incubation was 50  $\mu\text{M}$ . The final concentration of the test compounds and organic solvent were 50  $\mu\text{M}$  and 0.2% (v/v), respectively. After 24 h ( $t_{24}$ ), the reaction was terminated by addition of 2 mL of ice cold ACN/water (50:50 v/v). Initial time point samples ( $t_0$ ) were prepared by terminating the reaction immediately after adding the test compound to the THLE-2 cells with same quenching solvent. These samples were centrifuged at 13,000 rpm at  $4^\circ\text{C}$  for 10 min and the supernatants were removed and evaporated to dryness at  $35^\circ\text{C}$  for 8 h under a gentle flow of nitrogen gas using the Turbovap LV. Then, they were each reconstituted with 50  $\mu\text{L}$  of ACN/water (50:50 v/v), vortex-mixed and centrifuged at 13,000 rpm at  $4^\circ\text{C}$  for 2 min. 5  $\mu\text{L}$  of the supernatant was subjected to UPLC/MS/MS analysis. Negative control experiments were also performed in the absence of THLE-2 cells or substrates.

#### 6.3.1.2 LC/MS/MS conditions

For the profiling of sulfotransferase enzyme inhibition assay of both TGZ and QR using THLE-2 cells, chromatographic separations were performed on an ACQUITY UPLC



BEH C<sub>18</sub> 1.7 μm 100 × 2.1 mm i.d. column (Waters). The flow rate was set at 0.5 mL/min. The elution conditions were similar to the profiling of RM-GSH conjugates (Chapter 2). ESI-mode was employed throughout the experiments. MRM transition and single ion monitoring (SIM) were performed at *m/z* 520.0→440.0 for TGZS and *m/z* 381.0 for quercetin sulfate (QRS), respectively. The MS conditions are summarized in Table 8.

The common parameters of MS for TGZS and QRS were as follows: curtain gas (CUR); 10 psi, ion spray voltage; -4500 V, collision gas (CAD); medium, ion source gas (GS<sub>1</sub>); 40 psi, ion source gas (GS<sub>2</sub>); 45 psi, interface heater; On, temperature; 500°C, scan time; 250 ms.

Parameters	TGZS	QRS
Declustering potential, V	-49.0	55.0
Entrance potential, V	-5.6	-4.5
Collision cell entrance potential, V	-30.0	Nil
Collision energy, V	-4.0	Nil

**Table 8** Optimized MS parameters for identification and stability profiling of TGZS and QRS.

### 6.3.2 Stability study of synthesized TGZS in BEGM

Stability study was performed by the method which had been described previously (Chapter 4).

### *6.3.3 MTT viability assay*

MTT viability assay was performed by the method which had been described previously (Chapter 4). In another experiment, both TGZ and TGZS (1-125  $\mu$ M) were incubated with THLE-2 cells in absence and presence of TA (Chapter 4). In a separate experiment, 50  $\mu$ M QR was co-incubated with TGZ and TGZS at varying concentrations (1–125  $\mu$ M) in THLE–2 cells (Virginia et al., 2004). In parallel, another cell viability assay was performed using various concentrations of QR (1–125  $\mu$ M) in THLE–2 cells in the absence of TGZ and TGZS.

### *6.3.4 GSH depletion assay*

GSH depletion assay was performed by the method which had been described previously (Chapter 4).

### *6.3.5 PC assay*

PC assay was performed by the method which had been described previously (Chapter 4).

## *6.4 Results*

### *6.4.1 Sulfotransferase enzyme inhibition assay*

LC/MS/MS analysis of THLE-2 cells incubation with TGZ revealed the presence of TGZS using MRM at  $m/z$  520.0→440.0. The MRM experiment confirmed the presence of metabolically-generated TGZS (retention time 4.92 min) which was absent in “0 h TGZ-

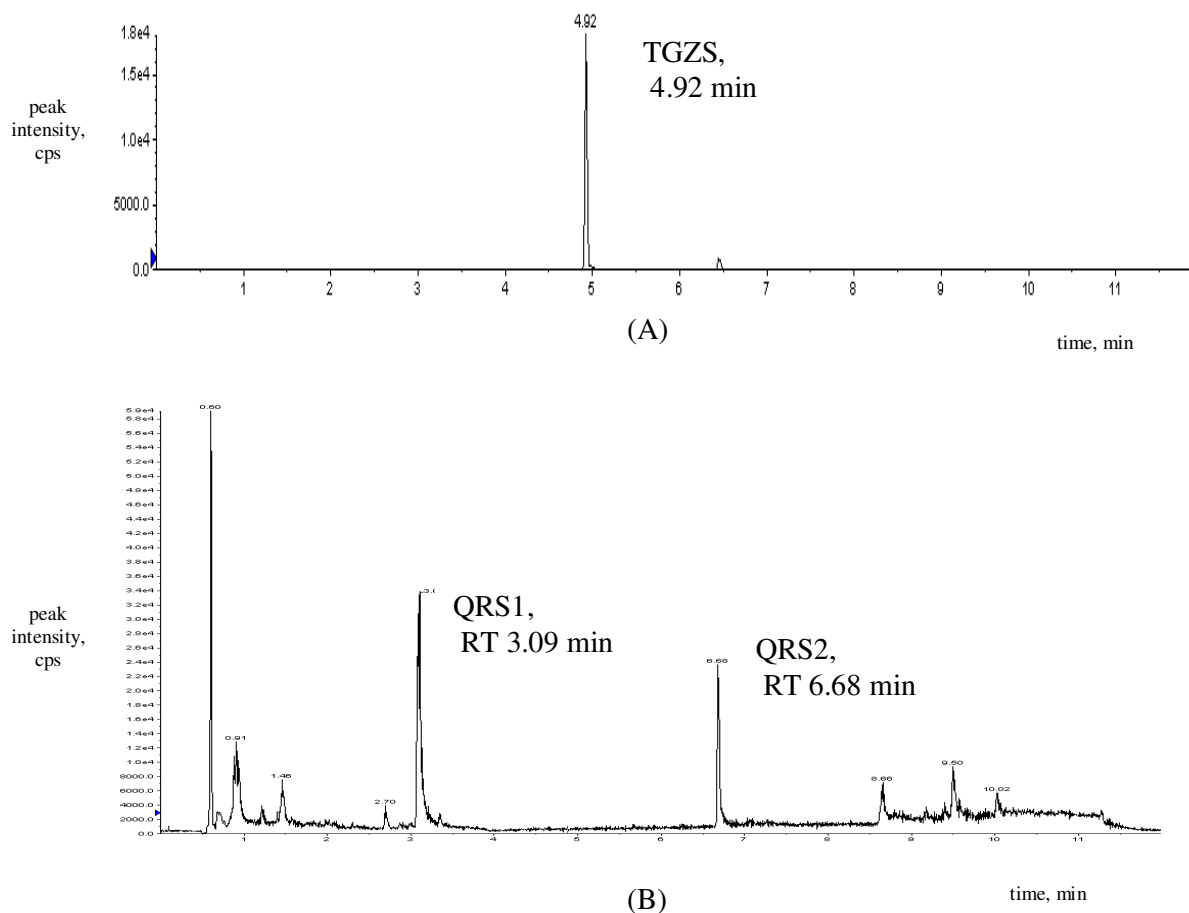


**Fig. 45** (A) Representative LC/MS/MS chromatogram of TGZS in “24 h TGZ-THLE-2” sample (retention time 4.92 min). (B) Representative LC/MS/MS chromatogram of “24 h TGZ-QR-THLE-2” sample (QRS1, retention time 3.09 min; QRS2, retention time 6.68 min).

THLE-2” and negative control samples but present in “24 h TGZ-THLE-2” incubation. TGZS is the sulfo-conjugate of TGZ where the conjugation with the bi-sulfate (-OSO<sub>3</sub>H) moiety occurred at the 6-hydroxyl (-OH) group of TGZ (Fig. 45A). TGZS was found to be

absent when TGZ and QR (“24 h TGZ–QR–THLE–2”) were co-incubated with THLE–2 cells for 24 h (data not shown). The absence of TGZS in the “24 h TGZ–QR–THLE–2” sample indicated that sulfotransferase enzyme activity blocked by QR. As shown in Fig. 45B, SIM at  $m/z$  381.0 of the “24 h TGZ–QR–THLE–2” sample exhibited the presence of quercetin sulfate–1 (QRS1, retention time 3.09 min) and quercetin sulfate–2 (QRS2, retention time 6.68 min). The presence of QRS1 and QRS2 in the “24 h TGZ–QR–THLE–2” sample confirmed the competition of QR for the sulfotransferase enzyme.

#### 6.4.2 Stability profile of TGZS using BEGM

To evaluate the contribution of the sulfo-conjugate to direct hepatotoxicity and mitigate the possible confounding factors coming from parental TGZ through hydrolysis of TGZS, we performed stability assessment of TGZS in our cell culture conditions. The stability study demonstrated that TGZS at 1.0 (86.02%) and 50  $\mu$ M (95.53%) was stable up to 72 h in BEGM at 37°C (Fig. 46). The stability ranges were  $100 \pm 15\%$  up to 72 h for TGZS. The levels of TGZS among the different time points (0, 24, 48 and 72 h) were not significantly different.

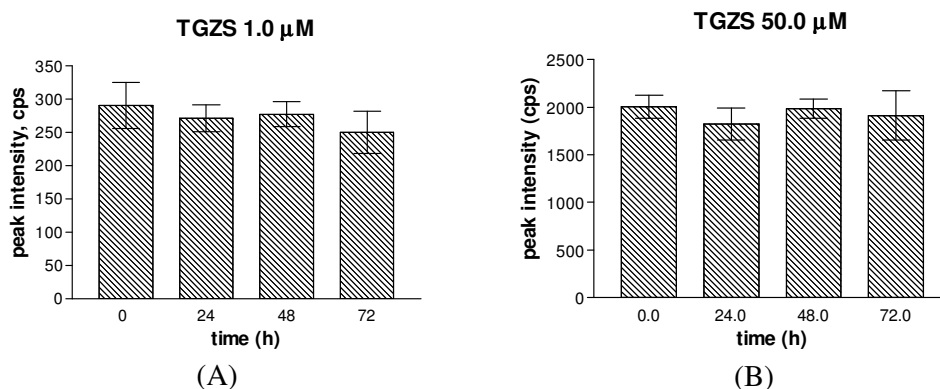


**Fig. 46** Stability profile of TGZS at (A) 1.0 and (B) 50.0  $\mu$ M in BEGM at 37°C up to 72 h.

### 6.4.3 MTT viability assay

THLE-2 cells were treated with TGZ and TGZS at various concentrations (1–125  $\mu\text{M}$ ) for 72 h. As shown in Fig. 47A, cell viability of the hepatocytes was dose-dependent for both TGZ and TGZS where an increase in dose of each test compound was associated with a consistent decline of cell viability. It was shown that when each compound was incubated with THLE-2 cells, toxicity was observed from 1  $\mu\text{M}$  with respect to control in both cases. However, the observed toxic effect of TGZS was greater than TGZ after 1  $\mu\text{M}$ . The THLE-2 cell viability was 50% at 75  $\mu\text{M}$  of TGZ and remained unchanged up to 125  $\mu\text{M}$ . On the other hand, cell viability decreased dramatically when dosed with TGZS and was below 10% at and above 50  $\mu\text{M}$  of TGZS. The calculated  $\text{EC}_{50}$  for TGZS and TGZ were  $21.76 \pm 5.34$  and  $41.12 \pm 4.3$   $\mu\text{M}$ , respectively. Statistical differences were demonstrated between control and test compounds (one-way ANOVA,  $P < 0.05$ ) and between TGZ and TGZS (paired T-test,  $P < 0.05$ ) at and above 10  $\mu\text{M}$  concentration, respectively.

To inhibit the biotransformation of TGZ to TGZS by sulfotransferase enzyme in THLE-2 cells, we co-incubated both compounds (TGZ and TGZS) with 50  $\mu\text{M}$  of QR. Our results demonstrated that TGZS was more toxic than TGZ at and above 50  $\mu\text{M}$  when co-incubated with QR (Fig. 47B). Statistical differences were observed between TGZ and TGZS in terms of percentage cell viability at and above 50  $\mu\text{M}$  (paired T-test,  $P < 0.05$ ). It was also confirmed that the viability of THLE-2 cells was not affected by QR alone up to a concentration of 125  $\mu\text{M}$  (data not shown). QR is a naturally occurring flavonoid having hepatoprotective activity (Gulati et al., 1995).

To determine if the increased cytotoxicity of TGZS was linked to oxidative stress, we co-incubated both treatments with the antioxidant, TA. The results further demonstrated that TGZS was more toxic than TGZ above 25  $\mu\text{M}$  when the compounds were co-incubated with

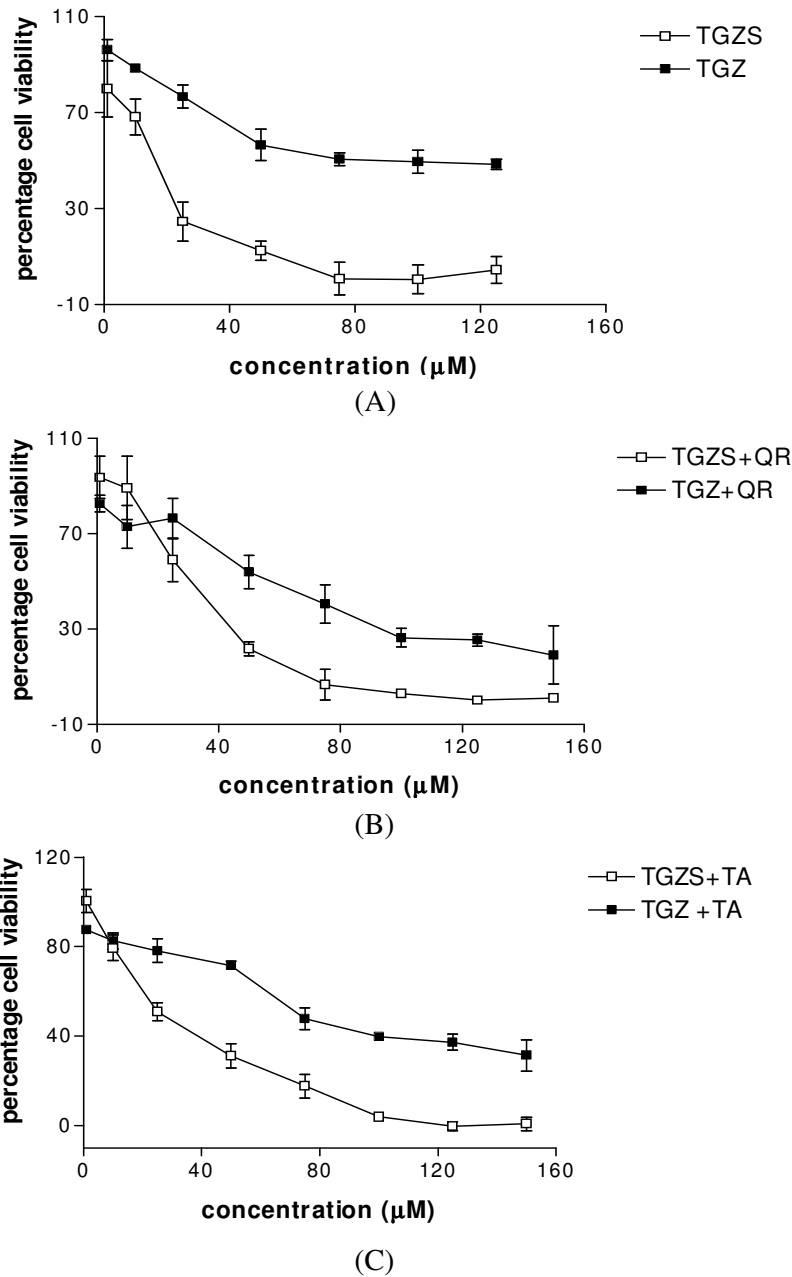


**Fig. 47** (A) Percentage MTT cell viabilities of THLE-2 cells at varying concentrations of TGZ and TGZS. Statistical differences were demonstrated between control and test compounds (one-way ANOVA,  $P < 0.05$ ) and between TGZ and TGZS (paired T-test,  $P < 0.05$ ) at and above 10  $\mu\text{M}$  concentration, respectively. (B) Percentage MTT cell viabilities of THLE-2 cells at varying concentrations of TGZ and TGZS co-incubated with 50  $\mu\text{M}$  of QR. Statistical differences were observed between TGZ and TGZS in terms of percentage cell viability at and above 50  $\mu\text{M}$  (paired T-test,  $P < 0.05$ ). (C) Percentage MTT cell viabilities of THLE-2 cells at varying concentrations of TGZ and TGZS co-incubated with 20  $\mu\text{M}$  of TA. Statistical differences were observed between TGZ and TGZS in terms of percentage cell viability at and above 25  $\mu\text{M}$  (paired T-test,  $P < 0.05$ ).

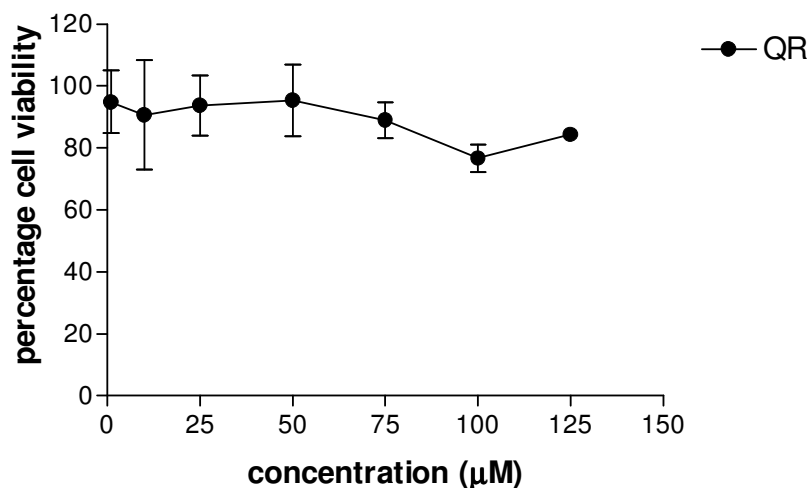


**Fig. 48** Percentage MTT cell viabilities of THLE-2 cells at varying concentrations of QR.

TA at 20 μM level (Fig. 47C). Statistical differences were observed between TGZS and TGZ in terms of percentage cell viability at and above 25 μM (paired T-test,  $P < 0.05$ ). By comparing Fig. 47A and 47C, it was clear that TGZS produced less toxicity in the presence of TA as compared to TGZS alone. The viabilities of THLE-2 cells were 20 and 50% in the absence and presence of TA at 25 μM of TGZS, respectively. As an experimental control, we confirmed that the viability of THLE-2 cells was not affected by TA alone up to a concentration of 100 μM (Fig. 48).

#### 6.4.4 GSH depletion assay

Determination of GSH-NEM adducts was performed in THLE-2 cells after 72 h incubation with TGZ and TGZS to measure any depletion of GSH. A linear regression performed over a range of 0.001 to 10 μM yielded a correlation coefficient ( $r^2$ ) of 0.9986.

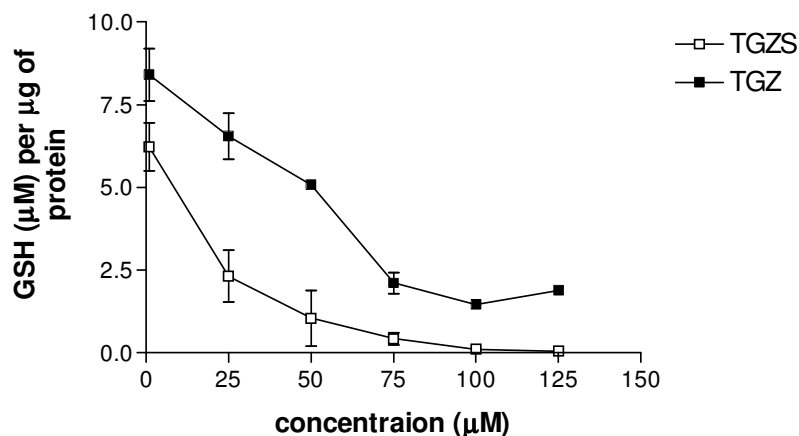


**Fig. 49** GSH depletion in THLE-2 cells at varying concentrations of TGZ and TGZS. Statistical differences were demonstrated between control and test compounds (one-way ANOVA,  $P < 0.05$ ) and between TGZ and TGZS (paired T-test,  $P < 0.05$ ) at and above 50  $\mu\text{M}$ , respectively.

The accuracy of the assay was found to be within 80 to 108%. The recoveries of the GSH-NEM complex in QC samples were 60 to 80%, respectively. The RT for GSH-NEM complex was 3.13 min. GSH depletion ( $\mu\text{M}$ ) per  $\mu\text{g}$  of protein was measured at varying concentrations of TGZ and TGZS after 72 h (Fig. 49). As shown in Fig. 49, TGZS depleted more GSH than TGZ after 50  $\mu\text{M}$ . Statistical differences were demonstrated between control and test compounds (one-way ANOVA,  $P < 0.05$ ) and between TGZ and TGZS (paired T-test,  $P < 0.05$ ) at and above 50  $\mu\text{M}$ , respectively.

#### 6.4.5 PC assay

Determination of PC content was performed in THLE-2 cells after 48 h incubation with TGZ and TGZS as a surrogate for ROS-mediated protein oxidation. For each compound, PC content ( $\mu\text{M}$ ) per  $\mu\text{g}$  of protein of THLE-2 cells was increased at all concentrations greater than 10  $\mu\text{M}$  with respect to control. As shown in Fig. 50, statistical differences were



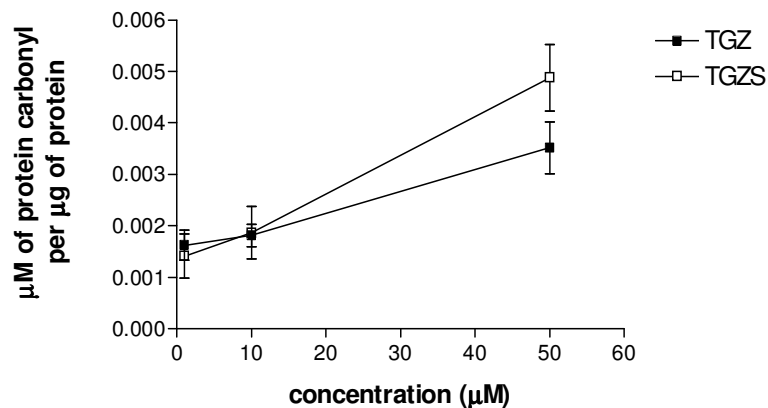


**Fig. 50** PC assay of THLE-2 cells at varying concentrations of TGZ and TGZS. Statistical differences were demonstrated between control and test compounds (one-way ANOVA,  $P < 0.05$ ) and between TGZ and TGZS (paired T-test,  $P < 0.05$ ) at 50  $\mu\text{M}$ .

demonstrated between control and test compounds (one-way ANOVA,  $P < 0.05$ ) and between TGZ and TGZS (paired T-test,  $P < 0.05$ ) at 50  $\mu\text{M}$ .

### 6.5 Discussion

In the chapters 3 and 4, we observed that the TZD ring of glitazones might be responsible for oxidative stress in THLE-2 cells via RM formation. We addressed that phase I metabolism is directly related to cytotoxicity in the subsequent chapters. In this chapter, we have discussed another issue about the cytotoxic effect of drug after phase II metabolism. Preliminary evidences suggested that the potential mechanism of hepatotoxicity of TGZS might be due to inhibition of BSEP (Smith, 2003). Therefore, it remains unclear if the sulfo-conjugated metabolite (TGZS) of TGZ has direct toxic effect on human liver cells. In the current chapter, the aim was to ascertain and establish the role of TGZS in causing direct toxicity in human hepatocytes.

To achieve this goal, TGZS was synthesized where 6-hydroxyl (-OH) group of TGZ was replaced by bi-sulfate (-OSO<sub>3</sub>H) group. In this study, the cytotoxicities of TGZS and TGZ were compared using THLE-2 cells, normal human hepatocytes with metabolizing capacity. The MTT assay results confirmed that TGZS was more toxic in human hepatocytes than TGZ. This data suggested a novel mechanism of toxicity of TGZ where TGZS is a direct toxicant in humans. In order to elucidate the cytotoxic effects of TGZ and TGZS more accurately, MTT assay was further performed where the sulfonation of TGZ to TGZS in THLE-2 cells was inhibited using QR, a specific phenol sulfotransferase inhibitor (Virginia et al., 2004). QR prevented the sulfonation of TGZ which was confirmed by LC/MS/MS experiments. Due to inhibition of sulfotransferase enzyme activity by QR, we observed toxicities of TGZ and TGZS individually in THLE-2 cells. MTT data using co-incubation of our test compounds with QR further supported that TGZS was more toxic than TGZ in the absence of biotransformation of TGZ to TGZS during incubation.

Based on earlier reports that TGZ mediated hepatotoxicity in part through generating oxidative injury (Smith, 2003), we raised the question whether the observed cytotoxicity was related to TGZS-induced oxidative stress in the biological system. To answer this question, MTT assay was performed by co-incubating 20 μM TA with TGZ and TGZS at various concentrations in THLE-2 cells. The data demonstrated that cell viability was improved when TGZS was co-incubated with TA. The partial salvation of human hepatocytes from the toxic effects of TGZS by an antioxidant indicated indirectly that TGZS might have exerted oxidative stress on the THLE-2 cells. In line with this observation, the GSH depletion assay established that TGZS depleted more GSH than TGZ, further underscoring the oxidative stress potential of TGZS. To further characterize the targets of oxidative stress, we performed PC assay which demonstrated that TGZS generated greater oxidation on cellular proteins than TGZ. Collectively, TGZS appeared to cause human liver toxicity by inducing oxidative

stress. Finally, the stability study confirmed that TGZS was stable in BEGM at 37°C up to 72 h. This finding was important to rule out the possibility of TGZS undergoing deconjugation to TGZ during incubation. Hence, we were able to attribute all observed toxicity effects to TGZS accurately.

The human blood concentration of TGZ is 0.3–0.5 µg/mL or 7–12 µM after oral administration (Loi et al., 1999). Our MTT, GSH and PC assays demonstrated that TGZS was more toxic towards THLE–2 cells at and above 10 µM concentration as compared to parent TGZ. As the pharmacological and *in vitro* concentrations of TGZ and TGZS are in the same dynamic order of magnitude, it suggested that the investigated *in vitro* concentrations of TGZS (1–125 µM) were clinically–relevant and associated with the human physiological concentrations.

This study yielded a surprising outcome in the light of some earlier works. Using primary cultures of human hepatocytes, Kostrubsky et al. (2000) proposed that TGZ was responsible for cytotoxicity rather than its metabolite TGZS. It was reported that inhibition of sulfation in these hepatocytes resulted in an accumulation of parent TGZ and cytotoxicity. Nonetheless, their findings were not confirmed using pure chemically–synthesized TGZS. Sulfo–conjugation is an essential metabolic pathway for many drugs, xenobiotics and endogenous substances. While the main role of sulfo–conjugation is to enhance the hydrophilicity of drugs and aid their excretion from the body, it has been reported that sulfation of certain allylic alcohols and polycyclic aromatic hydrocarbons may produce metabolites with increased toxicity (Chou et al., 1998; Banoglu, 2000; King et al., 2000). We reported for the first time that TGZS, a sulfo–conjugate of TGZ, exerted direct toxic effects on human hepatocytes, possibly via oxidative stress induction. It is noted that some phase II metabolites such as indoxyl sulfate, a sulfate metabolite of 3–hydroxyindole, causes renal failure via unknown mechanism (Banoglu and King, 2002). Similarly, the toxic mechanism

of TGZS is unknown. However, as both TGZ and TGZS had been shown to bind to similar biological receptor such as BSEP (Funk et al., 2001), it is possible that these compounds may bind to other similar biological receptors leading to oxidative stress and cell death. As TGZS is a major metabolite of TGZ in humans, the differential extent of phase II sulfation of TGZ in diabetic patients may be accountable for the idiosyncratic nature of TGZ-induced hepatotoxicity.

In summary, our present study reinforced the concept that hepatotoxicity of TGZ is possibly related to multiple mechanisms (Smith, 2003). Sulfonation at the 6-hydroxyl group of the chroman ring of TGZ is a potential cause of TGZ-induced hepatotoxicity. In addition to bile salt accumulation via inhibition of BSEP, we confirmed that TGZS is a direct human hepatotoxicant. Prospective studies involving other normal human hepatocytes, collagen-sandwiched hepatocytes, human liver slices and animal models are needed to confirm the interplay between the dual toxic mechanisms of TGZS.

## Chapter 7

### Conclusion and future direction

#### 7.1 Conclusion

The work presented in this thesis described the STR studies of the TZD antidiabetic drugs. The PRD analogues were prepared and examined for potential mechanism of toxicity using THLE-2 cells. Comparisons of toxicities of these compounds (both the TZD and PRD analogues) were also performed using THLE-2 cells. The sulfur moiety of the TZD ring was determined to be partially responsible for hepatotoxicity via the formation of reactive intermediates. These intermediates were detected in HLM and THLE-2 cells using GSH-trapping LC/MS/MS technique. No such intermediates were detected with regards to the PRD analogues. These findings suggested that the sulfur moiety was responsible for the RM formation either directly or indirectly.

A question arose whether TZD antidiabetic drugs produced toxicity via oxidative stress mechanism. To address this question, we performed MTT, GSH and PC assays. The MTT assay results confirmed that the TZD analogues, particularly TGZ and PGZ, produced greater toxicity than the PRD analogues in THLE-2 cells. TA-enriched MTT, GSH and PC assays were further performed to elucidate the mechanism of toxicity. MTT assay using TA (antioxidant) demonstrated that all the TZD analogues produced lesser toxicity than TZD alone. One possibility was that TA acted as a free radical oxygen scavenger and quenched the free oxygen species in the incubation system. In line with this observation, our GSH depletion assay further confirmed that all the TZD analogues depleted more GSH than the PRD analogues, further underscoring the oxidative stress capacity of the former. Finally, our PC assay exhibited the generation of more PC by the TZD analogues when compared to the

PRD analogues, confirming the occurrence of oxidative stress, In conclusion, the TZD antidiabetic drugs produce hepatotoxicity via oxidative stress mechanism mediated through the formation of RMs.

Our present study also focussed on the PPAR<sub>γ</sub> binding affinities of the TZD and PRD analogues to elucidate the importance of the sulphur moiety in binding to the receptor. Our PPAR<sub>γ</sub> binding assay depicted that both the TZD and PRD analogues had binding affinities to the PPAR<sub>γ</sub>. As expected, the TZD analogues showed higher binding affinities to the PPAR<sub>γ</sub> than the PRD analogues. Hence, the sulfur moiety was confirmed to be an important pharmacophore for the PPAR<sub>γ</sub> ligand. The results of the aP2 gene expression assay demonstrated expression of the gene by both types of analogues. While the TZD analogues expressed more aP2 gene than the PRD analogues, we confirmed that the PRD analogues possessed PPAR<sub>γ</sub> binding affinities and aP2 gene expression capacities. As both types of analogues were shown to bind to the PPAR<sub>γ</sub> and express the aP2 gene, the substitution of the TZD ring with PRD ring may be beneficial from a drug design perspective.

For a holistic STR study, we prepared sulfo-conjugated troglitazone (TGZS) synthetically and tested its toxicity using THLE-2 cells. Our MTT, GSH and PC results suggested that TGZS was more toxic than its parent TGZ and may be partially responsible for TGZ-induced hepatotoxicity via oxidative stress mechanism.

In conclusion, the PRD analogues demonstrated reduced toxicity in THLE-2 cells while sustaining the abilities to bind to the PPAR<sub>γ</sub> and stimulate aP2 gene expression. In particular, RSN retained aP2 gene expression activity that was comparable to that TGZ and PGZ. The substitution of the TZD ring by PRD ring is a viable strategy to develop safer PPAR<sub>γ</sub> agonists in future.

## 7.2 Limitation and future direction

The present study restricts the use of other oxidative stress assay like lipid peroxidation assay to prove oxidative stress mechanism strongly. Attempts should be made to investigate why this assay did not give positive results during our screening. TZD class of antidiabetic drugs may produce hepatotoxicity via multiple mechanisms (Smith, 2003). Oxidative stress may be another potential cause of hepatotoxicity. Lipid peroxidation assay gives strong measurement for oxidative stress. Future attempts should be made to investigate why this assay did not give positive results during our screening of the TZD compounds and PRD analogues. Future studies should also include animal experiments to further elucidate the exact mechanism of toxicity *in vivo*. The use of PRD analogues alone might not explain the mechanism of toxicity of the TZD drugs in this project completely. Future studies should explore other bio-isosteric analogues containing 2,4-oxazolidinedione in place of PRD to investigate their pharmacological and toxicological profiles. Finally, further investigation such as enantiomeric separation of synthesized racemic analogues and testing of each chiral compound should be performed.

## Bibliography

- American Diabetes Association., 2000. Clinical practice recommendations. *Diabetes* 23 (Supple. 1), 1–116.
- Andrade, R.J., Lucena, M.I., Martin-vivaldi, R., Fernandez, M.C., Nogueras, F., Pelaez, G., Gomez-Qutes, A., Garcia-Escano, M.D., Bellot, V., Hervas, A., Cardenas, F., Romero, M., Sameron, J., 1999. Acute liver injury associated with the use of ebrotidine, a new H<sub>2</sub>-receptor antagonist. *J. Hepatol.* 31, 641-646.
- Andrea, M.A.P., Katherine, E.C., Duane, T.S., Ainsley, W., John, D.F., Peter G.S., Jean-Michel V., Michel J., Michel M.L., Benjamin F.T., John F.L., Curtis C.H., 1993. Simian virus 40 large tumor antigen-immortalized normal human liver epithelial cells express hepatocyte characteristics and metabolize chemical carcinogens (serum-free medium/aflatoxin Bi/benzo[a]pyrene/N-nitrosodimethylamine). *Proc. Natl. Acad. Sci. USA.* 90, 5123-5127.
- Alvarez-Sánchez, R., Montavon, F., Hartung, T., Phler, A., 2006. Thiazolidinedione bioactivation: A comparison of the bioactivation potentials of troglitazone, rosiglitazone and pioglitazone using stable isotope-labeled analogues and liquid chromatography tandem mass spectrometry. *Chem. Res. Toxicol.* 19, 1106-1116.
- Banoglu, E., 2000. Current status of the cytosolic sulfotransferases in the metabolic activation of promutagens and procarcinogens. *Curr. Drug Metab.* 1, 1–30.
- Banoglu, E., King, R.S., 2002. Sulfation of indoxyl by human and rat aryl (phenol) sulfotransferases to form indoxyl sulfate. *Eur. J. Drug Metab. Pharmacokinet.* 27, 135–140.
- Bethesda, M.D., 1995. US department of health and human services, diabetes statistics, NIH publication 96, 236–239.
- Baughmam, T. M., Graham, R. A., Knecht, K. W., Silver I. S., Tyler, L. O., Knecht, M. W., and Zhao, Z., 2005. Metabolic activation of pioglitazone identified from rat and human liver microsomes and freshly isolated hepatocytes. *Drug Met. Dispos.* 33, 733-738.
- Bethesda, M.D., 1995. US department of health and human services, diabetes statistics, NIH publication 96, 236–239.
- Berger, J., and Moller, D.E., 2002. The mechanisms of action of PPARs. *Annu. Rev. Med.* 53, 409–435.
- Bigl, K., Schmitt, A., Meiners, I., Munch, G., Arendt, T., 2007. Comparison of results of the celltiter blue, the tetrazolium (3-[4,5-Dimethylthiazol-2-yl])-2,5-diphenyltetrazolium bromide) and the lactate dehydrogenase assay applied in brain cells after exposure to advanced glycation endproducts. *Toxicol. in vitro* 21, 952-971.
- Bolton, J.L., Trush, M.A., Penning, T.M., Dryhurst, G., Monks, T.J., 2000. Role of quinones in toxicology. *Chem. Res. Toxicol.* 13, 135–160.
- Burce, M., Psaty, M.D., Furberg, M.D., 2007. Rosiglitazone and cardiovascular risk. *New Eng. J. Med.* 356, 2522-2524.
- Camp, H.S., Li, O., Wise, L.S., Hong, Y.H., Frankowski, C.L., Roesler, W.J., 2000. Differential activation of peroxisome proliferators-activated-receptor-gamma by troglitazone and rosiglitazone. *Diabetes* 49, 539–547.
- Castillo, J.R., Torello, J., Hernandez, A., 2000. Liver injury caused by ebrotidine: A new example of the utility of the postmarketing surveillance. *Eur. J. Clin. Pharmacol.* 56, 187-189.



- Cereser, C., Guichard, J., Drai, J., Bannier, E., Garcia, I., Boget, S., Parvaz, P., Revol, A., 2001. Quantitation of reduced and total glutathione at the femtomole level by high-performance liquid chromatography with fluorescence detection: application to red blood cells and cultured fibroblasts. *J. Chromatogr. B* 752, 123–132.
- Chevion, M., Berenshtein, E., Stadtman, E.R. 2000. Human studies related to protein oxidation: protein carbonyl content as a marker of damage. *Free Radic. Res.* 33, 99–108
- Christine, M.D., Carmen, L.F., Richard, K., Paul, H.K., Thomas, A.B., 2005. Negative ion tandem mass spectrometry for the detection of glutathione conjugates. *Chem. Res. Toxicol.* 18, 630–638.
- Choi, S.S., Cha, B.Y., Lee, Y.L., Yonezawa, T., Teruya, T., Nagai, K., Woo, J.T., 2009. Magnolol enhances adipocyte differentiation and glucose uptake in 3T3-L1 cells. *Life sciences* 84, 908–914.
- Chojkier, M., 2005. Troglitazone and liver injury: in Search of answers. *Hepatology* 41, 237–246.
- Chou, H.C., Ozawa, S., Fu, P.P., Lang, N.P., Kadlubar, F.F., 1998. Metabolic activation of methyl-hydroxylated derivatives of 7,12-dimethylbenz[a]anthracene by 450 human liver dehydroepiandrosterone-steroid sulfotransferase. *Carcinogenesis* 19, 1071–1076.
- Day, C., 1999. Thiazolidinediones: a new class of antidiabetic drugs. *Diabetic Med.* 16, 179–192.
- Delzenne, N.M., Calderon, P.B., Taper, H.S., Roberfroid, M.B., 1992. Comparative hepatotoxicity of cholic acid, deoxycholic acid and lithocholic acid in the rat: in vivo and in vitro studies. *Toxicol. Lett.* 61, 291–304.
- Dieckhaus, C.M., Fernandez-Metzler, C.L., King, R., Krolikowski, P.H., Baillie, T.A., 2005. Negative ion tandem mass spectrometry for the detection of glutathione conjugates. *Chem. Res. Toxicol.* 18, 630–638.
- Fan, Y.H., Chen, H., Natarajan, A., Guo, Y., Harbinski, F., Layasere, J., Christ, W., Aktas, H., Halperin, J.A., 2004. Structure activity requirements for the antiproliferative effect of troglitazone derivatives mediated by depletion of intracellular calcium. *Bioorg. Med. Chem. Lett.* 2004, 2457–2550.
- Farris, M.W., Reed, D.J., 1987. High performance liquid chromatography of thiols and disulfides: dinitrophenol derivatives. *Methods Enzymol.* 143, 101–149.
- Forman, B.M., Tontonoz, P., Chen, J., Brun, R.P., Spiegelman, B.M., Evans, R.M., 1995. *Cell* 83, 803–812.
- Funk, C., Ponelle, C., Scheuermann, G., Pantze, M., 2001. Cholestatic potential of troglitazone as a possible factor contributing to troglitazone-induced hepatotoxicity. In vivo and in vitro interaction at the canalicular bile salt exportpump (Bsep) in the rat. *Mol. Pharmacol.* 59, 627–635.
- Gores, G.J., Miyoshi, H., Botla, R., Aguilar, H.I., Bronk, S.F., 1998. Induction of mitochondrial permeability transition as a mechanism of liver injury during cholestasis: a potential role for mitochondrial proteases. *Biochim. Biophys. Acta* 1366, 167–175.
- Grossman, S.L., Lessem, J., 1997. Mechanisms and clinical effects of thiazolidinediones . *Expert Opin. Invest. Drugs* 6, 1025–1040.
- Gulati, R.K., Agarwal, S., Agrawal, S.S., 1995. Hepatoprotective studies on *Phyllanthus emblica* Linn. and quercetin. *Indian J. Exp. Biol.* 33, 261–268.
- Harris M., Flegal K.M., Cowie C.C., 1998. Prevalence of diabetes, impaired fasting glucose, and impaired glucose tolerance in U.S. adults. The third national health and nutrition examination survey, 1988–1994. *Diabetes Care* 21, 18–24.

- Haskins, J. R., Rowse, P., Rahbari, R., Iglesia, F. A., 2001. Thiazolidinedione toxicity to isolated hepatocytes revealed by coherent multiprobe fluorescence microscopy and correlated with multiparameter flow cytometry of peripheral leukocytes. *Arch. Toxicol.* 75, 425-438.
- He, K., Talaat, R.E., Pool, W.F., Reily, M.D., Reed, J.E., Bridges, A.J., Woolf, T.F., 2004. Metabolic activation of troglitazone: identification of a reactive metabolite and mechanisms involved. *Drug Metab. Dispos.* 32, 639-646.
- He, K., Woolf, T.F., Kindt, E.K., Fielder, A.E., Talaat, R.E., 2001. Troglitazone quinone formation catalyzed by human and rat CYP3A: an atypical CYP oxidation reaction. *Biochem. Pharmacol.* 62, 191-198.
- Heel, R.C., Brogden, R.N., Carmine, A., Morley, P.A., Speight, T.M., Avery, G.S., 1982. Ketoconazole : A review of its therapeutic efficacy in superficial and systemic fungal infections. *Drugs* 23, 1-36,
- Henry, R.R., 1997. Thiazolidinones. *Endocrinol. Metab. Clin. North Am.* 26, 553–573.
- Hiji, A. K., Michalik, L., Wahli, W., 2002. PPARs: transcriptional effectors of fatty acids and their derivatives. *Cell Mol. Life Sci.* 59, 790-798.
- Huang, J., Shaiu, C.W., Yang, J., Wang, D.S., Chiu, H.C., Chen, C.Y., Chen, C.S., 2006. Development of small-molecule cyclin D1-ablative agents. *J. Med. Chem.* 49, 4684-4689.
- Ibrahimi, A., Teboul, L., Gaillard, D., Amri, E.Z., Ailhaud, G., Young, P., Cawthorne, M.A., Grimaldi, P.A., 1994. Evidence for a common mechanism of action for fatty acids and thiazolidinedione antidiabetic agents on gene expression in preadipose cells. *Mol. Pharmacol.* 46, 1070–1076.
- Jaakkola T., Backman, J.T., Neuvonen, M., 2006. Effect of rifampicin on the pharmacokinetics of pioglitazone. *Br. J. Clin. Pharmacol.* 61, 70-78.
- Joanna, Z., Li M., Baomin, X., Timothy, O.W., Griffith, H., Mingshe, Z., 2007. Screening and identification of GSH-trapped reactive metabolites using hybrid triple quadruple linear ion trap mass spectrometry. *Chem. Res. Toxicol.* 20, 757-766.
- Jinping, G., Timothy, W.H., Mei, H., Qinling, Q., Griffith, H.W., 2005. Dansyl glutathione as a trapping agent for the quantitative estimation and identification of reactive metabolites. *Chem. Res. Toxicol.* 18, 896-903.
- Kalgutkar, A.S., Vaz, A.D.N., Lame M.E., Henne, K.R., Sogila, J., Zhao, S.X., Abramov, Y.A., Lombardo, F., Collin, C., HendSch, Z., Hop. C.E.C.A., 2005. Bioactivation of the nontricyclic antidepressant nefazodone to a reactive quinone-imine species in human liver microsomes and recombinant P450 3A4. *Drug Metab. Dispos.* 33, 243-253.
- Kassahun, K., Pearson, P.G., Tang, W., McIntosh, I., Leung, K., Elmore, C., Dean, D., Wang, R., Doss, G., Baillie, T.A., 2001. Studies on the metabolism of troglitazone to reactive intermediates in vitro and in vivo. Evidence for novel biotransformation pathways involving quinone methide formation and thiazolidinedione ring scission. *Chem. Res. Toxicol.* 14, 62–70.
- Kassahun, K., Davis, M., Hu. P., Martin, B., Baillie, T., 1994. Metabolic activation of unsaturated derivatives of valproic acid. Identification of novel glutathione adducts formed through coenzyme A-dependent and –independent processes. *Chem. Biol. Interact.* 90, 253-275.
- Katrusiak, A.E., Paterson, P.G., Huse, K., Shoker, A., Lyon, A.W., 2001. Pre-column derivatization high-performance liquid chromatographic method for determination of cysteine, cysteinyl–glycine, homocysteine and glutathione in plasma and cell extracts. *J. Chromatogr. B* 758, 207–212.

- Kawai, K., Kawasaki-Tokui, Y., Odaka, T., Tsuruta, F., Kazui, M., Iwabuchi, H., 1997. Disposition and metabolism of the new oral antidiabetic drug troglitazone in rats, mice and dogs. *Arzneim. Forsch. Drug Res.* 104, 1507–1514.
- Khanna, S., Sobhia, M.E., Bharatam, P.V., 2005. Additivity of molecular fields: CoMFA study on dual activators of PPAR $\alpha$  and PPAR $\gamma$ . *J. Med. Chem.* 48, 3015–3040.
- Kliwer, S.A., Umesono, K., Noonan, D.J., Heyman, R.A., Evans, R.M., 1992. Convergence of 9-cis retinoic acid and peroxisome proliferators signalling pathways through heterodimer formation of their receptors. *Nature* 358, 771–774.
- Kletzien, R.F., Clarke, S.D., Ulrich, R.G., 1992. Enhancement of adipocyte differentiation by an insulin-sensitizing agent. *Mol. Pharmacol.* 41, 393–398.
- King, R.S., Teitel, C.H., Kadlubar, F.F., 2000. In vitro bioactivation of N-hydroxy-2- amino- $\alpha$ -carboline. *Carcinogenesis* 21, 1347–1354.
- Kostrubsky, V.E., Sinclair, J.F., Ramachandran, V., Venkataramanan, R., Wen, Y.H., Kindt, E., Galchev, V. Rose, K., Sinz, M., Strom, S.C., 2000. The role of conjugation in hepatotoxicity of troglitazone in human and porcine hepatocyte cultures. *Drug Metab. Dispos.* 28, 1192-1197.
- Kullak-Ublick, G.A., Beuers, U., Paumgartner, G., 2000. Hepatobiliary transport. *J. Hepatol.* 32 (suppl. 1), 3-18.
- Lee, W.M., 2003. Drug-induced hepatotoxicity. *New Engl. J. Med.* 349, 474–485.
- Lee, W.H., Kim, B.Y., Ahn, J.B., Kang, S.K., Jung, H.L., Jae, S.S., Ahn, S.K., Lee, S.J., Yoon, S.S., 2005. Molecular design, synthesis and hypoglycemic and hypolipidemic effect of novel pyrimidine derivatives having thiazolidinedione. *Eur. J. Med. Chem.* 40, 862-874.
- Lehmann, J.M., Moore, L.B., Smith-Oliver, T.A., Wilkison, W.O., Willson, T.M., Kliwer, S.A., 1995. An antidiabetic thiazolidinedione is a high affinity ligand for peroxisome proliferator-activated receptor  $\gamma$  (PPAR $\gamma$ ). *J. Biol. Chem.* 270, 12953-12956.
- Levine, R.L., Garland, D., Oliver, C.N., Amici, A., Climent, I., Lenz, A.G., Ahn, B.W., Shaltiel, S., Stadtman, E.R., 1990. Determination of carbonyl content in oxidatively modified proteins. *Methods. Enzymol.* 186, 464–478.
- Li, M., Bo, W., Qian, R., Mingshe, Z., 2008. Rapid screening of glutathione trapped reactive metabolites by linear ion trap mass spectrometry with isotope pattern-dependent scanning and postacquisition data mining. *Chem. Res. Toxicol.* 21, 1477-1483.
- Loi, C.M., Randiniis, E.J., Vassos, A.B., Kazierad, D.J., Koup, J.R., Sedman, A.J., 1997. Lack of effect of type II diabetes on the pharmacokinetics of troglitazone in a multiple-dose study. *J. Clin. Pharmacol.* 37, 1114-1120.
- Loi, C.M., Alvey, C.W., Randinitis, E.J., Sedman, A.J., Koup, S.R., 1999. Steady-state pharmacokinetics and dose proportionality of troglitazone and its metabolites. *J. Clin. Pharmacol.* 39, 920-926.
- Li, M., Bo, W., Qian, R., Mingshe, Z., 2008. Rapid screening of glutathione trapped reactive metabolites by linear ion trap mass spectrometry with isotope pattern-dependent scanning and postacquisition data mining. *Chem. Res. Toxicol.* 21, 1477-1483.
- Lloyd, S., Hayden, M. J., Sakai, Y., Fackett, A., Silber, P. M., Hewitt, N. J., Li, A. P., 2002. Differential in vitro hepatotoxicity of troglitazone and rosiglitazone among cryopreserved human hepatocytes from 37 donors. *Chem.-Biol. Interact.* 142, 57-71.
- Malinwski, J.M., Bolesta, P., 2000. Rosiglitazone in the treatment of type 2 diabetes mellitus: a critical review. *Clin. Ther.* 22, 1151-1168.
- Marcsek, Z.L., Kocsis, Z., Szende, B., Tompa, A., 2007. Effect of formaldehyde and resveratrol on the viability of vero, HepG2 and MCF-7 cells. *Cell Biol. Int.* 31, 1214–1219.

- Masubuchi, Y., 2006. Metabolic and non-metabolic factors determining troglitazone hepatotoxicity: a review. *Drug Metab. Pharmacokint.* 21, 347-353.
- Mingshe, Z., Li, M., Haiying, Z., Griffith, H.W., 2007. Detection and structural characterization of glutathione-trapped reactive metabolites using liquid chromatography high resolution mass spectrometry and mass defect filtering. *Anal. Chem.* 79, 8333-8341.
- Miller, V.A., Benedetti, F.M., Rigas, J.R., Verret, A.L., Pfister, D.G., Strarus, D., Kris, M.G., Crisp, M., Heyman, R., Loewen, G.R., Truglia, J.A., Warrell, R.P., 1997. Initial clinical trial of a selective retinoid X receptor ligand LGD1069. *J. Clin. Oncol.* 15, 790-795.
- Momose, Y., Maekawa, T., Yamano, T., Kawada, M., Odaka H., Hitoshi, I., Takashi, S., 2002. Novel 5-substituted 2,4-thiazolidinedione and 2,4-oxazolidinedione derivatives as insulin sensitizers with antidiabetic activities. *J. Med. Chem.* 45, 1518-1534.
- Mutlib, A., Lam, W., Atherton, J., Chen, H., Galatsis, P., Stolle, W., 2005. Application of stable isotope labeled glutathione and rapid scanning mass spectrometers in detecting and characterizing reactive metabolites. *Rapid Commun. Mass Spectrom.* 19, 3482-3492.
- New, L.S., Chan, E.C.Y., 2008. Evaluation of BEH C18, BEH HILIC, and HSS T3 (C18) column chemistries for the UPLC-MS-MS analysis of glutathione, glutathione disulfide, and ophthalmic acid in mouse liver and human plasma. *J. Chromatogr. Sci.* 46, 209-214.
- Park, B.K., Kitteringham, N.R., Maggs, J.L., Pirmohamed, M., Williams, D.P., 2005. The role of metabolic activation in drug-induced hepatotoxicity. *Annu. Rev. Pharmacol.* 45, 177-202.
- Park, B.K., Pirmohamed, M., Kitteringham, N.R., 1998. Role of drug disposition in drug hypersensitivity: A chemical molecular and clinical perspective. *Chem. Res. Toxicol.* 11, 969-988.
- Patrick, Y.M., Thomas, N., Jan, F., Elisabeth, S., Gerald, R., Luca, B., 2005. Comparative quantification of pharmacodynamic parameters of chiral compounds (RRR- vs. all-rac- $\alpha$ -tocopherol) by global gene expression profiling. *J. Plant Physiol.* 162, 811-817.
- Pastore, A., Piemonte, F., Locatelli, M., Lo R.A., Gaeta L.M., Tozzi, G., Federici, G., 2003. Determination of blood total, reduced and oxidized glutathione in pediatric subjects. *Clin. Chem.* 47, 1467-1469.
- Pomella, A., Visvikis, A., Paolicchi, A., De, T.V., Casini, A.F., 2003. The changing faces of glutathione, a cellular protagonist. *Biochem. Pharmacol.* 66, 1499-1503.
- Prabhu, S., Lloyd, A.F.S., Clellan, H.A., Terrell, C.M., Silber, P.M., Li, A.P., 2002. *Chem. Biol. Interact.* 142, 83-97.
- Rabkin, J.M., Smith, J.M., Orloff, S.L., Corless, C.L., Stenzel, P., Olyaei, A.J., 1999. Fatal fulminant hepatitis associated with bromfenac use. *Ann. Pharmacother.* 33, 945-947.
- Ramachandran, V., Kostrubsky, V.E., Komoroski, B.J., Zhang, S., Dorko, K., Esplen, J.E., 1999. Troglitazone increases cytochrome P-450 3A protein and activity in primary cultures of human hepatocytes. *Drug Metab. Dispos.* 27, 1194-1199.
- Ramachandran, U., Mital, A., Bharatum, P.V., Khanna, S., Rao, P.R., Srinivasan, K., Kumar, R., Chawla, H.P.S., Kaul, C.L., Raichur, S., Chakrabarti, R., 2004. Studies on some glitazones having pyridine as the linker unit. *Bioorg. Med. Chem.* 12, 655-658.
- Ranieri, R., Isabella, D.D., Alo, M., Daniela, G., 2006. Oxidized forms of glutathione in peripheral blood as biomarkers of oxidative stress. *Clin. Chem.* 52, 1406-1414.

- Rebeca G.M., Fausto S.M., Julio, C.A.P., Genoveva, D.R., Francisco, A.A., Miguel, C., 2008. Glycine increases mRNA adiponectin and diminishes pro-inflammatory adipokines expression in 3T3-L1 cells. *Eur. J. Pharmacol.* 587, 317-321.
- Reznick, A.Z., Packer, L., 1994. Oxidative damage to proteins: spectrophotometric method for carbonyl assay. *Methods Enzymol.* 233, 357-363.
- Rizvi, N.A., Marshall, J.L., Dahut, W., Ness, E., Truglia, J.A., Loewen, G., Gill, G.M., Ulm, E.H., Geiser R., Jaunakais, D., Hawkins, M.J., 1999. A phase I study of LGD1069 in adults with advanced cancer. *Clin. Cancer Res.* 5, 1658-1664.
- Robert L.D., Bruce M.B., Thomas T.C., David A.C., Bernard H., Ralph W.S., 1991. Benzylloxazolidine-2,4-diones as potent hypoglycemic agents. *J. Med. Chem.* 34, 1538-1544.
- Roman, K., Pavla, Ž., Halka L., Otto, K., Zuzana, Č., 2007. Determination of reduced and oxidized glutathione in biological samples using liquid chromatography with fluorimetric detection. *J. Pharma. Biomed. Annal.* 43, 1382-1387.
- Saha, S., New, L.S., Ho, H.K., Chui, W.K., Chan, E.C.Y., 2010. Investigation the role of the thiazolidinedione ring of troglitazone in inducing hepatotoxicity. *Toxicol. Lett.* 192, 141-149.
- Sahi, J., Hamilton, G., Sinz, M., Barros, S., Huang, M., Lesko, M.J., 2000. Effect of troglitazone on cytochrome P450 enzymes in primary cultures of human and rat hepatocytes. *Xenobiotica* 30, 273-284.
- Schulz, W.A., Eickelmann, P., Sies, H., 1996. Free radicals in toxicology: redox cycling and NADPH: quinone oxidoreductase. *Arch. Toxicol. Suppl.* 18, 217-222.
- Sherman, S.I., Gopal, J., Haugen, B.R., Chiu, A.C., Whaley, K., Nowlakha, P., Duvic, M., 1999. Central hypothyroidism associated with retinoid X receptor-selective ligands. *E. Engl. J. Med.* 340, 1075-1079.
- Smith, M.T., 2003. Mechanisms of troglitazone hepatotoxicity. *Chem. Res. Toxicol.* 16, 679-684.
- Soglia, J. R., Harriman, S.P., Zhao, S., Barberia, J., Cole, M.J., Boyd, J.G., Contillo, L.G. 2004. The development of a higher throughput reactive intermediate screening assay incorporating microbore liquid chromatography-micro-electrospray ionization-tandem mass spectrometry and glutathione ethyl ester as an in vitro conjugating agent. *J. Pharm. Biomed. Anal.* 36, 105-116.
- Tetty, J.N., Maggs, J.L., Rapeport, W.G., Primohamed, M., Park, B.K., 2001. Enzyme-induction dependent bioactivation of troglitazone and troglitazone quinone *in vivo*. *Chem. Res. Toxicol.* 14, 965-974.
- Thor, H., Smith, M.T., Hartzell, P., Bellomo, G., Jewell, S.A., Orrenius, S., 1982. The metabolism of menadione (2-methyl-1,4-naphthoquinone) by isolated hepatocytes. A study of the implications of oxidative stress in intact cells. *J. Biol. Chem.* 257, 12419-12425.
- Utrecht, J., 1999. New concepts in immunology relevant to idiosyncratic drug reactions: The "danger hypothesis" and innate immune system. *Chem. Res. Toxicol.* 12, 387-395.
- UK Prospective Diabetes Study (UKPDS) Group, 1998. Intensive blood glucose control with sulphonylureas or insulin compared with conventional treatment and risk of complications in patients with type2 diabetes. *Lancet.* 352, 837-853.
- Virginia, L.R., Dawn, V., Stefan, H., 2004. Sulfotransferase structural biology and inhibitor discovery. *Drug Discov. Today* 9, 1003-1011.
- Wagstaff, A.J., Goa, K.L., 2002. Rosiglitazone: a review of its use in the management of type 2 diabetes mellitus. *Drugs* 62, 1805-37.

- Yamamoto, Y., Nakajima, M., Yamazaki, H., Yokoi, T., 2001. Cytotoxicity and apoptosis produced by troglitazone in human hepatoma cells. *Life Sci.* 70, 471–482.
- Zhang, X.K., Hoffmann, B., Tran, P.B., Graupner, G., Pfahl, M., 1992. Retinoid X receptor is an auxiliary protein for thyroid hormone and retinoic acid receptors. *Nature* 355, 441–446.

## List of Publications

### Poster/Oral presentations:

1. **S Saha (Travel Award Winner)**, LS New, HK Ho, WK Chui, ECY Chan. Investigation of the role of thiazolidinedione ring and sulfo-conjugated troglitazone in inducing hepatotoxicity. **ADMET Profiling for Drug Discovery (Scientific workshops), Singapore**, 2009, September 15-16 (Oral).
2. **S Saha**, LS New, HK Ho, WK Chui, ECY Chan. Investigation of the role of thiazolidinedione of troglitazone in inducing hepatotoxicity in humans. **ISSX 3rd Regional Asia Pacific Meeting, Bangkok**, 2009, May 09-12 (Poster).
3. **S Saha**, WK Chui, LS New, ECY Chan. Reactive metabolites profiling of pioglitazone and pirosuccinimide in human liver microsomes using high performance liquid chromatography tandem mass spectrometry. **19<sup>th</sup> Singapore Pharmacy Congress, Singapore**, 2007, October 19-21 (Poster).

### Scientific abstract:

1. **S Saha**, LS New, HK Ho, WK Chui, ECY Chan. Investigation of the role of thiazolidinedione of troglitazone in inducing hepatotoxicity in humans. **Drug Metabolism Reviews**, 2009, 41(s2), 26.

**Journal articles:**

1. **S Saha**, LS New, HK Ho, WK Chui, ECY Chan. Direct toxicity effects of sulfo-conjugated troglitazone on human hepatocytes. **Toxicology Letters**, 2010, 195, 135-141.
2. **S Saha**, LS New, HK Ho, WK Chui, ECY Chan. Investigation of the role of thiazolidinedione of troglitazone in inducing hepatotoxicity. **Toxicology Letters**, 2010, 192, 141-149.